CORTICAL NETWORKS FOR CODING EGOCENTRIC VERSUS ALLOCENTRIC REACH GOALS

LINA MUSA

A DISSERTATION SUBMITTED TO THE FACULTY OF GRADUATE STUDIES
IN PARTIAL FULFILMENT OF THE REQUIREMENTS
FOR THE DEGREE OF
DOCTOR OF PHILOSOPHY

GRADUATE PROGRAM IN PSYCHOLOGY
YORK UNIVERSITY
TORONTO, CANADA

September, 2026

© Lina Musa, 2026

1 Abstract

Goal-directed actions require the integration of egocentric (body-centred) and allocentric (landmark-centred) spatial information to generate accurate movements. Although neuroimaging studies have identified cortical regions involved in each reference frame, the network-level organisation of these systems and the causal contribution of key network nodes to spatial behaviour remain poorly understood. This dissertation investigated the cortical mechanisms supporting memory-guided reaching using a multimodal approach that combined functional magnetic resonance imaging (fMRI), graph theory network analysis, and MRI-guided transcranial magnetic stimulation (TMS).

Study 1 characterised the functional network architecture underlying egocentric and allocentric reaching using graph theory analyses of event-related fMRI data. Functional connectivity analyses revealed distinct patterns of network organisation between spatial conditions. Allocentric reaching was associated with increased integration between dorsal visuomotor and ventral visual processing systems, consistent with the incorporation of landmark-centred information into motor planning. Network analyses identified task-specific hub regions within superior and inferior extrastriate cortex that exhibited high betweenness centrality, suggesting a role in facilitating communication across distributed cortical modules. These findings demonstrate that allocentric behaviour is supported by dynamic reconfiguration of large-scale functional brain networks rather than by recruitment of isolated cortical regions.

Study 2 examined the causal functional significance of these network hubs using MRI-guided TMS. Triple-pulse TMS delivered to the superior extrastriate hub disrupted behavioural performance across both egocentric and allocentric reaching, indicating that this region serves as a domain-general visuospatial processing node. In contrast, stimulation of the inferior extrastriate hub selectively impaired allocentric reaching, providing causal evidence that this region makes a specialized contribution to landmark-based spatial coding. Together, these findings establish that cortical hubs identified through graph-theoretical analyses are not merely correlates of network organisation but are functionally necessary for successful visuomotor behaviour.

Collectively, this dissertation demonstrates that memory-guided reaching emerges from coordinated interactions within distributed cortical networks whose organisation flexibly adapts to task demands. By integrating network neuroscience with causal brain stimulation, these studies provide novel insights into how egocentric and allocentric spatial information are coordinated to support goal-directed action and establish a framework for investigating distributed visuomotor networks in both healthy and clinical populations.

2 Dedication

This thesis is dedicated to my mother.

Your strength in the face of life's greatest challenges has been my greatest source of inspiration. Even during your own battles with your health, you have continued to face each day with courage, resilience, and unwavering love. Watching you persevere has taught me what it truly means to be strong and has inspired me to become a fighter in my own life.

Every obstacle I overcame during this journey was met with the lessons you unknowingly taught me: to never give up, to keep moving forward, and to face adversity with grace. This achievement is as much yours as it is mine.

Thank you for showing me that true strength is not measured by the absence of hardship, but by the courage to keep going despite it.

With all my love and gratitude, this work is dedicated to you.

3 Acknowledgements

First and foremost, I would like to express my deepest gratitude to my supervisor Dr. J. Douglas Crawford for his unwavering support throughout this journey. Through both the highs and the lows, he stood by me with patience, encouragement, and confidence in my abilities. During the most challenging moments, he reminded me of my strengths and gave me the determination to keep moving forward. His mentorship has shaped me not only as a researcher but also as a more confident and capable individual. I am especially grateful for the many opportunities he provided, including supporting my attendance at international conferences in beautiful countries, which broadened both my scientific perspective and my personal experiences. I could not have asked for a better mentor. Long before I began this journey, I looked up to my supervisor as one of my academic idols. Never in a million years did I imagine that I would one day have the privilege of working alongside him. Throughout these years, I have not only learned from his remarkable expertise and mentorship but have also come to admire him even more for his generosity, humility, and unwavering dedication to his students. It has truly been one of the greatest privileges of my academic career to learn from and work with someone I have respected for so long.

I would also like to sincerely thank my supervisory committee Dr. Jennifer Steeves and Dr. Dale Stevens, for their invaluable guidance throughout my graduate studies. Their wealth of knowledge, thoughtful feedback, and generosity with their time have been instrumental in strengthening this work. I greatly appreciate their willingness to share their expertise and their continued encouragement at every stage of this project. I would

also like to extend my sincere thanks to my examining committee, Dr. Shayna Rosenbaum, Dr. Jason Gallivan and Dr. Denise Henriques for taking the time to thoughtfully review my thesis and for their insightful questions, constructive feedback, and valuable perspectives.

To my lab mates, thank you for making the lab such a welcoming and enjoyable place to work. Your kindness, willingness to help, and readiness to share ideas made even the most difficult days more manageable. Beyond being wonderful colleagues, you became a strong support system, and I am grateful for the friendships, laughter, and sense of community we built together.

Finally, I would like to thank my family and friends who supported me throughout this journey, whether through words of encouragement, thoughtful advice, or simply by being there when I needed them. This thesis is the culmination of not only my efforts but also the generosity, guidance, and support of many remarkable people, for which I will always be grateful.

4 Table of Contents

1 Abstract ii

2 Dedication iv

3 Acknowledgements v

4 Table of Contents vii

5 List of Tables xi

6 List of Figures xii

7 List of Supplementary Figures xiii

1 CHAPTER ONE 1

1.1 Introduction 1

1.2 Spatial Reference Frames for Goal-Directed Action 2

1.3 Dorsal and Ventral Visual Streams 6

1.4 General Organization of the Cortical Reach System 12

1.5 Mechanisms for Egocentric vs Allocentric Reaching 18

1.5.1 Behavioural Mechanisms of Egocentric and Allocentric Reaching 19

1.5.2 Neuropsychology of Egocentric and Allocentric Reaching 23

1.5.3 Neurophysiology of Egocentric and Allocentric Reaching 26

1.5.4 Neuroimaging of Egocentric and Allocentric Reaching 28

1.5.5 Establishing Causality with Transcranial Magnetic Stimulation 32

1.6 Network Neuroscience and Graph Theory 35

1.7 Objectives and Hypotheses 39

2 CHAPTER TWO 41

2.1 Spatial Task Instructions and Global Activation Trends Influence Functional Modularity in the Cortical Reach Network 41

2.2 Abstract 42

2.3 Introduction 44

2.4 Methods 48

2.4.1 Data Source 48

2.4.2 Experimental Stimuli and Apparatus 49

2.4.3 Stimulus Specifications 49

2.4.4 Experimental Paradigm and Timing 50

2.4.5 Imaging Parameters 52

2.4.6 Univariate Data Analysis 52
2.4.6.1 Preprocessing 53
2.4.6.2 GLM Construction 53
2.4.6.3 Voxelwise Analysis 53
2.4.6.4 Statistical Corrections 54
2.4.7 Functional Connectivity Analysis 55
2.4.7.1 Regions of Interest and Time Series Computation 55
2.4.7.2 Detrending 59
2.4.7.3 Network Analysis (Adjacency Matrix Construction) 59
2.4.7.4 Graph Theory Analysis (GTA) 60
2.4.7.4.1 Global Network Topology 60
2.4.7.4.2 Global Network Dynamics 61
2.4.7.4.3 Mesoscale Network Topology (Modularity) 62
2.4.7.4.4 Modularity and Communication Analysis 64
2.4.7.4.5 Local Network Topology (Node Hubness) 65
2.4.7.4.6 Null Normalization 67
2.4.8 Statistical Analysis 70
2.4.9 Classification and Predictive Modeling 71
2.4.9.1 Classification of Task 71
2.4.9.2 Predicting Behaviour from Network Parameters 73
2.5 Results 75
2.5.1 Whole Brain Analysis: Cortical Trends Mediate Global Network Parameters 76
2.5.2 Intermediate Level Analysis: Behaviour Influences Signal Modularity 78
2.5.3 Local Analysis: Hubness of Egocentric and Allocentric Brain Networks 87
2.5.4 Decoding Task from Network Parameters 97
2.6 Discussion 103
2.6.1 Influence of Global Trends on Network 'Connectivity' 104
2.6.2 Global Network Parameters, Task, and Behaviour 105
2.6.3 The Egocentric Network 106
2.6.4 Changes Observed in the Allocentric Network 108
2.6.5 Lateralization 110
2.6.6 Possible Physiological Basis of Network 111
2.6.7 Relationship to Sensorimotor Transformation Models 112
2.6.8 General Implications 113
2.6.9 Conclusions 114
2.7 Funding 114
2.8 Supplementary Figures and Tables 115
3 CHAPTER THREE 117
3.1 Transcranial Magnetic Stimulation Differentiates Egocentric vs. Allocentric Network Hubs for Memory-Guided Reach 117

3.2 Abstract 118
3.3 Introduction 120
3.4 Materials and Methods 123
3.4.1 Participants 123
3.4.2 Experimental Design 123
3.4.3 Experimental Setup for TMS and Behavioural Recordings 124
3.4.4 Task Paradigm 126
3.4.5 Transcranial Magnetic Stimulation and Neuronavigation 126
3.4.6 Behavioural Data Acquisition and Analysis 127
3.4.7 MRI Data Acquisition 128
3.4.7.1 Structural Imaging 128
3.4.7.2 Retinotopic Mapping 128
3.4.7.3 Resting-State fMRI (Multi-Echo) 128
3.4.8 Individualized Functional Parcellation (GPIP) 129
3.4.9 Network Modularity Analysis 129
3.4.10 Statistical Analysis 130
3.4.11 Sample Size Analysis 130
3.5 Results 131
3.5.1 Overview of Experimental Paradigm 131
3.5.2 Reach Endpoint Errors 134
3.5.3 Influence of TMS in the Spatial Domain: Variable and Constant Error 136
3.5.4 Influence of TMS in the Temporal Domain: Reaction Time 139
3.5.5 Spatial Asymmetries: Visual Field and SAME vs. OPPOSITE Reaching 140
3.5.6 Network Analysis: Modularity Predicts Behavioural Changes Induced by TMS 143
3.6 Discussion 146
3.6.1 Behaviour in the Control Task Replicates Previous Observations 146
3.6.2 TMS Causally Dissociates Visual Streams and Spatial Behaviour 147
3.6.3 Implications for Cortical Network Organization 149
3.6.4 Potential Clinical Implications 150
3.6.5 Conclusions 150
3.6.6 Funding 151
3.7 Supplementary Materials 152
4 CHAPTER FOUR 156
4.1 Summary 156
4.2 The Role of Network Modularity in Spatial Goal Encoding 158
4.3 Global Activation Trends and Large-Scale Network Communication 159
4.4 Causal Evidence and the Convergence of Correlational and Interventional Methods 161

4.5 Relationship to Sensorimotor Transformation Models 163
4.6 Possible Physiological Basis of the Networks 164
4.7 Lateralization.....165
4.8 Limitations 166
4.9 General Implications and Clinical Relevance 167
4.10 Future Directions 168
4.11 Conclusions 169

5 References.....171

6 Appendix A. 197

8 Appendix B. 198

9 Appendix C. Author Contributions 199

9.1 Chapter 2 199
9.2 Chapter 3 199

5 List of Tables

Table 2.1 Glossary of Technical Terms Used in Graph Theory Analysis..... 68

Table 2.2 Eigenvector Centrality Hubs of the Egocentric and Allocentric Networks..... 90

Table 2.3 Betweenness Centrality Hubs of the Egocentric and Allocentric Networks 93

Table 2.4 Allocentric Inter-task Difference Nodes. 96

6 List of Figures

Figure 1.1 Schematic Illustration of Egocentric and Allocentric Reference Frames. 5

Figure 1.2 Two Visual Streams..... 11

Figure 1.3 Overview Visuomotor Brain Areas. 14

Figure 1.4 Reach Endpoints during Explicit Egocentric and Allocentric Reaching 22

Figure 1.5 Mechanisms for Egocentric and Allocentric Reach..... 30

Figure 1.6 Schematic of Graph Theoretical Analysis..... 37

Figure 2.1 Task. 51

Figure 2.2. Analysis Pipeline..... 56

Figure 2.3 Quantification of Global Network Properties. 77

Figure 2.4 Visualization of Networks / Modularity Analysis. 80

Figure 2.5 Quantification of Modularity in Original and Detrended Datasets. 83

Figure 2.6 Influence of Threshold and Detrending. 86

Figure 2.7 Eigenvector Centrality Hubs. 89

Figure 2.8 Betweenness Centrality Hubs. 92

Figure 2.9 Allocentric Inter-task Difference Nodes. 95

Figure 2.10 Classification Analysis. 100

Figure 2.11 Influence of Network Predictors on Behaviour by Condition. 102

Figure 3.1 Experimental Setup.....125

Figure 3.2 Stimulation Site and Experimental Paradigm. 133

Figure 3.3 Average Reach Endpoint Ellipses.....135

Figure 3.4 Influence of TMS in the Spatial and Temporal Domains. 138

Figure 3.5 Lateralization of Response. 142

Figure 3.6 Association of Network Modularity with Behaviour. 145

7 List of Supplementary Figures

Supplementary Figure 2.1 Influence of Network Predictors on Behaviour by Condition. 115

Supplementary Figure 2.2 Classification Analysis. 116

Supplementary Figure 3.1 Reach Accuracy and Precision Across Target-Movement Mappings. 152

Supplementary Figure 3.2 Reaction Time and Movement Time Across Target-Movement Mappings. 153

Supplementary Figure 3.3 Modularity Correlates to Behavioural Errors in Control Data. 154

Supplementary Figure 3.4 Timing of events. 155

1 CHAPTER ONE

GENERAL INTRODUCTION

1.1 Introduction

Successful interaction with the visual environment depends on the brain's ability to represent, maintain, transform, and utilise spatial information for action. Every visually guided behaviour, from reaching to grasp a cup to striking a moving ball, requires the nervous system to determine where a target is located in space and convert that positional information into motor commands appropriate for the intended movement (Andersen & Buneo, 2002; Crawford et al., 2011). Although this process appears to be effortless, it involves a complex series of neural computations that transform sensory signals encoded in one coordinate system into motor commands expressed in another. Understanding how the brain maintains and integrates these spatial representations remains a central question in systems and cognitive neuroscience.

Spatial coding has traditionally been described in terms of reference frames. Visual targets may be represented relative to the observer, termed egocentric coding, or relative to stable landmarks and objects in the environment, termed allocentric coding (Colby, 1998; Galati et al., 2000). Both forms of representation serve distinct functional roles. Egocentric coding provides direct access to information required for immediate action, whereas allocentric coding offers stability across movements, gaze shifts, and changes in body position (Burgess, 2006). Behavioural evidence indicates that humans use both sources of information simultaneously and combine them in a weighted fashion according to task demands and the relative reliability of each signal (Byrne &

Crawford, 2010; Fiehler et al., 2014). The present dissertation examines how egocentric and allocentric representations are organised across cortical networks and how specific network components contribute causally to behaviour.

Historically, research on spatial coding focused on identifying brain regions associated with egocentric and allocentric processing in isolation. Neuroimaging and neurophysiological studies established that posterior parietal cortex (PPC) is critical for egocentric visuomotor transformations, while ventral-stream regions in temporal cortex support allocentric and object-centred coding (Goodale & Milner, 1992; Milner & Goodale, 2006). More recently, attention has shifted toward understanding how distributed networks of regions interact to support behaviour, recognising that cognition arises from coordinated activity across large-scale cortical systems rather than from isolated specialised regions (Bressler & Menon, 2010). The current work builds upon this transition by combining functional magnetic resonance imaging (fMRI), graph theory analysis, and transcranial magnetic stimulation (TMS) to investigate both the organisation and causal significance of cortical networks supporting memory-guided reaching.

1.2 Spatial Reference Frames for Goal-Directed Action

The concept of a reference frame is fundamental to understanding sensorimotor interactions with the environment (Soechting & Flanders, 1992). Sensory information is initially encoded relative to the peripheral receptors that detect it. Visual signals, for example, are represented on the retina in eye-centred (retinocentric) coordinates, and afferent signals from mechanoreceptors are coded in skin- or joint-centred frames

(Cohen & Andersen, 2002). Motor systems, however, require information relative to the effectors that generate movement. Consequently, the nervous system must perform a series of coordinate transformations to translate target representations encoded in sensory coordinates into motor commands expressed relative to the hand, arm, or body (Andersen & Buneo, 2002; Buneo & Andersen, 2006). Failure at any stage of this transformation cascade can produce reaching errors, misreaches, and clinical deficits in spatial behaviour.

Egocentric reference frames specify target location relative to a body-centred origin. Targets may be encoded relative to gaze direction (retinocentric), as shown in Figure 1.1, where the position of the white cue ball is referenced relative to the gaze direction of the right eye. However, egocentric information can also be centered on head orientation (head-centred), trunk position (body-centred), or limb position (hand-centred), and representations at each level have been identified in distinct cortical and subcortical structures (Batista et al., 1999; Bremmer et al., 2001). Numerous behavioural, computational, and neurophysiological studies have demonstrated the importance of egocentric coding for visually guided action (Batista et al., 1999; Goodale & Milner, 1992). The dorsal visual stream, posterior parietal cortex (PPC), and frontal motor regions are strongly implicated in representing target location within egocentric coordinates suitable for action planning (Andersen & Buneo, 2002; Culham & Kanwisher, 2001).

Allocentric reference frames specify target location relative to external environmental landmarks or objects rather than the observer's body. The schematic in Figure 1.1

shows how the white cue ball is also encoded relative to the grey ball, which acts a landmark, external to the observer. Such representations are particularly useful when egocentric sensory information is uncertain, subject to noise, or when actions must be delayed beyond the period during which precise sensory signals are available (Milner & Goodale, 2006; Byrne & Crawford, 2010). Landmark-centred coding allows target information to remain stable despite movements of the eyes, head, or body, because the target's position is defined relative to stable external reference points rather than fluctuating internal signals (Burgess, 2006). Behavioural experiments have repeatedly demonstrated that visual landmarks influence reach endpoints even when participants are explicitly instructed to ignore them, indicating that allocentric processing operates automatically and in parallel with egocentric coding (Bridgeman et al., 1997; Fiehler et al., 2014).

A growing body of work suggests that egocentric and allocentric information are combined according to principles of probabilistic or Bayesian integration (Byrne & Crawford, 2010; Körding & Wolpert, 2004). Under this framework, the brain weights each source of spatial information according to its statistical reliability, combining signals in a manner that minimises overall uncertainty about target location. Byrne and Crawford (2010) formalised this account in a computational model showing that the relative weighting assigned to allocentric landmarks should increase as egocentric memory degrades over time or becomes noisier due to intervening eye movements. Experimental work by Fiehler and colleagues (2014) subsequently provided additional behavioural support for this proposal, demonstrating that manipulations of landmark stability, visual noise, and memory delay systematically altered the contribution of

allocentric information to reach planning. Collectively, these findings indicate that goal-directed actions emerge from the dynamic integration of multiple spatial representations rather than from a single dominant reference frame.

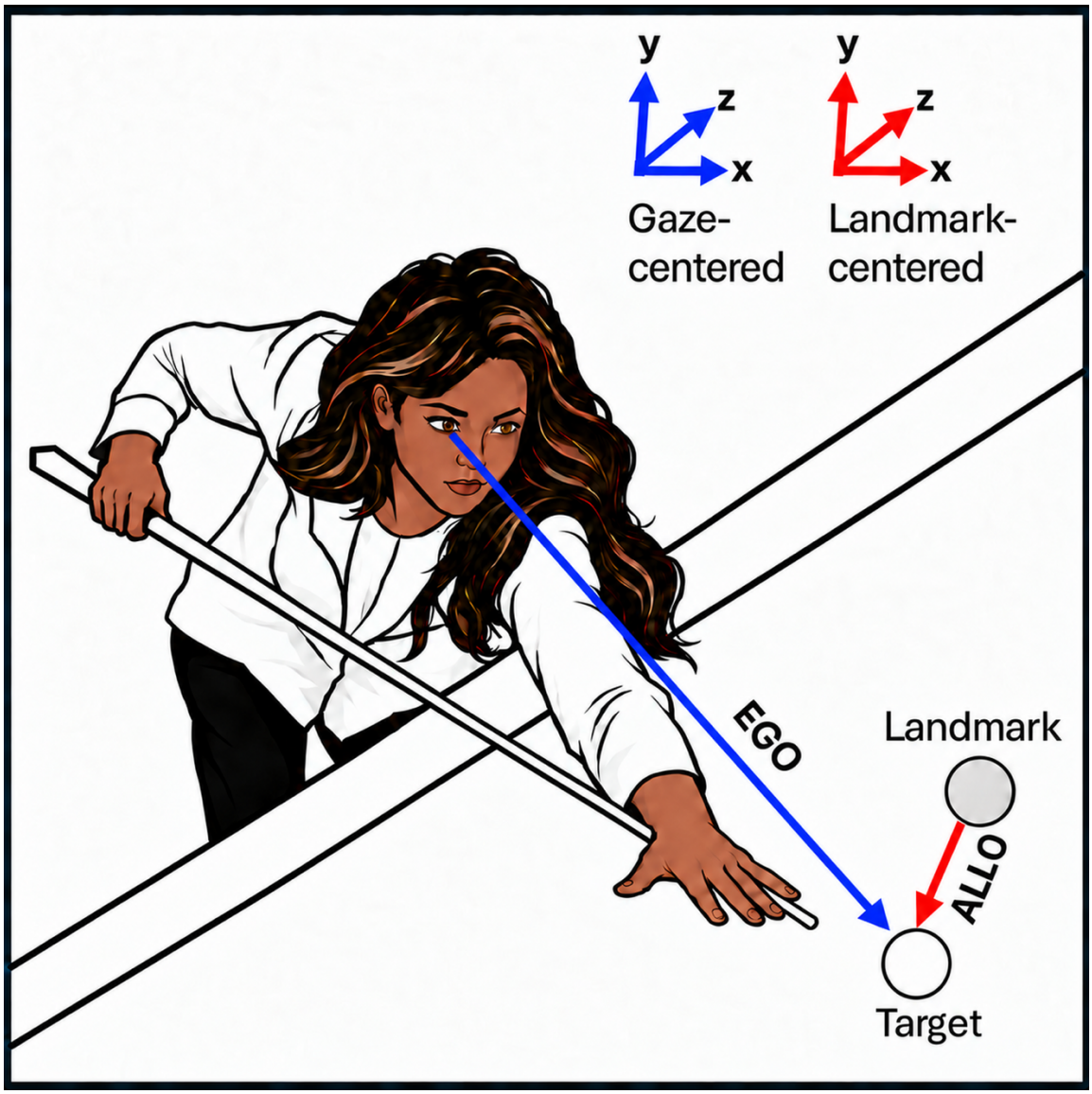


Figure 1.1 Schematic Illustration of Egocentric and Allocentric Reference Frames.

In egocentric coding (EGO; blue), the white ball (target) location is specified relative to the observer's gaze origin. In allocentric coding (ALLO; red), target location is specified relative to an external landmark (the grey ball), independently of the observer's position, both in all three orthogonal axes (x,y,z).

However, the distinction between egocentric and allocentric coding still has particularly important implications for memory-guided reaching. During delayed actions, sensory information about target location is no longer available, and target position must be maintained internally across the delay period (Gnadt & Andersen, 1988; Snyder et al., 1997). Studies examining motor-equivalent memory tasks have demonstrated that egocentric representations tend to degrade over time, consistent with progressive accumulation of noise in internal spatial signals (Hay & Redon, 1999). In contrast, allocentric representations anchored to stable landmarks remain comparatively stable across similar intervals. This asymmetry has led to the proposal that allocentric information may serve as a stabilising influence on memory-guided action, particularly under conditions of extended delay or uncertainty about egocentric state (Byrne & Crawford, 2010; Chen et al., 2018).

1.3 Dorsal and Ventral Visual Streams

Although vision is often regarded as a single sensory modality, decades of behavioural, neurophysiological, and neuroimaging research have demonstrated that visual information is processed through multiple specialized cortical pathways that differ in both their anatomical organization and functional roles (Goodale & Milner, 1992; Kravitz et al., 2011). Among these, the dorsal and ventral visual streams constitute the principal cortical networks responsible for transforming visual input into perception and action. Understanding the functional organization of these pathways is fundamental to explaining how the nervous system represents spatial information during reaching movements and, more specifically, how egocentric and allocentric reference frames emerge during visuomotor control.

Visual processing begins in the retina, where photoreceptors convert light into electrical signals that are transmitted through bipolar and retinal ganglion cells to the lateral geniculate nucleus (LGN) of the thalamus. From the LGN, visual information is projected to the primary visual cortex (V1), where fundamental stimulus characteristics such as orientation, contrast, spatial frequency, and edge information are extracted (Felleman & Van Essen, 1991). Rather than functioning as an isolated cortical area, V1 represents the first stage of a hierarchical network in which information is distributed to numerous extrastriate regions through extensive feedforward and feedback connections. These parallel pathways enable different aspects of the visual scene to be processed simultaneously, allowing the brain to extract information regarding object identity, spatial location, motion, depth, and behavioural relevance.

The concept that vision is organized into multiple cortical pathways originated largely from lesion studies conducted in non-human primates during the 1970s and early 1980s. In a landmark series of experiments, Ungerleider and Mishkin (1982) demonstrated that lesions involving the inferior temporal cortex impaired object discrimination while largely sparing spatial localization. Conversely, lesions affecting the posterior parietal cortex disrupted spatial discrimination despite relatively preserved object recognition. These observations led to the influential "what" versus "where" model of visual processing, proposing that the ventral pathway specializes in identifying objects, whereas the dorsal pathway computes their spatial location.

Although the "what/where" framework represented a major advance in understanding cortical specialization, subsequent research revealed that the distinction between object

identity and spatial location was insufficient to explain many aspects of visually guided behaviour. Individuals with damage to posterior parietal cortex frequently exhibited severe impairments in reaching and grasping despite retaining the ability to verbally identify target locations. Conversely, patients with ventral stream lesions often failed to recognize or consciously perceive objects while remaining capable of producing remarkably accurate reaching and grasping movements toward those same objects (Goodale et al., 1991). These dissociations suggested that the dorsal pathway performs computations extending beyond spatial localization and that visuomotor control cannot be explained solely by identifying where an object is located.

To account for these observations, Goodale and Milner (1992) proposed the perception–action model, one of the most influential theoretical frameworks in modern visual neuroscience. Rather than conceptualizing the dorsal stream as a "where" pathway, they argued that it functions primarily as a system for the visual control of action. According to this model, dorsal stream processing supports the rapid transformation of visual information into motor commands necessary for reaching, grasping, pointing, and object manipulation. In contrast, the ventral stream constructs perceptual representations that enable conscious object recognition, categorization, and long-term memory. This reinterpretation shifted emphasis away from the type of information being processed toward the computational goals served by each pathway.

A key distinction between the perception–action model and the earlier "what/where" hypothesis concerns the temporal characteristics of visual processing. Ventral stream representations are relatively stable and persist over time, supporting object recognition

across changes in viewpoint, illumination, and observer position. These representations are therefore well suited for perceptual judgments, semantic processing, and episodic memory. By contrast, dorsal stream representations are dynamic and continuously updated according to changes in gaze direction, body posture, and limb position. Such rapid updating allows movements to remain accurate despite ongoing changes in both the observer and the external environment (Goodale & Milner, 1992).

Nevertheless, the strict functional separation implied by early versions of the dual-stream model has become increasingly difficult to maintain in the face of accumulating evidence (Schenk & McIntosh, 2010; Freud et al., 2017). Neuroimaging studies consistently demonstrate that both streams are co-activated during most spatial tasks, and that their relative contributions depend on the specific demands imposed by task instructions, stimulus characteristics, and timing (Milner & Goodale, 2006; Filimon, 2010). Lesion studies reveal that dorsal stream damage can impair perceptual judgments in addition to motor performance (Rossetti et al., 2003), while ventral stream damage may produce deficits in grasping under conditions that require object recognition (Freud et al., 2017). Rather than functioning as entirely independent and informationally encapsulated systems, the two streams appear to exchange information extensively and to rely on partially overlapping cortical territories. Understanding the mechanisms that support this exchange, including the role of intermediate association areas, cross-stream projection pathways, and top-down modulatory signals, represents an important challenge for contemporary systems neuroscience.

Anatomically summarized in the schematic in Figure 1.2, the ventral visual stream extends from the occipital cortex through extrastriate visual areas, including V2 and V4, before projecting into the anterior temporal lobes (ATL). Along this pathway, receptive fields become progressively larger and increasingly selective for complex visual features. Neurons within inferior temporal cortex respond preferentially to object shape, colour, texture, faces, and learned object categories, supporting invariant object recognition despite substantial variations in retinal image characteristics (Kravitz et al., 2013). Beyond the temporal cortex, ventral stream projections communicate extensively with medial temporal lobe structures, including the hippocampus and parahippocampal cortex, which contribute to long-term memory formation and allocentric spatial representations.

The dorsal visual stream follows a markedly different anatomical trajectory. Originating within occipital visual areas, including V3, V6, MT and MST, the pathway projects dorsally toward the posterior parietal cortex before extending into premotor and frontal motor regions (Rizzolatti & Matelli, 2003). Unlike ventral stream neurons, which emphasize visual feature analysis, dorsal stream neurons are highly sensitive to spatial relationships, visual motion, binocular disparity, eye position, and limb configuration. These signals provide the sensory foundation required for transforming retinal coordinates into motor commands capable of guiding voluntary movements.

Importantly, the dorsal stream should not be viewed as a single homogeneous pathway. Advances in comparative neuroanatomy and tract-tracing techniques have revealed that it consists of multiple interconnected subnetworks with partially distinct functions.

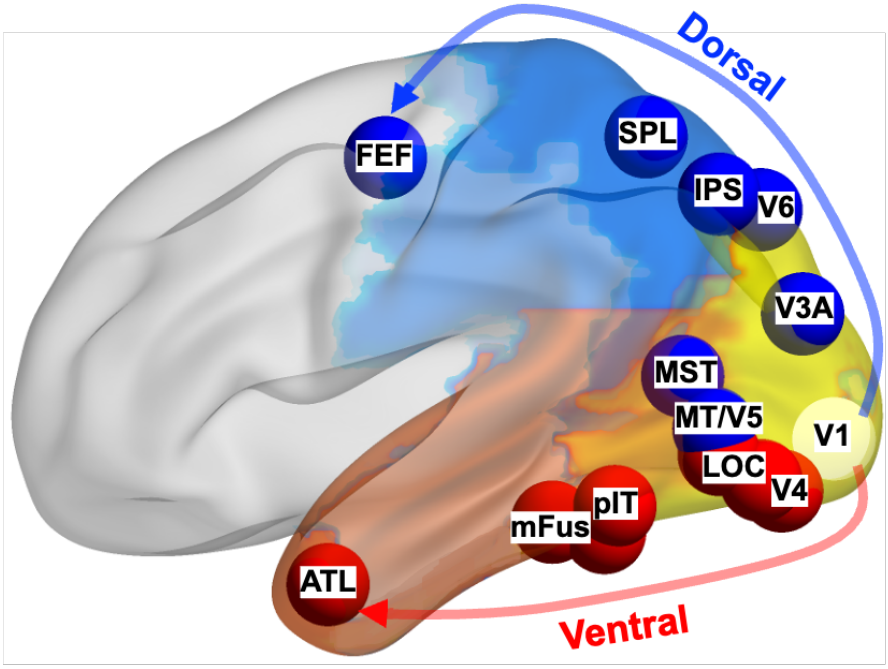


Figure 1.2 Two Visual Streams

Lateral view of the left human cerebral cortex illustrating the dorsal (blue) and ventral (red) visual processing streams. The dorsal stream projects from primary visual cortex (V1) in occipital cortex towards the parietal cortex (shown in blue). The ventral stream projects from V1 towards the temporal cortex (shown in red). Some of the key hub regions in both streams are shown, including the frontal eye fields (FEF), superior parietal lobule (SPL), intraparietal sulcus (IPS), visual areas V6 and V3A, and the motion-sensitive visual areas MT and MST in the dorsal stream, as well as visual area V4, the lateral occipital cortex (LOC), medial fusiform (mFus), posterior inferior temporal cortex (pIT), and the anterior temporal lobe (ATL) in the ventral stream. Regional boundaries were matched using the Human Connectome Project (HCP) multimodal cortical parcellation (Glasser et al., 2016). The organization of the dorsal and ventral visual streams is adapted from Kravitz et al. (2011).

Rizzolatti and Matelli (2003) proposed that the dorsal stream can be divided into dorsodorsal and ventrodorsal pathways. The dorsodorsal pathway, projecting through the superior parietal lobule to dorsal premotor cortex, is primarily involved in online movement control, visuomotor transformations, and reaching. In contrast, the ventrodorsal pathway, involving the inferior parietal lobule and ventral premotor cortex, contributes more strongly to object manipulation, skilled hand actions, action understanding, and tool use. This subdivision challenged earlier notions that the dorsal stream performs a single computational function and instead emphasized its functional heterogeneity. The next section examines the role of the dorsal stream during visually guided behaviour in greater detail by exploring how the dorsal stream is organized for reaching from occipital to frontal.

1.4 General Organization of the Cortical Reach System

Reaching is one of the most fundamental goal-directed behaviours performed by humans, requiring the precise coordination of sensory information, cognitive processes, and motor commands. Unlike simple reflexive movements, reaching requires the nervous system to determine the location of a target, transform this information into an appropriate movement plan, generate coordinated muscle activity, and continuously adjust movement based on sensory feedback. These processes depend on a widely distributed cortical network involving visual, parietal, premotor, and primary motor regions (Andersen & Cui, 2009; Vesia & Crawford, 2012), summarized in Figure 1.3. The cortical reach system can therefore be conceptualized as a hierarchical yet highly interactive network in which sensory representations are progressively transformed into motor commands.

A central feature of the cortical reach system is the transformation of visual information across multiple spatial reference frames. Visual input entering the cortex initially represents the external world relative to the retina. However, reaching requires information to be expressed in relation to the body and the intended movement. A target represented at a particular retinal location must ultimately be converted into a motor command specifying the direction, distance, and force required to move the arm. This transformation is not accomplished by a single brain region but emerges through interactions among interconnected cortical areas extending from occipital visual cortex to frontal motor regions (Andersen & Buneo, 2002).

A visual representation of the environment is transformed into an action-related motor plan through interactions between occipital, parietal, and frontal cortical networks. Processing begins in the occipital cortex, where primary visual cortex (V1) provides an organized retinotopic representation of visual space. Although V1 does not directly control movement, its outputs provide the foundation for higher-order visuomotor processing. Information is subsequently distributed across extrastriate areas, including V2, V3, V3A, and MT/MST, where increasingly complex features such as motion, depth, object boundaries, and spatial relationships are extracted (Felleman & Van Essen, 1991; Born & Bradley, 2005). These computations are essential for reaching because successful action requires not only identifying an object but also determining its location and three-dimensional relationship to the body.

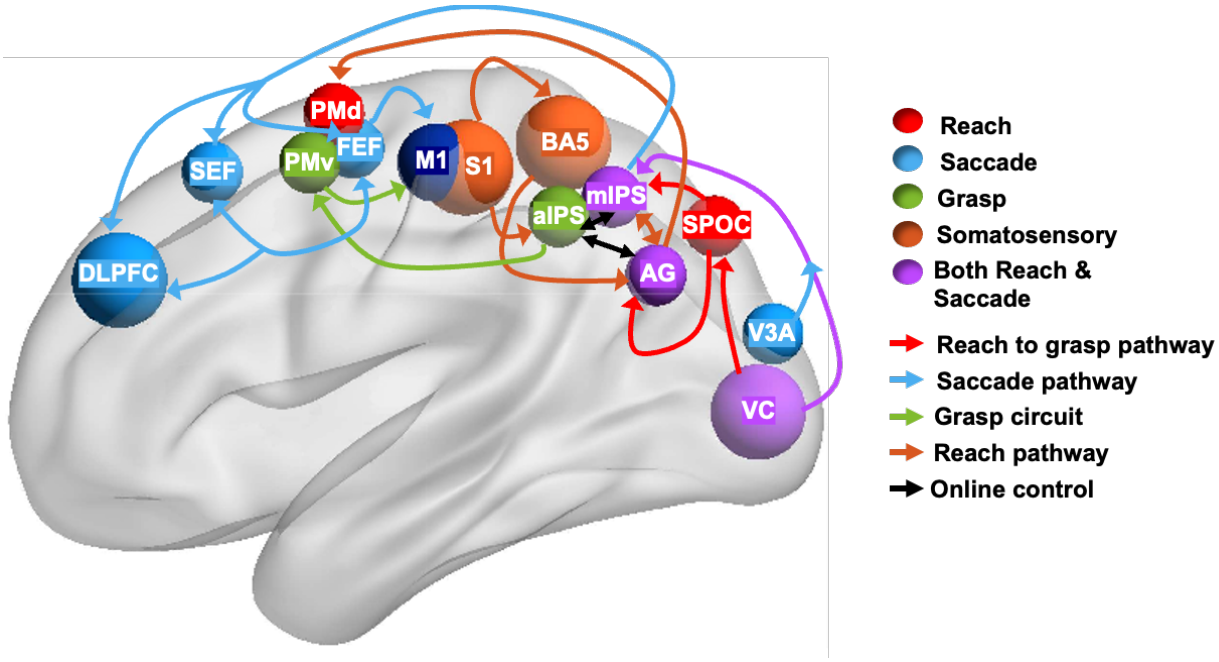


Figure 1.3 Overview Visuomotor Brain Areas.

Adapted from: Vesia & Crawford (2012). *Specialization of reach function in human posterior parietal cortex, Figure 7*. Schematic illustration of the left cerebral hemisphere highlighting cortical regions associated with visuomotor processing and eye–hand coordination. Labeled regions include the visual cortex (VC; V3A), angular gyrus (AG), anterior intraparietal sulcus (aIPS), mid-posterior intraparietal sulcus (mIPS), superior parieto-occipital cortex (SPOC), primary somatosensory cortex (S1; arm proprioception), Brodmann area 5 (BA5), primary motor cortex (M1), dorsal premotor cortex (PMd), ventral premotor cortex (PMv), frontal eye fields (FEF), supplementary eye fields (SEF), and dorsolateral prefrontal cortex (DLPFC). The figure has been redrawn, showing regions of interest (ROIs) in three dimensions, with some colors modified for clarity while preserving the general anatomical organization of the original illustration. The locations of the cortical regions were reconstructed by matching the reported anatomical locations to the closest corresponding regions in the Automated Anatomical Labeling (AAL) atlas, and the resulting atlas coordinates were used to position the ROIs.

The dorsal visual stream transforms these sensory representations into information suitable for guiding movement. Motion-sensitive areas such as MT and MST contribute information about object motion and optic flow, allowing the brain to distinguish movement of the environment from movement caused by changes in gaze or body position (Born & Bradley, 2005). Regions including V3A and the caudal intraparietal area (CIP) contribute to depth perception and three-dimensional object structure, which are necessary for accurate hand guidance in space (Culham et al., 2006). Research by Crawford and colleagues has emphasized that reaching requires complex visuomotor transformations because visual targets must be converted from external coordinates into gaze-, head-, and limb-centred representations before they can generate appropriate motor commands (Crawford et al., 2004; Crawford et al., 2011).

Following occipital processing, visual information converges within the posterior parietal cortex (PPC), which acts as a major sensorimotor interface between perception and action. Unlike early visual areas that primarily encode sensory features, PPC neurons integrate visual information with signals related to eye position, body posture, and intended movement. This allows objects to be represented according to their behavioural relevance rather than simply their retinal location (Andersen & Buneo, 2002). Crawford et al. (2011) demonstrated that goal-directed reaching depends on dynamic transformations between different spatial reference frames, with gaze-centred representations playing an important role in updating target location during coordinated eye and hand movements.

Several PPC regions contribute specifically to reaching behaviour. The medial intraparietal area (MIP) and parietal reach region (PRR) contain neurons that become active before movement initiation and encode intended reach goals rather than only visual targets (Andersen & Buneo, 2002; Snyder et al., 1997). These regions transform information between retinal-, eye-, and limb-centred coordinate systems, allowing the brain to determine how a movement should be directed toward a target (Batista et al., 1999; Chang & Snyder, 2010). The superior parietal lobule (SPL) contributes to online movement control by integrating visual feedback with proprioceptive information about limb position. Evidence from optic ataxia, where individuals show impaired reaching despite preserved visual perception, demonstrates that PPC is critical for converting spatial information into accurate motor behaviour (Perenin & Vighetto, 1988).

The transition from parietal to frontal cortex represents the conversion of spatial representations into movement plans. Frontal regions involved in reaching include the frontal eye fields (FEF), dorsal premotor cortex (PMd), ventral premotor cortex (PMv), supplementary motor area (SMA), and primary motor cortex (M1). The FEF contributes to eye–hand coordination by controlling voluntary saccades and providing gaze-related signals that assist in updating spatial representations during reaching. Because reaching frequently involves directing gaze toward a target before or during movement, FEF activity helps coordinate visual attention, eye position, and manual action (Crawford et al., 2011).

PMd receives substantial input from PPC and plays a central role in transforming spatial goals into motor plans. PMd neurons become active before movement onset and

encode factors such as reach direction, target selection, and movement strategy rather than only muscle activation (Wise et al., 1997; Cisek & Kalaska, 2005). PMv contributes to object-directed actions by integrating information about object properties and possible interactions, including grasp configuration and manipulation (Rizzolatti & Craighero, 2004). The SMA contributes to internally generated and memory-guided movements, particularly when reaching requires stored spatial information rather than immediate visual guidance (Nachev et al., 2008).

Finally, primary motor cortex (M1) generates the descending corticospinal commands required for movement execution. M1 neurons encode movement parameters including direction, force, velocity, and muscle activation patterns (Georgopoulos et al., 1982). However, M1 functions within a continuous sensorimotor loop rather than as a simple final output stage. Visual and proprioceptive feedback are continuously compared with predicted movement outcomes, allowing corrections throughout the reach (Shadmehr & Krakauer, 2008). Together, these interconnected regions form a distributed cortical reach network in which occipital areas analyze visual information, PPC transforms sensory inputs into action-related representations, FEF supports gaze coordination, premotor regions prepare movements, and M1 executes motor commands.

The visuomotor transformations described above highlight that reaching requires continuous updating of spatial information across multiple reference frames. As demonstrated in the previous literature, the brain must convert visual signals from external coordinates into body-centred representations while maintaining accurate relationships between gaze, the hand, and surrounding objects (Crawford et al., 2004;

Crawford et al., 2011). These transformations provide the basis for understanding the complementary roles of egocentric and allocentric mechanisms in guiding reaching behaviour.

1.5 Mechanisms for Egocentric vs Allocentric Reaching

Every goal-directed reaching movement requires the brain to answer a fundamental question: where is the target located, and how should the body move to acquire it? Although this appears to be a straightforward computation, it requires the integration of multiple sources of sensory information, including vision, proprioception, vestibular signals, and prior knowledge about the environment. One of the central challenges in visuomotor neuroscience is understanding how the brain represents spatial information and transforms these representations into appropriate motor commands.

Two major classes of spatial representation have been identified as particularly important for reaching behaviour: egocentric and allocentric reference frames. Egocentric representations define the location of objects relative to the observer or the body, whereas allocentric representations define the location of objects relative to other objects or environmental landmarks (Klatzky, 1998; Byrne & Crawford, 2010). These reference frames provide complementary strategies for representing space, with egocentric coding supporting immediate interactions with the environment and allocentric coding supporting stable representations that remain useful across changes in viewpoint and body position.

The distinction between egocentric and allocentric representations is a central framework for understanding visuomotor behaviour because it provides an explanation

for how the brain can simultaneously control rapid actions and maintain stable knowledge of the external world. During an immediate reach toward a visible object, information about the object's location relative to the body is essential because the motor system must rapidly calculate the trajectory required to move the limb. However, during delayed reaching, navigation, or interactions involving multiple objects, information regarding the relationship between objects and environmental structure becomes increasingly valuable.

1.5.1 Behavioural Mechanisms of Egocentric and Allocentric Reaching

Reaching behaviour requires the representation of target location within different spatial reference frames. Behavioural studies have examined these representations using open-loop reaching, memory-guided reaching, landmark manipulation, and realistic virtual environments. Differences in endpoint accuracy, movement variability, and spatial biases provide evidence that egocentric and allocentric representations contribute differently depending on the demands of the task.

Early studies established that reaching is strongly influenced by egocentric reference frames, particularly during conditions where visual feedback is unavailable. Henriques et al. (1998) demonstrated that when participants viewed a target, shifted their gaze, and then reached in darkness, reach endpoints showed systematic gaze-dependent errors. These errors indicated that remembered target locations were maintained within gaze-centred coordinates and required transformation before being converted into motor commands. Similarly, Henriques and Crawford (2000) demonstrated direction-dependent distortions in remembered visual space, showing that errors reflected

systematic transformations between retinal, gaze, and motor coordinates rather than random variability. These studies provided the foundation for understanding how spatial information is transformed during goal-directed action.

However, reaching behaviour is not determined exclusively by body-centred information. A large body of work has demonstrated that external landmarks can influence reaching accuracy, particularly when targets must be remembered over a delay. Landmark-based reaching studies showed that shifting surrounding objects during the memory period produces systematic endpoint biases toward the altered landmark configuration, indicating that environmental information contributes to the remembered location of targets (Diedrichsen et al., 2004; Krigolson & Heath, 2004). Importantly, these allocentric effects are typically reflected in endpoint accuracy rather than changes in movement initiation or movement time, suggesting that landmarks primarily stabilize spatial memory rather than alter the motor execution process.

Byrne and Crawford (2010) further demonstrated that allocentric information can be used implicitly during memory-guided reaching. Participants reached toward remembered targets while the reliability and stability of surrounding landmarks were manipulated. When landmarks provided a reliable spatial reference, changes in landmark position produced corresponding shifts in reach endpoints. In contrast, unstable landmarks had a reduced influence on performance. These findings demonstrated that environmental landmarks act as a stabilizing reference frame, reducing uncertainty in remembered target location and improving spatial accuracy when they provide reliable information.

More recent studies have investigated allocentric reaching in more realistic environments. Fiehler et al. (2014) used naturalistic scenes containing multiple objects and demonstrated that participants incorporated environmental structure when reaching toward remembered targets. When relevant objects were displaced, reach endpoints shifted toward the altered object locations, demonstrating that allocentric information contributes during realistic spatial behaviour. Virtual reality studies have extended these findings by allowing controlled manipulation of three-dimensional environments. Klinghammer et al. (2016) showed that participants used allocentric cues during memory-guided reaching in immersive environments, with landmark manipulations producing measurable changes in endpoint accuracy, particularly when landmarks provided depth information.

While earlier studies primarily demonstrated implicit allocentric influences, explicit allocentric tasks examined whether participants could intentionally adopt an external reference frame to improve performance. Chen et al. (2010) examined the stability of different reference frames during memory-guided reaching and found that egocentric representations showed greater decay across delays, whereas allocentric representations provided a more stable representation of target location. Musa et al. (2024) addressed this question more directly by instructing participants to encode target locations relative to either themselves or surrounding landmarks. Explicit allocentric instructions improved reaching accuracy and precision when reliable landmarks were available, as reflected by the visibly smaller reach endpoint confidence ellipses shown in Figure 1.4, demonstrating that participants can deliberately use environmental reference points to enhance spatial performance. Importantly, the benefit of allocentric

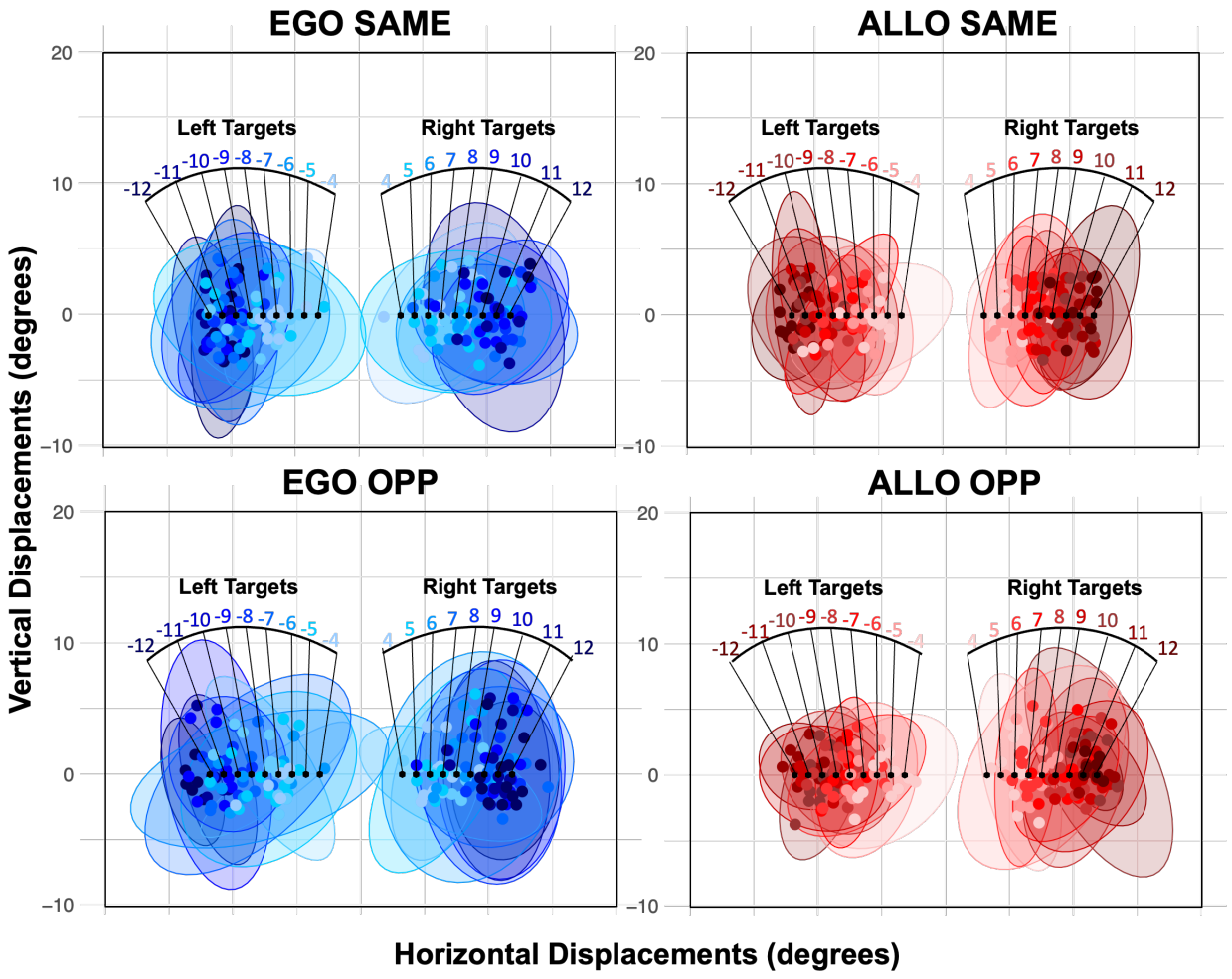


Figure 1.4 Reach Endpoints during Explicit Egocentric and Allocentric Reaching

Adapted from: Musa et al. (2024) *Instruction alters the influence of allocentric landmarks in a reach task, Figure 4.* The figure was reconstituted to display only the mean 95% confidence ellipses, representing two-dimensional reach endpoint variability, for the **SAME** (top) and **OPP** (bottom) conditions. Small filled circles indicate individual reach endpoints relative to the central fixation point. The confidence ellipses and reach endpoints are color-coded according to the initial target reference frame, with **EGO** shown in blue and **ALLO** shown in red.

encoding was greatest when landmarks provided stable and informative spatial cues, highlighting that allocentric strategies improve behaviour by reducing uncertainty in target localization rather than by changing the mechanics of movement execution.

Overall, behavioural studies demonstrate distinct contributions of egocentric and allocentric representations during reaching. Egocentric coding is characterized by gaze-dependent and body-centred errors when visual information must be transformed into motor commands, particularly during open-loop and delayed reaching. In contrast, allocentric coding improves spatial stability by anchoring remembered targets to external landmarks and reducing endpoint variability across delays and environmental changes. Thus, the behavioural signature of egocentric reaching is primarily expressed through coordinate-transformation errors, whereas allocentric reaching is reflected in improved accuracy and reduced uncertainty when reliable environmental references are available. Together, these findings demonstrate that the two reference frames support different aspects of reaching behaviour, with egocentric representations being closely tied to movement execution and allocentric representations providing a stable framework for spatial memory and planning.

1.5.2 Neuropsychology of Egocentric and Allocentric Reaching

Neuropsychological studies provide strong evidence that egocentric and allocentric representations contribute differently to reaching behaviour. Studies of patients with selective visual and visuomotor impairments demonstrate that reaching depends on specialized transformations between visual information and motor commands, requiring

both body-centred representations for action and stable spatial representations of the external environment (Goodale & Milner, 1992; Milner & Goodale, 2006).

The most influential evidence comes from patient DF, who developed visual form agnosia following bilateral occipitotemporal damage. Although DF was unable to consciously perceive object shape and orientation, she retained relatively accurate visually guided reaching and grasping. For example, she could appropriately adjust her hand orientation when grasping objects despite being unable to verbally report their orientation (Goodale et al., 1991). This dissociation suggested that reaching can rely on egocentric visuomotor representations that specify object location and orientation relative to the body, even when allocentric object perception is impaired. These findings provided key evidence for the distinction between vision-for-action and vision-for-perception.

In contrast, patients with optic ataxia demonstrate impaired reaching despite preserved visual perception. Following posterior parietal damage, these patients show increased endpoint errors, impaired online corrections, and difficulty directing the hand toward visual targets, particularly when reaching requires transformations between gaze, body, and hand coordinates (Perenin & Vighetto, 1988). These deficits indicate that posterior parietal cortex is critical for constructing egocentric representations required for accurate reaching. Importantly, optic ataxia reflects a disruption of visuomotor transformation rather than a general inability to represent spatial information.

Further studies demonstrated that patients with optic ataxia can often identify target locations or make perceptual judgments accurately while failing to reach toward the

same targets, suggesting that allocentric spatial representations may remain intact while egocentric action representations are disrupted (Pisella et al., 2000). Schenk (2006) showed that optic ataxic patients could use allocentric information about object relationships but were impaired when actions required encoding target location relative to the body. This finding demonstrated that allocentric representations can support spatial perception while egocentric transformations are specifically required for visually guided reaching. Schenk and McIntosh (2010) further argued that reaching deficits reflect damage to action-specific spatial processing rather than a general spatial impairment.

Although allocentric deficits are less commonly observed than egocentric impairments, neuropsychological evidence suggests that environmental representations contribute to reaching when actions depend on memory or contextual information. Patients with posterior cortical or medial temporal damage can show difficulties using spatial relationships between objects and landmarks, complementing behavioural studies showing that landmarks improve reaching accuracy during delayed conditions. Thus, neuropsychological evidence indicates that egocentric representations are essential for immediate movement control, whereas allocentric representations provide a stable framework for spatial memory and context-dependent reaching.

Together, patient studies demonstrate distinct behavioural consequences of egocentric and allocentric representations during reaching. Egocentric impairments primarily disrupt movement accuracy and online control, producing deficits such as optic ataxia,

whereas allocentric impairments affect the ability to use environmental structure to maintain spatial information.

1.5.3 Neurophysiology of Egocentric and Allocentric Reaching

Behavioural and neuropsychological studies demonstrate that egocentric and allocentric representations contribute differently to reaching behaviour. Neurophysiological studies in non-human primates have provided further evidence that these reference frames are supported by distinct neural computations within cortical networks. Recordings from parietal and frontal regions demonstrate that egocentric reaching depends on transformations between visual information and motor commands, whereas allocentric representations involve coding spatial relationships relative to external landmarks.

Egocentric reaching has been extensively studied within the parietofrontal reach network, including the posterior parietal cortex, parietal reach region, medial intraparietal area, dorsal premotor cortex, and primary motor cortex. Early recordings demonstrated that neurons in PPC become active before movement initiation and encode intended reach goals rather than simply responding to visual targets (Snyder et al., 1997). Batista et al. (1999) further showed that PPC neurons represent reach targets primarily in eye-centred coordinates, providing a mechanism for transforming retinal information into motor plans. These representations are not rigid, however, as neuronal activity is influenced by eye position, limb position, and other contextual variables, allowing flexible transformations between spatial reference frames (Andersen & Buneo, 2002; Chang & Snyder, 2010).

Further studies have shown that egocentric representations are distributed across multiple stages of the motor system. Neurons in parietal and premotor regions encode reach goals using different coordinate systems, including eye-, hand-, and world-centred representations, suggesting that reaching depends on progressive transformations across the dorsal visuomotor pathway (Gail et al., 2009). As information moves through parietofrontal circuits, spatial representations become increasingly linked to movement planning and execution, allowing visual targets to be converted into appropriate motor commands.

Compared with egocentric reaching, the neural basis of allocentric reaching has been investigated more recently. Electrophysiological studies have demonstrated that frontal regions involved in spatial behaviour can incorporate information from external landmarks. Neurons in the frontal eye fields (FEF) have been shown to encode both eye-centred and landmark-centred spatial information during memory-guided tasks. When landmark position was manipulated, neuronal activity reflected changes in external spatial relationships, indicating that FEF contributes to maintaining spatial representations beyond a purely gaze-centred reference frame (Bharmauria et al., 2020). These findings demonstrate that frontal circuits involved in goal-directed behaviour can integrate environmental information when body-centred information alone is insufficient.

Additional work has shown that allocentric and egocentric signals emerge at different stages of neural processing. Landmark-based information becomes increasingly represented during delay periods, suggesting that external spatial cues contribute to

maintaining stable target representations over time. This landmark-related activity provides a neural mechanism through which environmental structure can influence future actions and guide behaviour when immediate visual information is unavailable (Bharmauria et al., 2020; Bharmauria et al., 2023).

Overall, primate neurophysiology supports the existence of distinct neural systems underlying egocentric and allocentric reaching. Egocentric representations are primarily associated with parietofrontal circuits that transform target location into body-centred motor commands required for accurate reaching. In contrast, allocentric representations involve additional cortical networks that encode relationships between objects and environmental landmarks.

1.5.4 Neuroimaging of Egocentric and Allocentric Reaching

Following evidence from primate neurophysiology, human neuroimaging studies provide a complementary whole-brain perspective on how egocentric and allocentric representations are organized during reaching. These studies have demonstrated that egocentric and allocentric reaching rely on partially distinct cortical systems, with egocentric representations preferentially engaging parietofrontal motor networks and allocentric representations involving visual and temporal regions associated with spatial memory and landmark-based coding (Chen et al., 2014; Chen & Crawford, 2020).

Early neuroimaging studies of egocentric reaching consistently identified the superior parietal lobule, intraparietal sulcus, dorsal premotor cortex, and supplementary motor areas as key regions involved in representing reach goals relative to the body.

Functional MRI studies demonstrated that these regions become active during delayed reaching tasks, where participants must maintain a target location and prepare a movement after a delay. Activity within these parietofrontal networks reflects the transformation of visual target information into motor plans, consistent with the role of dorsal-stream regions in visuomotor control (Connolly et al., 2000; Culham et al., 2006). These findings parallel monkey electrophysiology showing that parietal and premotor regions encode intended movements and reach direction.

A major advance came from studies directly comparing egocentric and allocentric representations within the same participants. Chen et al. (2014) used event-related fMRI to examine remembered reach targets encoded either relative to the body (egocentric) or relative to an external landmark (allocentric). During the memory period, both conditions recruited overlapping cortical regions; however, egocentric reaching produced stronger activation in parietofrontal areas associated with motor planning, whereas allocentric reaching produced greater activity in visual regions. Directional selectivity for egocentric targets was observed in occipital and parietal areas, whereas allocentric target coding was more strongly associated with inferior temporal and occipital regions. These findings, also shown in Figure 1.5, demonstrated that remembered reach targets are represented differently depending on whether spatial information is encoded relative to the body or the surrounding environment (Chen et al., 2014).

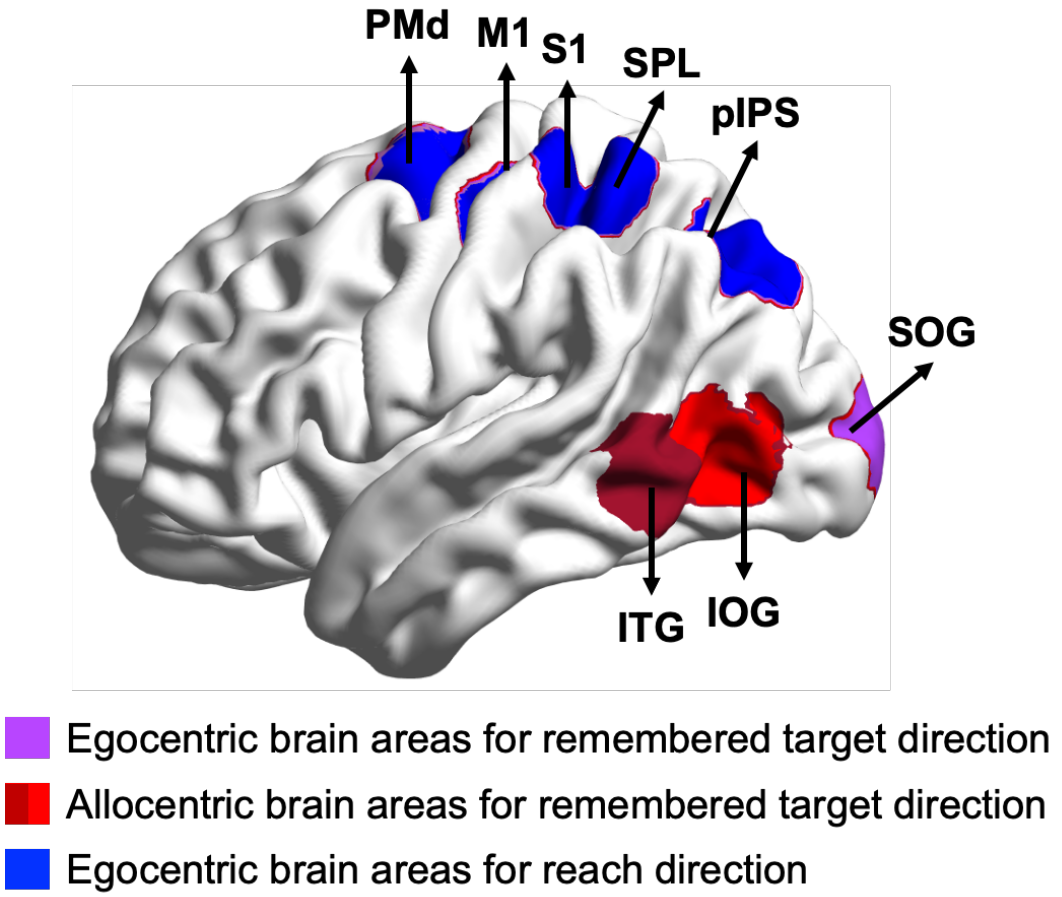


Figure 1.5 Mechanisms for Egocentric and Allocentric Reach

Adapted from: Chen and Crawford (2020), *Allocentric representations for target memory and reaching in human cortex, Figure 3.* Regions of interest (ROIs; 12 mm radius for visualization) were defined by matching the anatomical locations reported in the original study (Chen et al., 2014) to the closest corresponding regions in the Harvard–Oxford Cortical Structural Atlas (2 mm maximum-probability atlas, thresholded at 25%). The ROIs comprised the inferior temporal gyrus (ITG) and inferior occipital gyrus (IOG), associated with allocentric target localization; the superior occipital gyrus (SOG), associated with egocentric target localization; and the dorsal premotor cortex (PMd), supplementary motor area (SMA), primary somatosensory cortex (S1), primary motor cortex (M1), superior parietal lobule (SPL), and posterior intraparietal sulcus (pIPS), which are involved in reach planning and direction. Distinct colors were assigned to each ROI to facilitate visualization of the cortical network.

The neural mechanisms underlying the transition between allocentric memory and egocentric action planning have been further examined using whole-brain fMRI approaches. Chen et al. (2018) investigated allocentric-to-egocentric conversion during memory-guided reaching and identified a network involving the right precuneus, bilateral dorsal premotor cortex, and right presupplementary motor area. These regions were proposed to mediate the transformation of landmark-based target representations into body-centred motor plans required for reaching. The findings suggest that allocentric and egocentric representations are maintained by different cortical systems but can be transformed through interactions between posterior visual regions and parietofrontal motor areas (Chen et al., 2018).

Additional neuroimaging evidence has shown that egocentric and allocentric representations are not completely independent but interact during spatial behaviour. Neggers et al. (2006) demonstrated that visual context and external reference frames influence spatial representations in human cortex, showing that allocentric information can bias spatial judgments while having different effects on pointing behaviour. Their findings supported the idea that parietal regions are more strongly associated with body-centred visuomotor processing, whereas temporal regions contribute to object- and landmark-centred spatial representations. This distinction parallels the broader organization of dorsal and ventral visual pathways, with dorsal regions supporting action and ventral regions contributing to perceptual and spatial memory processes.

The broader framework proposed by Chen and Crawford (2020) integrates these neuroimaging findings by suggesting that allocentric and egocentric representations are

initially maintained in partially separate cortical systems. Allocentric representations provide a stable representation of remembered target locations relative to landmarks, whereas egocentric representations support the preparation and execution of reaching movements. During action, these representations interact through parietofrontal networks that transform environmental information into motor commands. Thus, neuroimaging evidence supports a dual-stream organization of reaching behaviour, where different cortical systems specialize in environmental spatial memory and body-centred motor control.

1.5.5 Establishing Causality with Transcranial Magnetic Stimulation

Neuroimaging provides a powerful tool for characterizing the organization of cortical networks supporting spatial cognition and reaching behaviour. However, measures of brain activity are inherently correlational. The observation that a cortical region is active during a task does not establish that the region is necessary for successful performance. Demonstrating a causal contribution requires experimentally disrupting neural processing within candidate regions and examining the resulting behavioural consequences.

Transcranial magnetic stimulation (TMS) provides a non-invasive and reversible approach for establishing causal brain–behaviour relationships in humans (Pascual-Leone et al., 2000; Hallett, 2007). By delivering a magnetic pulse through a coil positioned over the scalp, TMS induces transient electrical currents within underlying cortical tissue, altering local neuronal excitability. The behavioural effects of stimulation depend on stimulation parameters, including intensity, frequency, and timing relative to

task events, allowing researchers to examine the contribution of specific cortical regions to distinct stages of behaviour (Walsh & Cowey, 2000; Silvanto & Pascual-Leone, 2008). When combined with structural MRI and neuronavigation, TMS can target cortical regions with high anatomical precision, providing a method for testing whether areas identified through neuroimaging are functionally necessary (Sack et al., 2009).

The majority of TMS studies examining reaching have focused on egocentric visuomotor transformations within the dorsal stream. Early studies targeting the posterior parietal cortex demonstrated that disrupting parietal activity impairs the transformation of visual information into motor commands. Stimulation of the intraparietal sulcus and superior parietal lobule has been shown to increase reaching errors, disrupt spatial updating following changes in gaze position, and interfere with the online control of visually guided movements (Desmurget et al., 1999; Vesia et al., 2010). These effects are consistent with the role of PPC in representing target locations relative to the body and updating these representations during movement.

Work from Vesia and colleagues further demonstrated that PPC contributions to reaching are reference-frame dependent. Disruption of the human PPC using repetitive TMS impaired memory-guided reaching, particularly when participants were required to transform visual target information across different coordinate systems (Vesia et al., 2010). Additional studies from the same research program showed that stimulating parietal regions involved in visuomotor integration can selectively disrupt reaching and pointing accuracy without producing generalized motor impairments, indicating that these regions contribute specifically to spatial transformations required for action (Vesia

et al., 2006; Vesia et al., 2010). These findings provide causal support for the involvement of PPC in egocentric reaching and complement neurophysiological evidence from primates demonstrating reference-frame coding within parietofrontal circuits.

TMS studies have also begun to investigate the causal contribution of occipitotemporal regions involved in allocentric spatial processing. Because allocentric reaching depends on representing targets relative to external landmarks, rather than the body, candidate regions include higher-order visual areas involved in object and scene representation. Studies targeting the lateral occipital complex (LOC) and occipitotemporal cortex have demonstrated that disrupting these regions can impair object-based spatial processing and landmark-related judgments, suggesting a causal role for ventral-stream regions in allocentric representations (Ellison & Cowey, 2009). However, compared with egocentric reaching, direct TMS evidence for allocentric reaching remains relatively limited.

Together, TMS studies provide causal evidence that egocentric and allocentric reaching depend on partially distinct cortical systems. Egocentric reaching relies strongly on dorsal-stream parietofrontal regions that transform visual information into body-centred motor commands, whereas allocentric reaching depends more heavily on occipitotemporal and posterior cortical regions involved in representing relationships between objects and environmental landmarks. However, causal investigations of allocentric reaching remain substantially less developed than those examining egocentric visuomotor control. The second study of this dissertation addressed this gap

by applying MRI-guided TMS to the superior and inferior extrastriate hub regions identified through graph theory analysis of fMRI data in Study 1. Details of this analysis are described in the next section.

1.6 Network Neuroscience and Graph Theory

Traditional neuroimaging approaches to spatial cognition have focused primarily on identifying localised changes in the blood-oxygen-level-dependent (BOLD) signal associated with specific task conditions (Friston et al., 1994; Culham & Kanwisher, 2001; Finn et al., 2023; Zeidman et al., 2025). Although mass-univariate activation analyses have yielded fundamental discoveries regarding the regional specialisation of cortical systems, they provide inherently limited insight into how communication between regions supports cognition and behaviour. Cognitive functions emerge from coordinated interactions among distributed neural systems, not from the activity of isolated cortical areas, making it essential to examine patterns of functional connectivity in addition to regional activation profiles (Bressler & Menon, 2010; Park & Friston, 2013; Finn et al., 2023; Huang et al., 2024; Zeidman et al., 2025).

Network neuroscience provides a principled mathematical framework for characterising the large-scale organisation of the brain (Bullmore & Sporns, 2009; Rubinov & Sporns, 2010). In graph theoretic analyses, the brain is modelled as a network composed of nodes—corresponding to anatomical or functional regions of interest or parcels—and edges—corresponding to statistical relationships between the time-series activity of those regions (Sporns, 2011). This approach enables researchers to quantify organisational properties of the brain's functional architecture that are entirely invisible to standard activation analyses, including network-level features such as modularity,

path length, and the centrality of individual regions within information flow hierarchies (Bullmore & Sporns, 2009; Rubinov & Sporns, 2010).

Figure 1.6 illustrates the general principles of network analysis used to characterize the organization of brain connectivity. Rather than considering brain regions as isolated functional units, network approaches represent the brain as a graph composed of nodes and edges, where nodes represent individual brain regions or recording sites and edges represent the strength of communication between these regions. First, the brain is divided into predefined regions of interest (ROIs) or recording locations, which serve as the fundamental units of analysis. For each node, time-series data are collected, representing changes in neural activity over time. Association between nodes is then calculated to determine their relationships. In functional connectivity analyses, this is typically measured using statistical associations such as temporal correlations between regional time series. These relationships form the edges of the network. The resulting network can then be visualized as a graph, where the organization of connections reveals important properties of brain architecture (Figure 1.6).

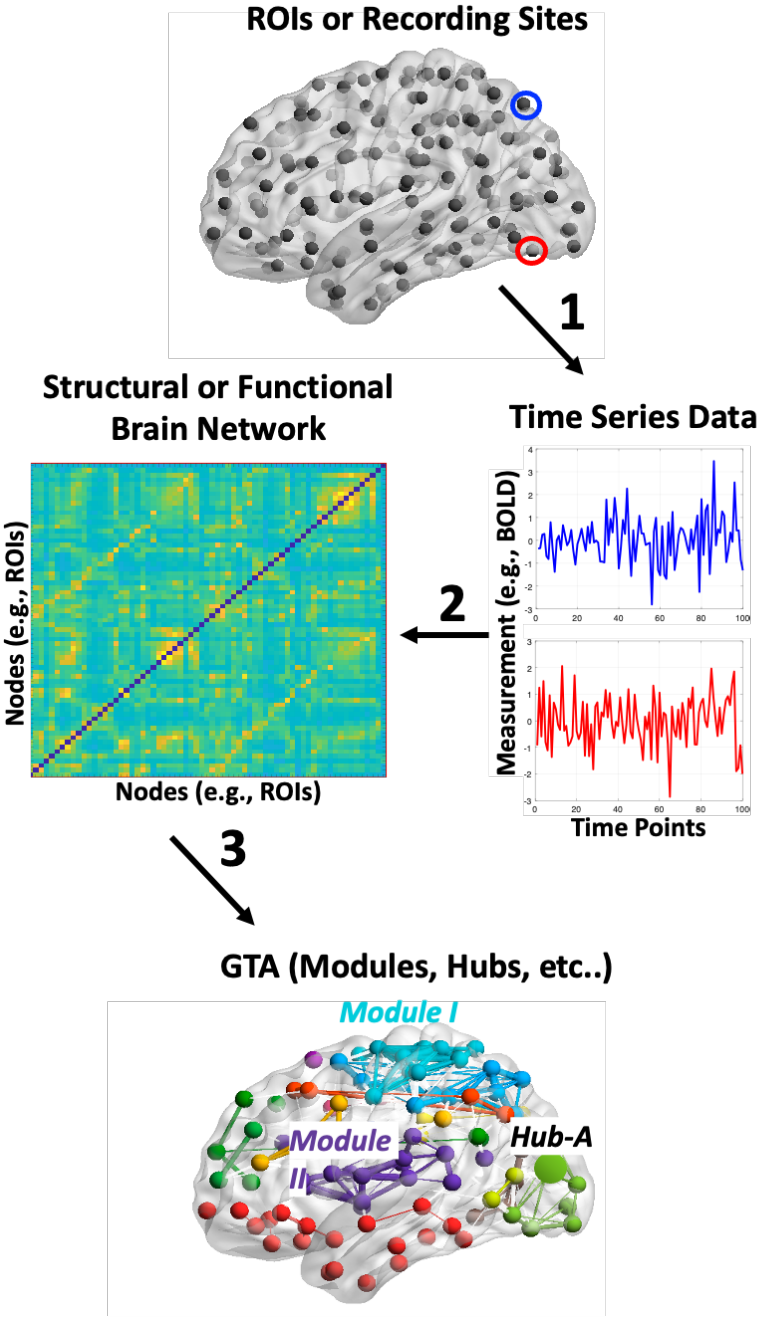


Figure 1.6 Schematic of Graph Theoretical Analysis

1- The brain is parcellated into regions of interest (nodes), or recording sites are selected for analysis. **2-** Timeseries data is obtained for each node. **3-** Structural or functional connectivity (e.g., correlation) between pairs of regions is determined (edges). (B) Resulting graph depicting modular organisation: nodes cluster into communities (modules; represented by different colors), that can correspond to known functional systems. A hub node (large circle) can exhibit high within- and/or between-module connectivity, positioning them to facilitate information flow.

Graph theory metrics can be evaluated at multiple spatial scales of network organisation (Rubinov & Sporns, 2010). At the global scale, measures such as global efficiency and the clustering coefficient characterise the overall balance between network integration—enabling fast communication across the whole network, and segregation—enabling specialised local processing within distinct subnetworks (Latora & Marchiori, 2001; Watts & Strogatz, 1998). At the mesoscale, modularity analysis identifies clusters of nodes that form cohesive communities with dense internal connectivity and sparse between-community connections (Newman, 2006; Sporns & Betzel, 2016). At the local scale, nodal centrality measures such as betweenness centrality, eigenvector centrality, and participation coefficient identify hub nodes that occupy strategically important positions in network topology and disproportionately influence information flow (van den Heuvel & Sporns, 2013).

Although functional connectivity studies have demonstrated that reaching depends on coordinated interactions between posterior parietal, premotor, and motor regions (Grol et al., 2007; Tunik et al., 2007), most have focused on general visuomotor transformations rather than the distinct spatial reference frames that support action. Similarly, graph-theoretical studies have shown that motor behaviour depends on dynamic changes in network segregation and integration (Bassett et al., 2011), but whether egocentric and allocentric reaching rely on different patterns of network organization remains unclear. Neuroimaging studies have identified partially distinct cortical systems supporting these representations (Chen et al., 2014; Chen & Crawford, 2020), yet the network-level mechanisms that allow these systems to interact during

goal-directed reaching remain largely unexplored. This was the goal of Study 1 of this dissertation.

1.7 Objectives and Hypotheses

The overarching objective of this dissertation is to advance understanding of how egocentric and allocentric spatial information is represented, integrated, and transformed into goal-directed action. Specifically, the dissertation employs a convergent multimodal approach combining functional neuroimaging, graph theory network analysis, and causal brain stimulation to investigate both the organisational principles and the functional significance of cortical systems supporting memory-guided reaching in healthy human participants.

Study 1 examined the network-level organisation of egocentric and allocentric reaching using graph theory analysis of event-related fMRI data. It was hypothesised that allocentric behaviour would be associated with increased functional communication between dorsal parietal and ventral temporal stream modules, reflecting the need for cross-stream integration of landmark information. Additionally, it was predicted that allocentric reaching would recruit task-specific hub nodes within extrastriate and occipitotemporal cortex not engaged during egocentric performance, and that these hubs would be distinguished by high cross-module participation coefficients.

Study 2 examined the causal necessity of these network hubs using MRI-guided TMS delivered to hub sites identified in Study 1. Based on the network analysis results, it was predicted that TMS targeting the superior extrastriate hub would impair reaching accuracy under both egocentric and allocentric conditions, reflecting its role as a

general visual-spatial processing node active across task conditions. It was further predicted that TMS to the inferior extrastriate hub would selectively impair allocentric reaching relative to egocentric performance, consistent with its task-specific emergence as a hub during allocentric conditions. This network-guided targeting strategy represents a methodological advance over traditional anatomically defined approaches to TMS site selection. Rather than targeting regions based solely on their gross anatomical location or prior activation in unrelated tasks, stimulation sites were selected on the basis of their quantified functional importance, as indexed by hub centrality measures, within the network supporting the specific behaviour of interest. This approach generates stronger and more hypothesis-driven predictions: regions that serve as critical, task-relevant hubs should produce greater behavioural impairments when perturbed, with the magnitude of these deficits depending on the specific task.

Together, the two studies provide complementary and mutually constraining evidence regarding the organisation and causal functional significance of cortical networks supporting spatial behaviour. By integrating the descriptive power of network neuroscience with the inferential strength of causal brain perturbation, this dissertation advances theoretical understanding of how distributed cortical systems are coordinated to support goal-directed reaching in environments that contain both egocentric and allocentric spatial information.

2 CHAPTER TWO

2.1 Spatial Task Instructions and Global Activation Trends Influence Functional Modularity in the Cortical Reach Network

Musa, L.[1-3], Ghaderi, A. [2,6], Chen, Y.[2,4], and Crawford, J.D[1-5]

Affiliations: [1]Centre for Integrative and Applied Neuroscience (CIAN) and [2]Centre for Vision Research, York University, Toronto, Canada; Departments of [3]Psychology, [4]Kinesiology & Health Sciences and [5]Biology, York University, Toronto, ON, Canada

[6]Centre for Affective Neuroscience, Development, Learning and Education (CANDLE), University of Southern California (USC), Los Angeles, USA

Publication status:

Published in NeuroImage, Volume 320, Article 121460 (15 October 2025).

Special Issue: Neuroscience of Action.

DOI: 10.1016/j.neuroimage.2025.121460.

Ethics Approval:

Investigating cortical mechanisms underlying visuomotor control using functional Magnetic Resonance Imaging (fMRI) in humans [EthicsProtocol #3730]

Certificate #: e2023-336

2.2 Abstract

Humans can be instructed to ignore visual cues or use them as landmarks for aiming movements (Musa et al. 2024), but it is not known how such allocentric cues interact with egocentric target codes and general planning activity to influence cortical network properties. To answer these questions, we applied graph theory analysis (GTA) to a previously described fMRI dataset (Chen et al. 2014). Participants were instructed to reach toward targets defined in egocentric or landmark-centered (allocentric) coordinates. During *Egocentric* pointing, cortical nodes clustered into four bilateral modules with correlated BOLD signals: a superior occipital-parietal / somatomotor module, an inferior parietal / lateral frontal module, a superior temporal / inferior frontal module, and an inferior occipital-temporal / prefrontal module. The *Allocentric* task showed only three modules, in part because inferior occipital nodes were incorporated into the superior occipital-parietal / somatomotor module. Both tasks engaged local (within module) and global (between module) cortical hubs, but the *Allocentric* task recruited additional hubs associated with allocentric visual codes and ego-allocentric integration. Removing reach-related activation trends reduced global synchrony and increased clustering, specifically diminishing dorsoventral coupling in the allocentric task. Cross-validated decoding and network parameter – reach error correlations confirmed that modularity was the best predictor of both task and specific behavioural measures. These results demonstrate that activation trends related to motor plans influence global network integration, whereas task instructions influence intermediate / local network properties, specifically the increased modular integration and hub recruitment observed in our *Allocentric* task.

Keywords

1. Allocentric cues
2. Cortical reach network
3. Graph theory analysis (GTA)
4. Modularity and Integration

2.3 Introduction

The neural mechanisms that process spatial information are central to our ability to interact with the environment. Typically, this involves an *egocentric* transformation of spatial information defined in a sensory frame of reference, e.g., visual photoreceptors fixed relative to the eye, into motor commands defined in another frame of reference, e.g., for arm motion relative to the shoulder (Andersen & Buneo, 2002; Crawford et al., 2011; Soechting & Flanders, 1992). However, our external environment also provides a rich set of cues to object location in world-fixed, i.e., *allocentric* frames of reference. For example, humans can also be instructed to reach toward locations defined relative to another visual landmark (Byrne & Crawford, 2010, Byrne et al., 2010; Lemay et al., 2004; Musa et al., 2024). It is thought that the visual system processes egocentric versus allocentric information through different cortical 'streams' (Milner & Goodale, 2006), but it is not known how task specific task instructions interacts with these signals and motor planning signals to influence segregation and integration of this information at whole-brain, intermediate, and local levels. The present study investigated this question by identifying whole brain network parameters, modules, hubs derived from neuroimaging data collected during egocentric versus landmark-centered pointing tasks.

Neuropsychological studies suggest that the dorsal visual stream, running from occipital to parietal cortex, is associated with egocentric coding of vision-for-action, whereas the ventral stream is associated with allocentric coding and perception (Goodale & Milner 1992; Milner & Goodale, 2006; Schenk & McIntosh, 2010). This distinction was supported by subsequent neuroimaging studies (e.g. Committeri et al. 2004; Galati,

2000; Zaehle et al., 2007), although the ventral stream is engaged when a memory delay precedes action (Budisavljevic, 2018; Goodale et al., 2005; Vesia & Crawford, 2012; Khan et al., 2013).

In a more recent neuroimaging study, Chen et al. (2014) presented participants with both reach targets and visual landmarks and either instructed them to ignore the landmark (*Egocentric* task) or remember target location relative to the landmark (*Allocentric* task). They then shifted the landmark during a memory interval, to dissociate egocentric and allocentric coordinates. Their imaging results suggest that the task instruction reproduced a dorsoventral dissociation for egocentric / allocentric coding during the memory interval. Further, directional selectivity for target location was evident in both egocentric and allocentric frames, with areas like the inferior occipital gyrus (IOG) and superior occipital gyrus (SOG) showing preferential activity for egocentric direction coding, while the inferior temporal gyrus (ITG) was more selective for allocentric coding, requiring an interaction between target and landmark information in the ventral stream.

Other studies have emphasized the need to integrate information across these streams for real-world behaviour (Prime et al., 2007; Freud et al., 2018, Baltaretu, et al., 2020). For example, various behavioural studies have shown that allocentric cues influence reach, even when participants are instructed to ignore visual landmarks (Byrne & Crawford, 2010; Fiehler et al., 2014). Based on the two visual streams hypothesis, this would ultimately require the incorporation of ventral stream allocentric target information into the dorsal stream processes associated with action planning (Chen et al., 2014).

For example, precuneus, supplementary motor, and dorsal premotor cortex were selectively activated when participants are cued to reach toward a target location that was stored and remembered relative to a landmark (Chen et al., 2018). Consistent with this, neurophysiological studies have shown that prefrontal visual, memory, and motor signals integrates egocentric and allocentric signals for action (Bharmauria et al. 2020, 2021; Schutz et al., 2023). Overall, these results support the classic dorsal/ventral distinction for ego/allocentric coding during memory-guided reach but suggest that multiple cortical areas may be involved in integrating this information for action.

Finally, when participants are instructed to perform landmark-centred reach, the parietofrontal networks for egocentric action planning and execution are recruited, along with a progressive rise in BOLD activation across large swaths of cortex (Chen et al. 2014, 2018). The latter phenomenon has been observed in various sensorimotor imaging studies (Medendorp et al., 2003, Cappadocia et al. 2017) and might be attributed to recurrent feedback from the motor system (Gallivan & Culham, 2015; Blohm et al., 2019; Monaco et al. 2024). However, the possible functional role of this widespread, progressive BOLD activation for signal integration has not been considered, to our knowledge.

These findings suggest that understanding the interaction between egocentric and allocentric codes requires an integrated, whole-brain approach, based not just on regions of interest, but also on how information is propagated across these areas. Recent advances in network science, for example through the application of graph theory analysis (GTA), provide a valuable framework for modeling the complex neural

interactions of signals within and between different brain regions (Sporns, 2011). Specifically, GTA provides a means of formalizing large-scale patterns of 'functional connectivity' (i.e., correlations between time series data derived from local 'nodes') at the whole-brain level. This technique is employed most often in conjunction with resting-state neuroimaging data (Braun et al., 2012) but can also be used to derive task-related networks from event-related data (Ghaderi et al., 2023; Tomou et al., 2025).

This approach provides an objective means to quantify network parameters at the whole brain level (i.e., global parameters), intermediate levels (i.e., modular clusters of nodes with similar signals), and local levels (i.e., Hubs: nodes that correlate strongly with other important nodes). For example, if the dorsal-ventral theory of ego / allocentric coding for vision is correct (Goodale & Milner 1992; Milner & Goodale, 2006; Schenk & McIntosh, 2010), one would expect a modular separation to emerge between superior occipital-parietal-frontal cortex and occipital-temporal cortex. Further, this approach allows one to evaluate if functionally-defined regions of interest (e.g. Chen et al. 2014; Committeri et al. 2004; Galati, 2000; Vesia & Crawford 2012; Zaehle et al., 2007) correspond to network hubs, how these ROIs communicate (or at least share information with) other nodes in the network, and their potential functional contributions to the network.

The current study investigated the influence of an allocentric (vs. egocentric) instruction on the cortical reach network by applying graph theory analysis to the dataset collected by Chen et al. (2014). Specifically, we aimed to contrast the cortical networks for egocentric vs. allocentric memory-guided reach, based on global network parameters for segregation and integration of information, objectively identified modules, and

important hubs for sharing local and global task information. Based on previous findings by Chen et al. (2014, 2018) and others, we hypothesized that 1) removing overall whole-brain trends related to sensorimotor planning and execution would affect global and intermediate network properties, whereas 2) task instruction would influence intermediate and local levels, i.e., increased communication between dorsal and ventral visual network modules, and recruitment of network hubs associated with specific task requirements. Finally, we evaluated the capacity of these networks to predict behaviour by decoding reach task (egocentric vs. allocentric) from global and intermediate network parameters, and by examining modularity - error correlations within and across participants.

2.4 Methods

2.4.1 Data Source

This study involved a secondary analysis of data that were previously published in a univariate 'region of interest' study (Chen et al. 2014). The dataset consisted of neuroimaging data of twelve right-handed participants (8 females, 4 males; aged 23–40 years). All participants had normal or corrected-to-normal vision and were free of any known neuromuscular impairments. All procedures involving human participants were performed in accordance with the relevant laws, institutional guidelines, and the Declaration of Helsinki. Ethical approval for the use of data in this study, including secondary analyses, was obtained from the Human Participants Review Sub-Committee at York University (Certificate #: e2023-336; Ethics Protocol #3730). Renewal of approval was granted on November 9, 2023.

2.4.2 Experimental Stimuli and Apparatus

Complete details of the experiment are provided in Chen et al. 2014; here we repeat the main points necessary to understand the task and analysis. The experiment was conducted at York University's neuroimaging center using a 3-T Siemens Magnetom TIM Trio MRI system. A 12-channel head coil (6 channels posterior, 4-channel flex coil anterior) was used for data acquisition. Experiments were performed in near-complete darkness (participants reported that they could not see the workspace or hand) to minimize extraneous visual cues. Visual stimuli consisted of 3 mm LED lights controlled by fiber optic cables embedded in a custom board mounted above the participant's abdomen. The platform was adjustable for optimal comfort, visibility and reach accessibility, and affixed to the MRI bed. A touch screen (Keytec) recorded reaching endpoints, while gaze was tracked using an iView X eye-tracking system with an MRI-compatible Avotec Silent Vision system. The head was slightly tilted (20°) to allow direct viewing of the stimuli. Participants wore headphones to receive audio instructions for the upcoming trial and before pointing.

2.4.3 Stimulus Specifications

Visual stimuli were color-coded: yellow for gaze fixation, green/red for reach targets, and blue for landmarks (Figure 2.1). Reach targets and landmarks were located to the left and right of central gaze fixation points (Figure 2.1). Target and landmark positions varied horizontally (with a range of 1-2° visual angle from target), with 40 possible configurations. A 'mask' consisting of 20 LEDs was positioned above and below the visual stimuli, vertically aligned between the target and landmark. The mask was presented to minimize

aftereffects from the target and landmark stimuli, ensuring memory encoding rather than afterimage reliance. Light intensity was set to a level that was clearly visible for the participant but did not illuminate the hand or workspace.

2.4.4 Experimental Paradigm and Timing

The experiment featured two primary tasks: *Egocentric* and *Allocentric* (Figure 2.1). A third non-spatial *control* task (not shown) was used in the original univariate analysis (Chen et al. 2014) but was not required here. Each trial began with an audio cue to indicate the task: *Egocentric*, where participants were instructed to remember where they saw the object or *Allocentric*, where participants were instructed to remember the location of the object relative to the landmark. Participants then looked at the gaze fixation point, followed by a 2-second display of the target and landmark. The fixation stimulus then shifted slightly left or right so that it could not be used as an allocentric landmark. This was followed by a 12-second memory delay, during which the mask was presented. Afterward, the landmark reappeared either at the same or a different location, and participants were cued to perform the reach toward the target (in egocentric or allocentric coordinates, as initially instructed). Since the landmark appeared in the opposite hemifield 50% of the time, tasks were equalized by providing a *Pro/Anti* instruction before *Egocentric* reaches, i.e., to reach toward or opposite (mirrored across midline) to remembered target location. A 16-second inter-trial interval was provided to allow for hemodynamic baseline recovery. Participants practiced the tasks until they did them correctly, one day before recordings.

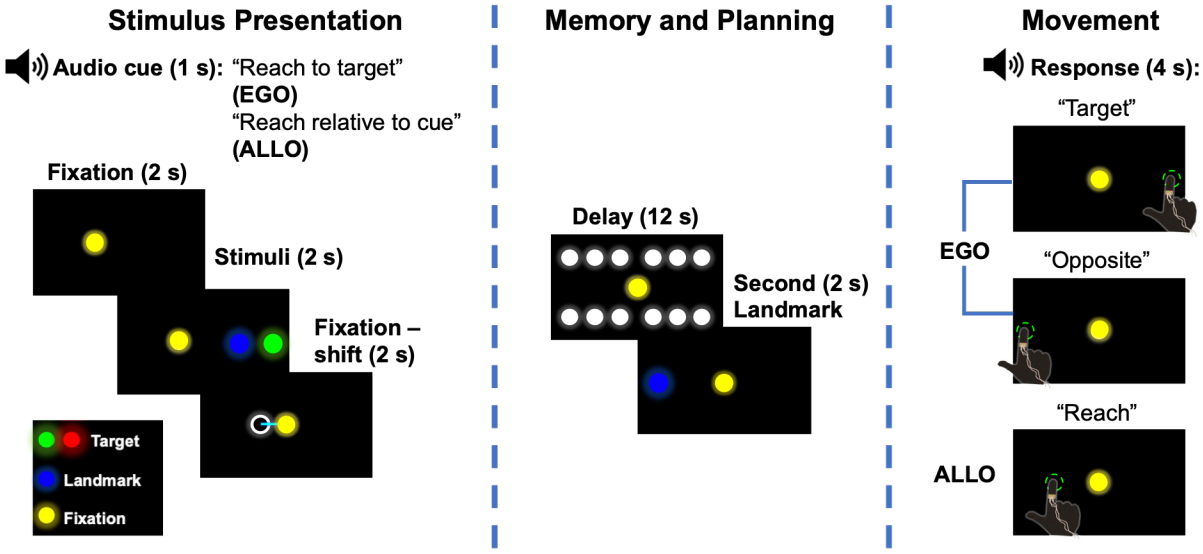


Figure 2.1 Task.

Experimental paradigm, divided into three sequential phases: stimulus presentation (6 seconds total), memory and planning (14 seconds total), and movement (4 seconds). Audio task instructions preceded stimulus presentation and differed based on the type of task, Egocentric – participants were instructed to remember the target location only, Allocentric – participants were instructed to remember the target location relative to the landmark. Black boxes represent the stimulus pad / touch screen, and the dots represent the fixation point (yellow), target (red or green), landmark (blue) and mask (white). With the exception of the initial task audio instructions, the stimuli presented during the stimulus presentation phase and the memory and movement planning phases are the same for the Egocentric and Allocentric task. However, during the movement planning phase participants also heard differing instructions to execute distinct types of movements based on the final task-relevant audio instructions, which prompted participants to perform a pro or anti point in the Egocentric task or point to the remembered position relative to the second landmark. See text for details.

The design incorporated three factors: task (*Egocentric, Allocentric*), target position relative to gaze (left or right), and target position relative to the landmark (left or right). This resulted in 12 counterbalanced conditions across six experimental runs, each consisting of 18 trials. Note that the distribution of stimuli (targets and landmarks) was essentially the same for each task, only the instruction differed.

2.4.5 Imaging Parameters

Functional data were acquired with an echo-planar imaging (EPI) sequence (TR = 2000 ms, TE = 30 ms, FA = 90°, FOV = 192 x 192 mm, matrix = 64 x 64, slice thickness = 3.5 mm, 35 slices, angled at 25°, ascending interleaved). T1-weighted anatomical images were acquired using an MPRAGE sequence (TR = 1900 ms, TE = 2.52 ms, inversion time = 900 ms, FA = 9°, FOV = 256 x 256 mm, voxel size = 1 x 1 x 1 mm^3).

2.4.6 Univariate Data Analysis

The first step in the analysis involved defining statistical contrasts following the approach of Chen et al. (2014), which were later used to relate regional activation patterns to network topology and to extract time series data isolating variability associated with the effect of interest—specifically, delay phase activity in the Egocentric and Allocentric tasks. The steps for the univariate analysis, functional connectivity analysis, statistical testing, and classification learning are outlined in **Supplementary Figure 2.1**.

2.4.6.1 Preprocessing

Data preprocessing was performed using FSL (FMRIB Software Library). The first two volumes of each run were discarded to account for saturation effects. Slice time correction, motion correction, and high-pass temporal filtering (to remove low-frequency noise) were applied. Motion correction was performed using FSL's MCFLIRT. Functional data were co-registered to the T1 anatomical scan using FLIRT (FMRIB's Linear Image Registration Tool) and then normalized to MNI space. Spatial smoothing was applied using a Gaussian kernel with a 6-mm full-width half-maximum (FWHM).

2.4.6.2 GLM Construction

For individual analysis, a General Linear Model (GLM) was constructed using FSL's FEAT (FMRIB's Expert Analysis Tool) for each participant, including task-specific predictors for different phases of the experiment (eye movement, target presentation, delay, landmark, and response phases). Six motion correction parameters were included as regressors of no interest to control for head movement. Task conditions included EGOCENTRIC and ALLOCENTRIC reaches, each with target positions defined relative to gaze or landmark.

2.4.6.3 Voxelwise Analysis

Voxelwise analysis was conducted using a group-level mixed-effects analysis with FLAME (FMRIB's Local Analysis of Mixed Effects). Group contrasts were performed using higher-level FEAT analysis in FSL. The following contrasts were tested:

1. **EGOCENTRIC vs. Baseline (Delay Phase)**: Areas coding target location during the delay phase in the **EGOCENTRIC** task.

2. **ALLOCENTRIC vs. Baseline (Delay Phase)**: Areas coding target location during the delay phase in the **ALLOCENTRIC** task.

3. **EGOCENTRIC Left vs. EGOCENTRIC Right (Delay Phase)**: Directional selectivity within the **EGOCENTRIC** task (left vs. right relative to gaze).

4. **ALLOCENTRIC Left vs. ALLOCENTRIC Right (Delay Phase)**: Directional selectivity within the **ALLOCENTRIC** task (left vs. right relative to landmark).

5. **Reach Left vs. Reach Right (Response Phase)**: Directional selectivity in the **EGOCENTRIC** and **ALLOCENTRIC** reach tasks based on the actual movement direction.

2.4.6.4 Statistical Corrections

To correct for multiple comparisons, we applied cluster-based correction using FSL's randomise tool (1000 permutations) to estimate the significance of contiguous clusters of activation. The minimum cluster size for inclusion was 11 voxels (297 mm^3). A Bonferroni correction was applied to post-hoc paired-sample t-tests to control for Type I error across multiple comparisons, with a corrected p-value threshold of 0.0167.

2.4.7 Functional Connectivity Analysis

In this section, we describe the steps taken to perform the functional connectivity analysis, following the panels depicted in Figure 2.2.

2.4.7.1 Regions of Interest and Time Series Computation

We chose 200 regions of interest (ROIs) as nodes, each defined as a 6-mm diameter spherical region based on the centroid coordinates of the Schaefer-Yeo atlas (Schaefer et al., 2018) (Figure 2.2A). Average timeseries for entire runs were then extracted at each ROI (Figure 2.2B) using the fslmeants function. For every ROI (200) and each run (6 in total) we computed a contrast-reduced time series (described below) for both **Contrast 1: EGOCENTRIC vs. Baseline (Delay Phase)** and **Contrast 2: ALLOCENTRIC vs. Baseline (Delay Phase)** outlined in **Methods section 2.6.3.** We then isolated the appropriate epoch from the relevant contrast. For each run, there were 6 egocentric task trials and 6 allocentric task trials, which were analysed independently by isolating the time series from the start of the stimulus presentation phase until the end of the delay epoch (18 s in total), from Contrast 1 reduced time series for the egocentric task trials and Contrast 2 reduced timeseries for the allocentric task trials, creating timeseries as shown in red in the example in Figure 2.2C.

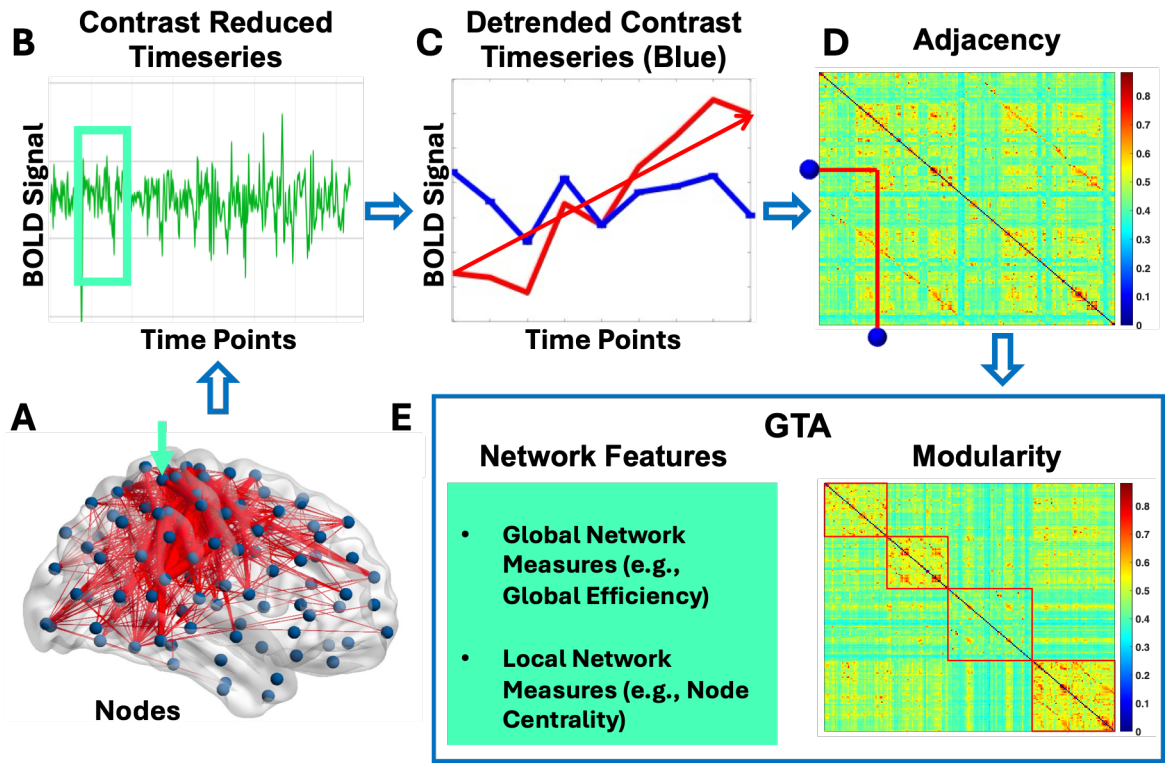


Figure 2.2. Analysis Pipeline

A, Nodes: 200 ROIs shown in blue (6mm diameter) were defined based on the centroid coordinates of the Schaefer-Yeo parcellation atlas. Red lines show example thresholded connections between them (top 5%). The cyan arrow points to the example ROI that was used for the timeseries in **B**, Contrast reduced timeseries of the example ROI an entire run: A delay predictor and GLM residuals were used to derive the contrast reduced time series. The cyan box represents a single trial (18s, 9 data points), shown in C. **C**, The time series from the beginning of each trial until the end of the delay period is shown in red. (the red arrow shows the linear trend) A detrending algorithm was used to derive the detrended time-series shown in blue. **D**, Adjacency matrices were computed for the 200 ROIs using the data with and without the trend. The example ROI indicated by the cyan arrow in A and its neighbour are shown in the x and y axis and the connection between them in the adjacency matrix is traced by the red lines. The colormap shows areas of low to high correlations (blue to red) **E**, GTA: The global, mesoscale, and local network features were derived for each participant and trial. The modularity of the same adjacency matrix shown in D is shown by resorting the nodes based on their strongest connections and defining the different modules by the red boxes.

The contrast-reduced time series, representing a cleaned version of the voxel time course for a specific task condition, was used to remove irrelevant variability associated with shared task components (e.g., stimulus color), which could otherwise inflate correlations between ROIs. This signal reflects the partial model fit for a given contrast combined with the residual error from the GLM estimation, effectively isolating the contribution of the contrast of interest (e.g. **Contrast 1: EGOCENTRIC vs. Baseline (Delay Phase)**) while preserving noise structure. A customized Matlab code was used to automatize the steps required to compute a contrast reduced timeseries are described below and in *the FSLeyes FEAT mode user documentation (2024)*.

The contrast vector C is normalized by scaling it as follows:

$$C = \frac{\sqrt{n}\ x\ C}{\sqrt{\sum_{e=1}^{p} C_e^2}}$$

Where:

- C**:** Contrast vector (before and after normalization)
- n**:** Number of non-zero elements in the contrast vector **C**
- p**:** Total number of elements in C
- C_e**:** The *e*th element of C

This ensures that partial model fits are scaled appropriately.

For each contrast vector C, the model fit F_C at each time point 't', F_C^t was computed using the following formula:

$$F_C^t = \sum_{e=1}^{p} X_e^t \ \beta_e |C_e|$$

Where:

- p: the number of explanatory variables (EVs) in the design matrix,
- X_e^t: the value in the design matrix for EV ‘e’ at time ‘t’,
- βe: the parameter estimate for EV ‘e’,
- |Ce|: the absolute value of the contrast vector element ‘Ce’.

Additionally, in the first-level analysis (i.e., fitting a model to time series data), the mean of the data is added to the model fit since FSL de-means the time series data before model fitting.

The final contrast-reduced time series, D_C was computed as the sum of the partial model fit and the residual error ϵ from the GLM estimation:

$$D_C \ = \ F_C \ + \ \epsilon$$

Where:

- F_C: Partial model fit of all time points (i.e., the predicted time course of contrast C for a run)
- ε: Residual error time series from the GLM (observed − predicted)

2.4.7.2 Detrending

As in many previous sensorimotor studies (e.g., Medendorp et al., 2003; Cappadocia et al. 2017), we noted a consistent upward linear trend in the BOLD time series for most nodes (Figure 2.2C, thin red line). To assess the role of this general trend in network dynamics, we created a comparison dataset by linear detrending using the detrend function in MATLAB. The detrend function automatically fits a first-degree polynomial (a straight line) to the data y using a least squares approach. It then subtracts the fitted line from the data, effectively removing the linear trend and leaving only the residuals. The goal was to assess what network properties were missing after detrending, and what properties remained in the remaining fluctuations around the linear trend (Figure 2.2C, blue line).

2.4.7.3 Network Analysis (Adjacency Matrix Construction)

To determine how networks functionally interact during egocentric and allocentric task conditions in the original and de-trended data, functional 'connectivity' edges (e.g., Figure 2.2A, red lines) were computed by taking the absolute values of correlations between all the nodes, computed for each participant, trial and separated into condition. Note that these edges represent the degree of temporal signal sharing between nodes, not anatomic connections. These correlations were then used to construct an 'adjacency matrix' for each participant / condition (Figure 2.2D). Each entry of this matrix represents the correlation between nodes in the corresponding rows and columns. For example, the two blue dots in Figure 2.2D illustrate the connection

between the node highlighted by the cyan arrow and its neighbour. These fully connected adjacency matrices were then used for graph theory analysis.

2.4.7.4 Graph Theory Analysis (GTA)

Using a GTA, described in this section, we aimed to uncover differences in **integration and segregation** of brain regions, offering insight into the distinct functional architectures that support each spatial reference frame and changes in functional architectures due to the linear trend. Following the construction of the adjacency matrices, we evaluated the topological and dynamical properties of the functional brain networks for both the EGOCENTRIC and ALLOCENTRIC tasks (Figure 2.2E), obtaining network measures per participant, per trial and separated into condition. Two common graph-theoretical measures were used to assess the network's topology: clustering coefficient (CC) and global efficiency (EF), as explained below (Bonacich, 1972; Latora & Marchiori, 2001; Sporns et al., 2005; Watts & Strogatz, 1998).

2.4.7.4.1 Global Network Topology

Clustering Coefficient (CC) measures the level of local processing within the network, indicating how interconnected the nodes are. Networks with a high CC reflect functional segregation, with nodes highly connected to one another. This is important because the brain typically organizes itself into segregated modules for efficient neural processing. In a weighted network, connectivity strength between three nodes (triangles) indicates the clustering coefficient.

$$C_i^{wei,O} = \frac{1}{d_i(d_i-1)} \sum_{\substack{1 \le j,l \le N \\ j,l \ne i}} \frac{\left(w_{ij} w_{il} w_{lj}\right)^{1/3}}{max w_{i,j,l}}$$

d_i: The *degree* of a given node *'i'*

w_{ij}: The weight of connection between the pair of nodes *('i'* and *'j')*

$max w_{i,j,l}$: maximum weight between neighbor nodes that make a triangle (Saramäki et al., 2007).

Global Efficiency (EF) quantifies the ability of the network to integrate information across distributed regions. Higher global efficiency indicates that the network can rapidly and effectively exchange information between distant nodes, facilitating efficient brain function. In weighted functional networks, stronger connections contribute to shorter weighted path lengths and, consequently, higher EF. This measure is the average over all pairs in the network.

$$Ef = \frac{1}{n(n-1)} \sum\nolimits_{i,j \in N} \left(L_{ij}\right)^{-1}$$

L_{ij}: Strongest connection between pair of nodes (*i* and *j)*

n: Total of number of nodes (Rubinov & Sporns, 2010)

2.4.7.4.2 Global Network Dynamics

Aside from topology, we employed graph theory analysis to investigate the dynamics of network synchronization across all pairs of brain regions (Bassett & Sporns, 2017; Breakspear, 2017; Ghaderi et al., 2020; Honey et al., 2010; Vidaurre et al., 2018). In this analysis, the following measure was used:

Energy (E), which reflects the stability of synchronization in the network. Higher energy values suggest stable coupling between nodes over time, indicating more consistent functional interactions. In a weighted network, the *E* is the summation of absolute values of eigenvalues.

$$E = \sum_{i=1}^{n} |\lambda_i|$$

λ_i: Set of network eigenvalues

n: Total of number of nodes (Ghaderi et al., 2020)

2.4.7.4.3 Mesoscale Network Topology (Modularity)

Modularity refers to a measure of the structure of a network, which quantifies the degree to which a network can be divided into relatively independent, densely connected groups or communities. A *community* in this context is a subset of nodes that are more densely connected to each other than to nodes outside the subset. We assessed modularity to understand how the brain functionally organizes into distinct subnetworks or communities during egocentric and allocentric tasks, which may support different cognitive strategies or processing demands associated with each spatial frame of reference and to determine whether the trend influences this organization. By comparing modularity in data with and without a linear trend, we aimed to reveal whether removing such trends exposes more specific network structures that reflect task-dependent functional segregation.

To evaluate condition-specific correlation patterns, we initially applied a Fisher r-to-z transformation to each individual correlation matrix. This transformation is commonly

used to stabilize the variance and normalize the distribution of Pearson correlation coefficients, particularly when averaging correlations across participants or samples. After transforming, the matrices were averaged within each condition, and the resulting means were converted back to correlation coefficients using the inverse Fisher z-to-r transformation. This procedure allows for statistically appropriate averaging of correlation values. However, upon comparison, we observed that the Fisher-transformed and non-transformed averages produced negligible differences in the resulting matrices. Given the lack of meaningful divergence, and to preserve interpretability in terms of raw correlation coefficients, we opted to retain the original, untransformed correlation matrices for subsequent analysis and visualization. We then found the community assignments using the modularity function in the Brain Connectivity Toolbox (Rubinov & Sporns, 2010), and it is mathematically based on Newman modularity algorithm (Newman, 2006), modularity Q s defined as:

$$Q = \frac{1}{2m} \sum_{ij} \left(A_{ij} - \frac{k_i k_j}{2m} \right) \delta(c_i, c_j)$$

Where:

- Aij: Adjacency matrix (with 1 if there is an edge between nodes ii and jj, and 0 otherwise),
- ki: degree of node i,
- m: total number of edges in the network,
- ci: community assignment of node i,

- δ(ci,cj): Kronecker delta function, which is 1 if nodes ii and jj are in the same community, and 0 otherwise.

In addition, the modularity function in the Brain Connectivity Toolbox (Rubinov & Sporns, 2010) accounts for the resolution parameter γ which adjusts the scale of community detection, influencing the size and granularity of the modules (communities) detected in the network.

2.4.7.4.4 Modularity and Communication Analysis

To evaluate modularity of subnetworks we implemented a self-developed function (Ghaderi et al., 2025) on the Newman modularity algorithm (Newman, 2006) in MATLAB 2022b. It is available as open access code at https://github.com/AHGhaderi/Amir-Hossein-Ghaderi/commit/df636b2105e578a8969ffa88856e54f3267a40a7.

Steps in this algorithm are (Ghaderi et al., 2025):

1) Identify a group of nodes (e.g., brain regions) to form a subnetwork.
2) Calculate the average connectivity between the selected nodes.
3) Randomly shuffle the connections between nodes in the entire network.
4) Recalculate the average connectivity between the selected nodes after randomizing the network.
5) To find the modularity score, divide the connectivity average from step 2 (original subnetwork) by the connectivity average from step 4 (randomized network).

If the modularity score in step 5 is greater than 1, it suggests that the connectivity pattern within the selected group of nodes (subnetwork) is more structured than a random connectivity pattern. This implies that the selected nodes are connected in a modular fashion, forming a modular subnetwork.

2.4.7.4.5 Local Network Topology (Node Hubness)

Eigenvector Centrality (EigC) measures the influence of a node based on its connections to other well-connected nodes (Bonacich, 2007). Nodes with high eigenvector centrality are often considered hubs (Ghaderi et. al, 2023), as they are central to the flow of information and have strong connections to other highly influential nodes. However, hubs with high Eigc lack diverse connections, giving rise to their role of within-module hubs. In a weighted network, the eigenvector corresponded to largest eigenvalue of adjacency matrix is Eig_C.

$$Ax = \lambda x, \lambda x_i = \sum_{j=1}^{n} a_{ij}\ x$$

A: Adjacency matrix

λ: The largest eigenvalue of *A*

x: Eigenvector associated with λ

n: Total of number of nodes

Betweenness centrality is a measure of centrality in a graph that quantifies the extent to which a node (or edge) acts as a "bridge" between other nodes. It is based on the idea that a node is important if it lies along the shortest paths (geodesics) between other pairs

of nodes in the network (Freeman, 1977). Nodes with high betweenness centrality fulfill the role of hubs (Sporns, 2007), since they are important for the flow of information, but function as between-module hubs due to their diverse connections. In other words, betweenness centrality captures how often a node is an intermediary or a connector in the network, influencing the flow of information, goods, or influence between different parts of the network. For a weighted graph, where edges have weights representing distances, costs, or capacities, the definition of the shortest path must take the weights into account. In this case, the betweenness centrality formula is adjusted to consider the weighted shortest paths between pairs of nodes.

$$C_B(v) = \sum_{s \neq v \neq t} \frac{\sigma_{st}(v)}{\sigma_{st}}$$

σst(v): the number of shortest weighted paths between nodes s and t that pass through node v.

σst: the total number of shortest weighted paths between nodes s and t.

Significant network hubs were then determined by comparing the eigenvector centrality and betweenness centrality values across all brain regions (200 Schaefer-Yeo ROIs) using a penalized regression binary logistic model (glmnet package, R Core Team, 2024). This analysis utilized the LASSO (Least Absolute Shrinkage and Selection Operator) regression, which is a form of penalized regression that adds a penalty (L1 penalty: encourages sparse solutions by shrinking some coefficients to zero) to the loss function. This provides both regularization (preventing overfitting) and variable selection (shrinking

some coefficients to zero). This approach compares multiple nodes at once and only leaves behind the nodes with a large difference as significant predictors.

The clustering coefficient, global efficiency, eigenvector centrality, and betweenness centrality functions in the Brain Connectivity Toolbox (Rubinov & Sporns, 2010) were used to determine those measures.

2.4.7.4.6 Null Normalization

The graph network measures, including the clustering coefficient, global efficiency, and energy were normalized using a null model generated using a self-developed Matlab code. It is available for open access at: https://github.com/AHGhaderi/Null-model.

A null model is typically used in network science to create a random version of the data, without any of the underlying structure or dependencies present in the original adjacency matrix (Váša, & Mišić, 2022). Using the Matlab function, a "null matrix" was produced for each adjacency matrix (individual trials within runs). This was done by permuting elements within the adjacency matrix in a random fashion. For each node (row), this is done by randomly shuffling elements from the lower triangular part (below the diagonal) and placing them in the upper triangular part of the matrix. The matrix is then symmetrized to maintain the structure of the original input matrix, but with randomized values. The graph network measures are then computed again from the average null matrix. The final reported values were found by dividing the value of the graph network measure in the original data by the value of the graph measure found in the average null matrix, e.g., Clustering coefficient = $CC_{raw\ matrix}$ / $CC_{null\ matrix.}$

For convenient reference, the GTA terms that are described above, and repeated in the results / discussion sections are summarized in Table 2.1.

Table 2.1 Glossary of Technical Terms Used in Graph Theory Analysis

Term	Definition	Purpose in Study	Network Scale
Adjacency Matrix	A table showing how strongly each pair of brain regions (nodes) are functionally connected.	Used to build the brain network for each condition.	General Tool
Betweenness Centrality	Measures how often a node acts as a bridge between other nodes.	Identifies *between-module hubs* that connect different communities.	Local
Clustering Coefficient (CC)	Describes how tightly a node's neighboring regions are connected to each other.	Measures local connectivity and functional segregation.	Local
Detrending	Removing steady trends (like gradual increases) from time-based brain data.	Focuses on meaningful fluctuations in brain activity.	General Tool
Edge	A connection between two nodes, showing how similar their brain activity is over time.	Absolute correlation represents functional communication between brain regions.	General Tool
Eigenvector Centrality (EigC)	Highlights nodes connected to other highly connected nodes.	Identifies *within-module hubs* central to information flow.	Local
Energy (E)	Reflects how stable and consistent the connections are over time.	Measures synchronization and network stability.	Global
Global Efficiency (EF)	Describes how easily information can travel between distant brain regions.	Indicates the brain's capacity for integration.	Global

Term	Definition	Purpose in Study	Network Scale
Hub	A highly connected or influential node.	Central to efficient communication across the brain network.	Local
Modularity	Measures how well the network divides into tightly connected communities.	Reveals brain subsystems active during different tasks.	Mesoscale
Modularity Score (Subnetwork-based)	Compares how structured a subnetwork is to a random version.	Determines whether selected brain regions form meaningful modules.	Mesoscale
Node	A brain region included in the network.	Represents a single functional unit of brain activity.	General Tool
Null Model	A randomized version of the brain network.	Helps identify meaningful patterns vs. chance.	General Tool
Null Normalization	Compares real network metrics to those from a null model.	Ensures results are not due to randomness.	General Tool

Note: For detailed quantitative definitions, see Methods section and Ghaderi et al. (2023).

2.4.8 Statistical Analysis

To explore the differences between the EGOCENTRIC and ALLOCENTRIC tasks in terms of their functional brain network properties, nonparametric permutation tests were performed across participant means. These tests compared the whole network measures—such as clustering coefficient (CC), global efficiency (EF), energy (H), and Modularity (M)—between the two tasks.

The original study obtained a medium to large, standardized effect size of d = 0.67, but only analyzed 12 participants after exclusion criteria were applied. To account for the relatively small sample size (by current standards), which did not meet distributional assumptions, permutation testing was used. We randomly shuffled task conditions between participants and recalculated the t-statistic for each permutation. This process was repeated 5000 times to ensure that the resulting distribution of t-values approximated a normal distribution, allowing us to determine statistical significance at a 0.05 level. Multiple comparisons were corrected using false discovery rate (FDR) analysis to account for the potential inflation of Type I error.

The resolution limit problem arises when the resolution parameter γ is set too high or too low, causing the modularity optimization to miss communities that are smaller or larger than what the parameter was tuned for (Blondel et al., 2008; Fortunato, 2010; Good et al., 2010; Traag et al., 2011). To account for this, the modularity and number of modules was determined at different values of γ to see which gives the most meaningful community structure (including γ=1 - 1.3). A linear multilevel regression module (lme4

package, R Core Team, 2024) was used to determine task and trend differences in the number of modules at different resolution parameters, while a quadratic multilevel model was used to determine differences in modularity at different resolution parameter.

2.4.9 Classification and Predictive Modeling

2.4.9.1 Classification of Task

We used all available trials and applied a supervised cubic Support Vector Machine (SVM) classification algorithm to identify which network features (clustering coefficient, global efficiency, energy and modularity) best distinguish between the EGOCENTRIC and ALLOCENTRIC tasks. Traditional statistical comparisons can reveal group-level differences but may overlook complex multivariate patterns. By using a supervised cubic Support Vector Machine classifier, we evaluated the discriminative power of these features at the level of individual trials, capturing variability at a finer scale. In addition, this approach not only identifies which features most effectively separate the tasks but also strengthens external validity by using cross-validation to assess how well these network patterns generalize to unseen data. A cubic SVM is an extension of the SVM algorithm, where the kernel function used is the cubic kernel. This is a non-linear classification method where the decision boundary between classes is learned by transforming the input data into a higher-dimensional space, making it easier to find a linear separation in that space. In general, an SVM aims to find the best hyperplane that separates data points of different classes with the maximum margin. When the data are not linearly separable in the original feature space, we can use a kernel approach to map the data to a higher-dimensional feature space where a linear separator may exist.

To prevent overfitting, fivefold cross-validation was used during the training phase, which is a widely recognized and effective method in machine learning. This approach enhances the reliability of the results by dividing the dataset into five distinct subsets, or "folds." In each iteration, the model is trained on four of these subsets and tested on the remaining one. This process is repeated five times, with each fold serving as the test set once. By systematically using different portions of the data for training and testing, this technique minimizes the risk of overfitting and provides a more comprehensive assessment of the model's generalizability across diverse data.

We tested the ability of different classification models to classify the EGOCENTRIC and ALLOCENTRIC conditions accurately using the Classification Toolbox in MATLAB. The MATLAB Classification Toolbox provides a variety of models for classification tasks, each suitable for different types of data and tasks, ranging from simple linear models (Logistic Regression, LDA) to complex non-linear models (SVM, Neural Networks, Random Forests). Depending on the nature of the data (e.g., linear vs. non-linear, large vs. small datasets), the best classification model is selected. The overall performance of the best model was assessed using the receiver operating characteristic (ROC) curves, which helps evaluate the model's ability to distinguish between positive and negative cases across various thresholds by calculating the Area Under the Curve (AUC). A higher AUC indicates that the model is better at making accurate predictions, with a larger separation between the positive and negative classes, which generally reflects better overall performance. We reported the model’s overall accuracy and presented confusion matrices, including positive predictive values (PPV) and false

discovery rates (FDR), to provide deeper insights into the model's classification outcomes and reliability. The most important feature was determined using the Kruskal-Wallis importance score, which quantifies the relative contribution of each feature in explaining the variance between different groups. All classification analyses were performed in MATLAB (R2022b).

2.4.9.2 Predicting Behaviour from Network Parameters

To model the relationship between the network and behavioural performance, we employed a multiple linear regression framework to predict constant and variable reach errors from our various network parameters using two separate models. The constant reach error was determined by averaging the absolute reach error of trials per participant, and the variable reach error was determined by calculating the standard deviation of the absolute reach error per participant. An initial full model was specified including all candidate network predictors, Energy, Global Efficiency, Clustering Coefficient, and the modularity of modules (MOD) 1–4, and their interactions with the Condition (EGO vs. ALLO) variable. A mixed effects model for constant error was also tested, incorporating random intercepts for participants to account for individual variability; however, it did not significantly improve model fit compared to the simpler linear model. This is likely because averaging across trials reduces the amount of variability between participants. Importantly, we maintained a consistent modeling approach across both constant and variable error to facilitate direct comparison of effects across outcome types, ensure interpretability, and avoid unnecessary complexity.

To reduce the full model complexity and identify the most parsimonious set of predictors, we used a stepwise selection approach based on Akaike Information Criterion (AIC), implemented through the stepAIC() function from the MASS package in R (R Core Team, 2024). This method performs both forward and backward selection, evaluating potential models based on their AIC values to balance model fit and complexity. To assess the model's generalizability and estimate its predictive performance, we applied 5-fold cross-validation using the caret package (R Core Team, 2024). The data were randomly partitioned into five folds; the model was trained on four folds and tested on the remaining fold, repeated across all folds. Performance metrics including Root Mean Squared Error (RMSE), Mean Absolute Error (MAE), and R-squared (R^2) were computed to evaluate prediction accuracy and explained variance.

To visualize the effects of individual predictors on the outcome variable, we generated predicted values from the fitted linear model by constructing a grid of new data points. First, we defined a sequence of values spanning the observed range of a target predictor (e.g., MOD1 or MOD2) while holding the remaining predictors at their mean values. We accounted for group-level effects by including all observed levels of the Condition variable. This allowed us to estimate model-predicted outcomes across different values of a focal predictor, while controlling for the others. Using the predict function in R (R Core Team, 2024), we obtained predicted values and associated confidence intervals for each row in the constructed grid. The resulting dataset of predictions was then used to plot the relationship between each predictor and the outcome.

2.5 Results

In this study, we applied graph theoretical analysis to investigate network properties in a previously published fMRI dataset (Chen et al. 2014). To summarize, participants were shown a set of visual stimuli (targets and landmarks), instructed to either remember the target location and ignore the landmark (*Egocentric* task) or remember target relative to a visual landmark (*Allocentric* task), and then after a delay in which the landmark shifted, they reached toward the goal (**Figure 2.1**). Univariate analysis confirmed 'ventral stream' coding of landmark-centered goals versus 'dorsal stream' coding of egocentric visual goals, with further activation in parietofrontal reach pathways during movement execution (Chen et al. 2014). Other studies suggested that ego-allocentric integration is completed in frontal cortex (Chen et al. 2018; Bharmauria et al. 2020, 2021; Schutz et al., 2023).

Based on these results, we hypothesized that the *Allocentric* condition would induce a general increase in cortical signal sharing: specifically, increased sharing of information between dorsal and ventral pathways and recruitment of additional hubs in temporal and frontal cortex. We further investigated whether removal of the general rising trend of BOLD activation would decrease network parameters related to global integration. To these ends, we examined functional network properties at the whole brain level (global network parameters), intermediate level (network modularity), and local level (network 'hubs'), and then used a classifier model to test if the task instruction (egocentric vs. allocentric) could be decoded from these network parameters.

Note that the original study of Chen et al. (2014) reported that participants accurately pointed toward the originally viewed target location (or opposite in the anti-reach task) in

the *Egocentric* Task and accurately shifted pointing direction with the landmark in the *Allocentric* Task. This suggests that participants engaged the egocentric system and effectively ignored intervening shifts in the former task but effectively utilized landmark-centred codes in the latter task. Based on this, we henceforth refer to the functional networks associated with these tasks as the egocentric and allocentric networks.

2.5.1 Whole Brain Analysis: Cortical Trends Mediate Global Network Parameters

To investigate the global topological and dynamical attributes of our networks, we computed three distinct metrics: Clustering Coefficient, Global Efficiency, and Energy (**Figure 2.3**), which assess network segregation, integration, and stability / synchronization of connections between nodes, respectively. Each 'violin plot' shows the distribution of these scores across participants for the Egocentric network (blue) and allocentric network

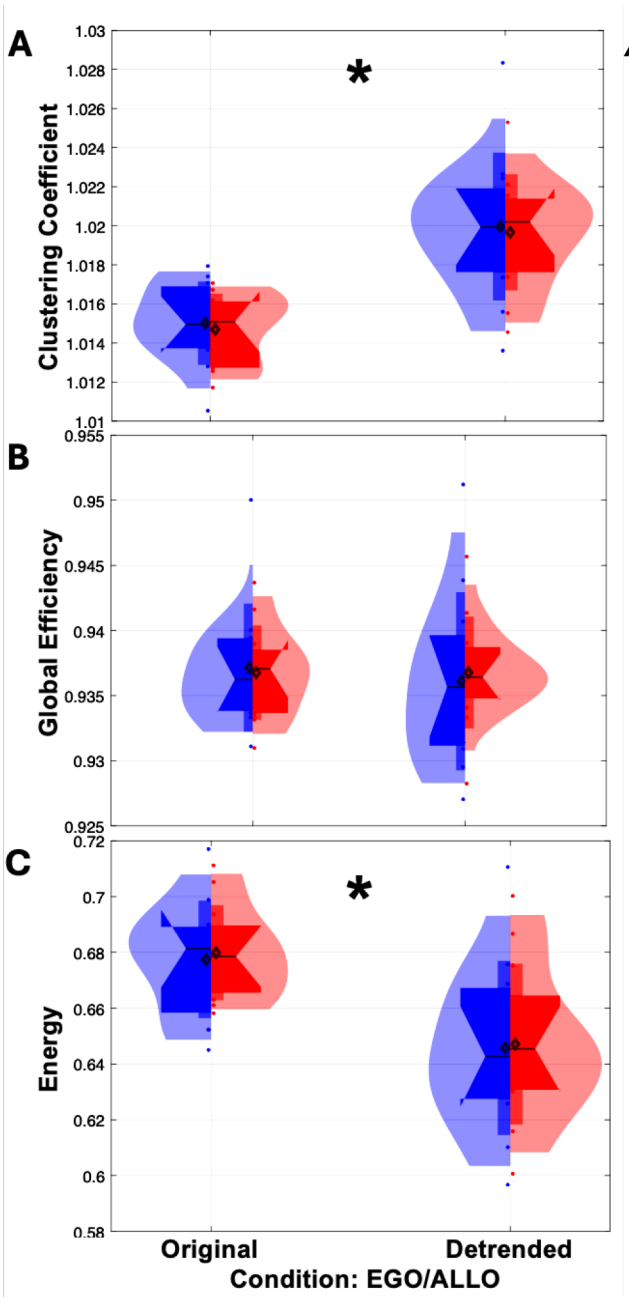


Figure 2.3 Quantification of Global Network Properties.
The average clustering coefficient (**A**), global efficiency (**B**) and energy (**C**) for each participant (n=12) were compared between the Egocentric (blue) and Allocentric networks (red), for the original (left) and detrended (right) data.

(red), contrasting scores from the original dataset (left) versus the detrended dataset (right). If overall temporal trends in brain activation mediate long range communications, detrending should result in increased local clustering and decreased integration. We found this to be the case for two of our parameters: detrending the data increased network segregation, as indicated by a significant rise (0.048 increase, t = 3.64, p= 0.0034) in the average clustering coefficient of nodes in both tasks (**Figure 2.3A**) and significantly reduced synchrony (**Figure 2.3C**) when the data were detrended (0.386 decrease, t = 5.20, p= 2e-04). However, there was no significant effect on Global Efficiency (**Figure 2.3B**) and none of the measures were significantly modulated by task. To discriminate the influence of behaviour on these networks, we next examine the intermediate level: cortical modularity in both tasks, in original and detrended datasets.

2.5.2 Intermediate Level Analysis: Behaviour Influences Signal Modularity

Graphic Analysis. Modularity analysis sorts nodes into 'communities' with signals that tend to correlate with each other and not to the other communities. **Figure 2.4** provides a graphic summary of our general network and modularity analysis for group data from the *Egocentric* condition (A), *Allocentric* condition (B), and detrended *Allocentric* data (C). The small dots indicate the location of the nodes analyzed, the larger dots local network hubs (these will be discussed in a later section), and the lines indicate 'edges' (signal correlations) that exceeded the 90^{th} percentile correlation (thin lines) or 95^{th} percentile correlation (thick lines). Note that the nodes, hubs, and edges have been color-coded based on the results of a modularity analysis at standard (1.0) resolution parameter γ.

As shown in **Figure 2.4 A,** the *Egocentric* network was divided into four bilateral modules: a superior occipital-parietal / somatomotor module (Module 1; red), an inferior parietal / lateral frontal module (Module 2; yellow), a superior temporal / inferior frontal module (Module 3; purple), and an inferior occipital-temporal / prefrontal module (Module 4; blue). In contrast, the *Allocentric* network (**Figure 2.4 B**) was divided into three modules, because the blue module 4 was incorporated into modules 1 and 3, forming an inferior occipital / superior parietal / somatomotor module (red), and a temporal / inferior frontal module (purple). Only the inferior parietal / lateral frontal module (2, yellow) remained largely the same.

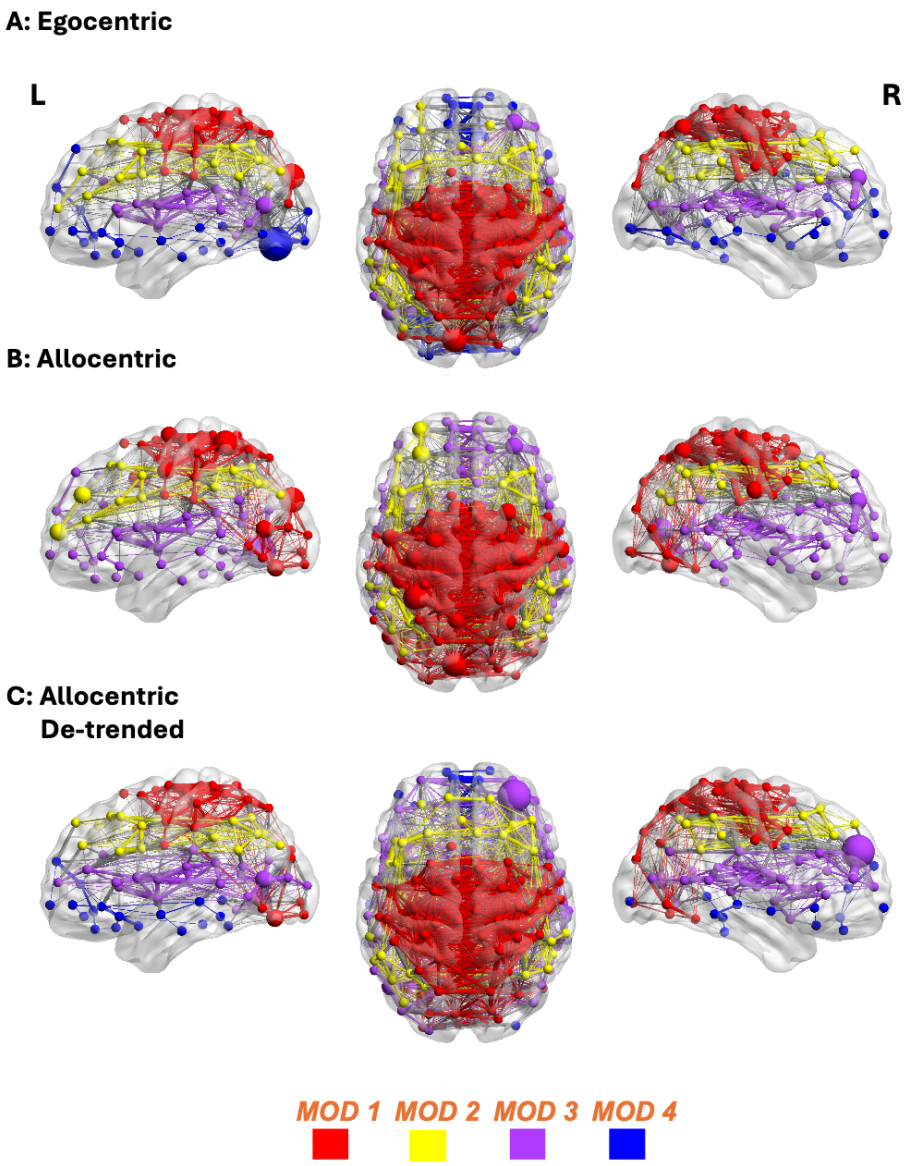


Figure 2.4 Visualization of Networks / Modularity Analysis.

Egocentric (**A**), *Allocentric* **(B**) and *detrended Allocentric* (**C**) datasets are shown**.** Each row provides an 'above' view of bilateral cortex along with lateral views of the left and right hemispheres. Small dots: node locations. Only nodes that are connected to edges exceeding the threshold shown below are shown. Larger dots: Eigenvector network hubs (scaled by statistical significance-based importance). Lines: 'edges' (signal correlations) exceeding a threshold of 90th percentile correlation (thin lines) or 95th percentile correlation (thick lines), thresholded for illustrative purposes only. Nodes, hubs, and edges have been color-coded by module (up to four): yellow, purple, blue, and red. For this analysis, a standard modularity resolution parameter of 1.0 was used.

In light of our hypotheses, it is noteworthy that the *Allocentric* network showed an increased conjoining of ventral and dorsal stream nodes (compared to Egocentric), toward a single (red) occipital / superior parietal / somatomotor module. However, after detrending the data (**Figure 2.4 C**), this network reverted to four modules, and the conjoining of dorsal-ventral visual stream modules was reduced. We will quantify these and other observations in the following sections.

Quantitative Analysis. **Figure 2.5** shows the distributions of modularity score across participants for each module (color coded red, yellow, purple, blue). Each color plot is further segregated into scores for the egocentric (left halves) and allocentric (right halves) networks. In simple terms, higher distributions signify greater modularity: increased connectivity within the module and reduced connectivity without.

Figure 2.5 A quantifies modularity in the original dataset. Most of the original modules, except for Allocentric module 2 (yellow) and Egocentric module 3 (purple), had a connectivity pattern that was more specific than a random null distribution. Comparing between tasks, the *Egocentric* network exhibited significantly higher modularity in the inferior-parietal / lateral frontal module (yellow) (1.25 increase, $t = 4.43$, $p = 8e\text{-}04$), whereas the *Allocentric* Network demonstrated significantly higher modularity in the superior temporal / inferior frontal module (purple) (1.29 increase, $t = 4.00$, $p = 0.00$). This suggests a trend toward greater dorsal modularity in the egocentric task vs. ventral modularity in the Allocentric task, consistent with dorsal-ventral stream theory.

As noted above (**Figure 2.4 C)**, the Allocentric network reverted to four modules after detrending **(Figure 2.5 B**). Detrending produced dramatic changes in the distribution of

modularity coefficients. In this case, only Egocentric module 3 had a connectivity pattern more specific than a random null distribution, whereas Allocentric modules 1, 2, 3 were no more specific than random null distributions or the corresponding egocentric modules. Together with **Figure 2.4**, this analysis suggests that the trend plays a role in integrating ventral occipital and dorsal parietal regions in the Allocentric network, as well as in forming specialized modules within the dorsal stream.

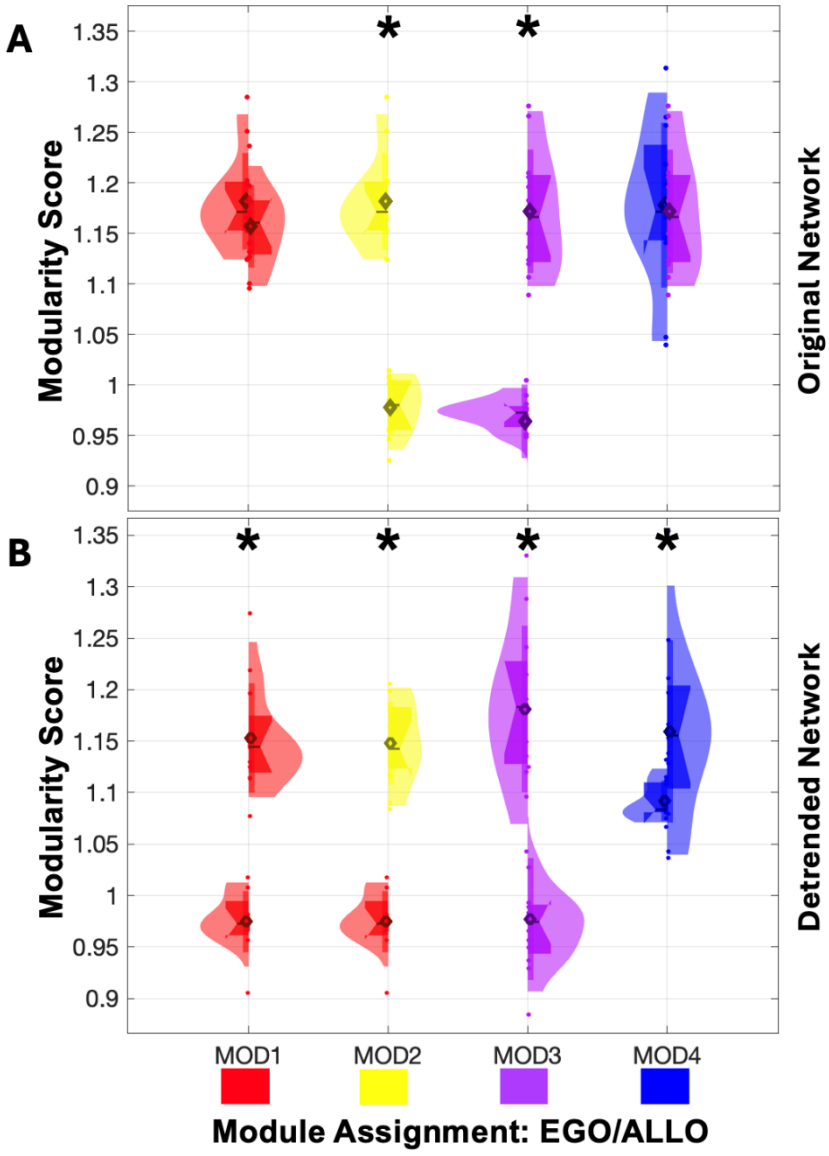


Figure 2.5 Quantification of Modularity in Original and Detrended Datasets. The left halve of each violin plot shows Egocentric network data and the right half shows Allocentric network data. A standard resolution parameter of 1 is used here. The color key is based on the original modules shown in Fig. 4. **A**: Original Ego/Allocentric datasets. Since Egocentric module 4 (blue) disappeared in the Allocentric dataset, mostly joining module 3, it is compared to allocentric module 3 (purple). **B**: Detrended Ego/Allocentric datasets. Since Allocentric modules 1 and 4 were merged in the detrended Egocentric dataset, the same values (red) were used for comparison to the Allocentric modules. Significant differences between task are indicated with an asterisk '*' in the plot.

Consistency Across Resolution Parameters. The proceeding modularity analysis was performed with an arbitrary standard resolution parameter of 1.0, but GTA parameters are known to be parameter-dependent (Blondel et al., 2008; Fortunato, 2010; Good et al., 2010; Traag et al., 2011). Therefore, it is possible that we just 'got lucky' by using the standard parameter. To assess the influence of this arbitrary choice on task- and trend-dependence, we calculated modularity scores and the number of modules for the original and detrended datasets across a range of resolution parameters (**Figure 2.6**).

Across different resolution parameters, we found that the influence of task was best revealed in the modularity score (**Figure 2.6 A**). The relationship between resolution and mean modularity was quadratic (e.g. for Egocentric modularity at a resolution parameter of 1, mean modularity score = average modularity score of all 4 egocentric modules in **Figure 2.5**). All scores generally rose with resolution, with original *Egocentric* data (blue) showing significantly higher scores (0.137, $t(596) = 2.56$, $p = 0.011$) than original *Allocentric* (red) below 1.18, and significantly lower above 1.18 resolution (-0.161, $t(596) = -2.62$, $p = 0.009$). The detrended data (dark red / black) essentially followed the same curves. It is noteworthy that both the standard (1.0) and optimal (1.13) resolutions (vertical dotted lines) fall to the left of this reversal point. Color coded modularity scores of individual nodes for the *Allocentric* networks are illustrated in the graphic plots shown below, where the score for most nodes rises (lighter colors) from standard resolution (**C**) to optimal resolution 1.13 (**D**) and show slightly different topological patterns for original (left) vs. detrended (right) data, such as a reduction in occipital modularity. In contrast, the influence of resolution parameter on module number was linear (**Figure 2.6 B**) and not task dependent. Instead, it showed significantly different slopes 0.31 difference ($t(596)$

= 2.97, p = 0.003) for original (red/blue) vs. detrended (dark red/black) data. Overall, **Figure 2.6** suggests that, although modularity depends on the resolution parameter, task- and trend- dependent differences are retained across different values.

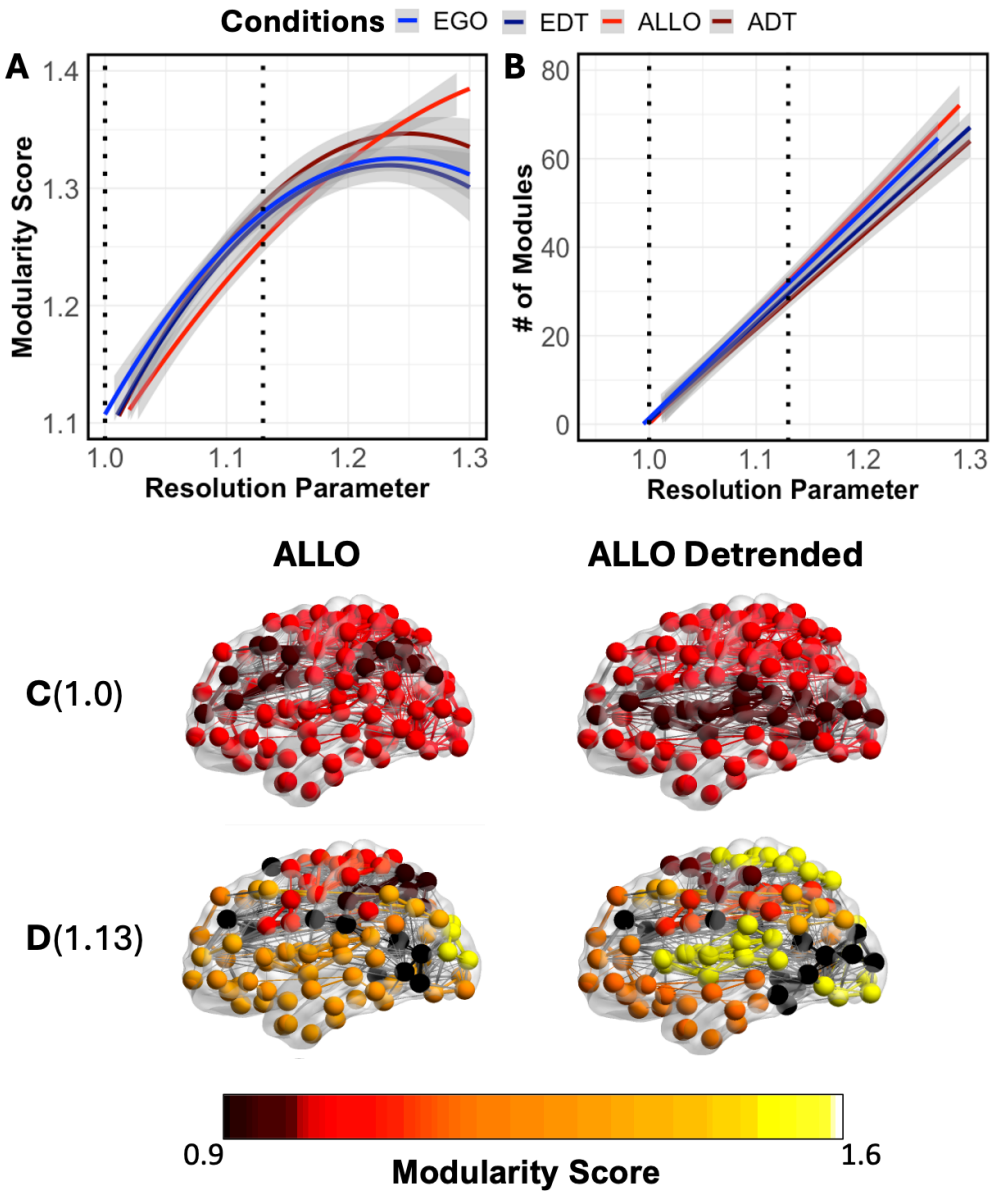


Figure 2.6 Influence of Threshold and Detrending.

The change in the modularity score (**A**) and the number of modules (**B**) is shown as a function of resolution parameter (top) is shown in the Egocentric (blue) and Allocentric (red) task, in the original (EGO/ALLO) and detrended (EDT/ATD) networks (darker colors). Network connectivity is shown in different resolution parameters for the Allocentric dataset, **C**: 1.0 (Standard) and **D**: 1.13 (Optimal for ALLO) (bottom), for original (left) and detrended (right data). The nodes are separated based on the module assignments based on the respective resolution parameters, but color coded based on the modularity score from part **B**.

2.5.3 Local Analysis: Hubness of Egocentric and Allocentric Brain Networks

Hubs are nodes that highly correlate to other areas that in turn are well 'connected' to other nodes and are thus thought to play important roles in the network. *Eigenvector Centrality* is used to compute locally important hubs (i.e., functional connectivity within modules) whereas *Betweenness Centrality* is used to compute hubs for global (i.e. across module) connectivity (Freeman, 1977; Rubinov & Sporns, 2010).

Local Hubs. **Figure 2.7** illustrates significant Eigenvector Centrality hubs for the significant Egocentric (**A**) and Allocentric (**B**) modules, overlaid on clusters of significant BOLD activation (orange). Eigenvector Centrality identifies nodes that are well-connected to other influential nodes (Freeman, 1977). In the figure, these nodes are scaled by size and color related to their hub importance and modularity assignment, respectively, which indicates their relative contribution to the network.

In the *Egocentric* network (**Figure 2.7 A**) local hubs were primarily confined to posterior parietal and occipital areas, including the superior parietal lobule (SPL), post-central cortex (PC), and the inferior and superior extra striate visual cortex (ExStr, ExStrSup). Based on their coordinates (**Table 2.2**), some, but not all, of these hubs overlap with significant BOLD activation clusters in occipital and parietal cortex (although one cannot conclude absence of activity in the other hubs). In short, the Egocentric task engaged local hubs in areas associated with visual processes, attention, and the bottom-up visuomotor transformations for this task (Cappadocia et al. 2017; Blohm et al., 2019).

The *Allocentric* task (**Figure 2.7 B**) engaged more occipital hubs in the inferior and superior extra striate visual cortex (ExStr, ExStrInf, ExStrSup), and also engaged several dorsal hubs such as somatomotor and postcentral visual cortex areas (SomMotA, PC, Precuneus) and more anterior hubs, including the lateral and dorsal prefrontal cortex (PFCl & PFCd) and the frontal eye fields FEF) (**Table 2.2**). Again, some of these hubs overlap with significant BOLD activation clusters, especially in occipital cortex.

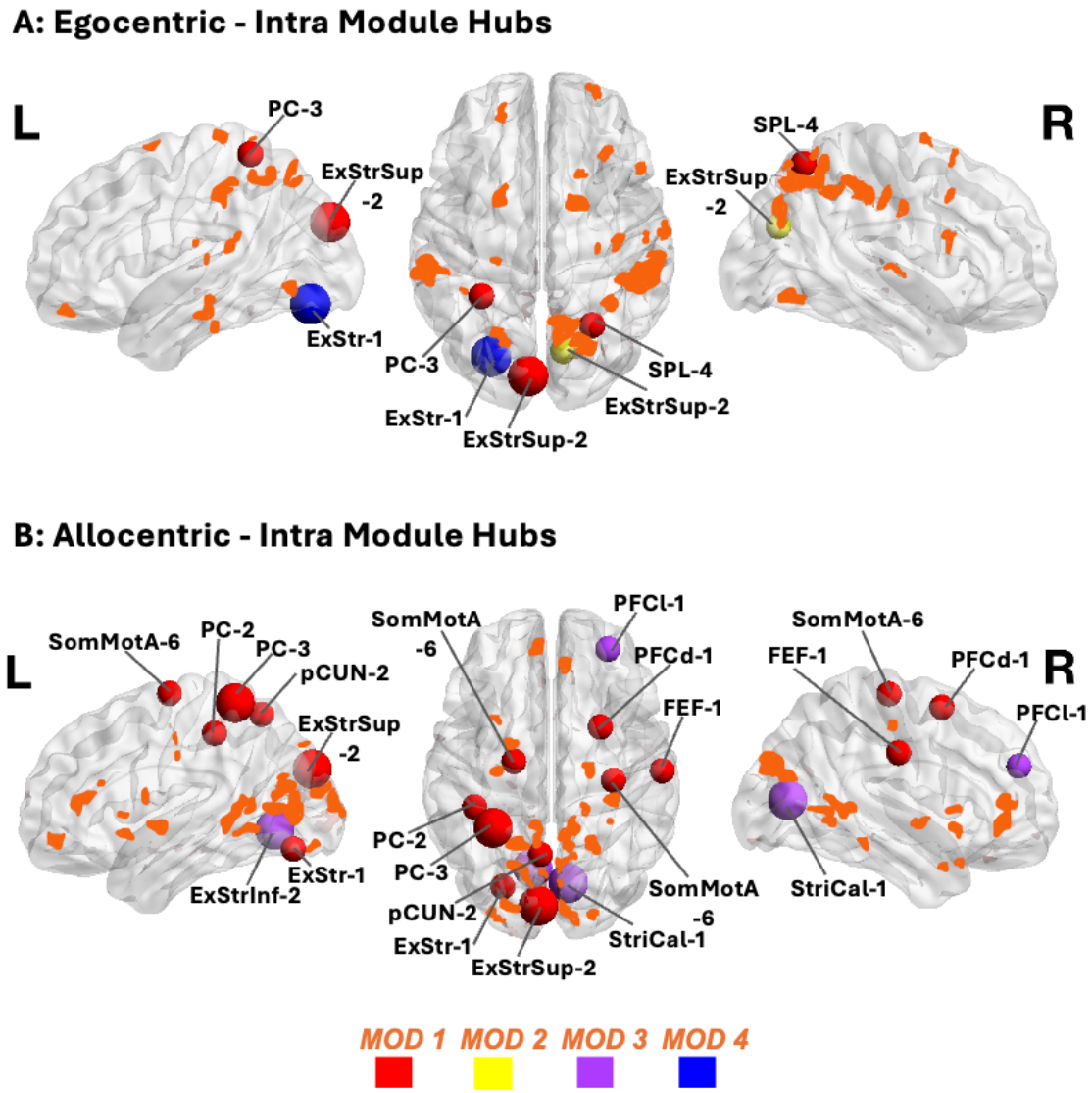


Figure 2.7 Eigenvector Centrality Hubs.

A: Egocentric, **B**: Allocentric hubs with significant eigenvector centrality are shown overlaid on the cluster map for the Allocentric vs Baseline Mixed-effects analysis, clusters with a corrected p-value threshold of 0.0167 are shown. See Table 2.2 for definitions of acronyms, their coordinates, and correspondence to functional areas. The node sizes are scaled according to significance-based importance ($p<0.01$ larger nodes, $p<0.05$ smaller nodes), whereas the color scheme shown at the bottom of the figure is based on the same modularity conventions of Figures 2.4 & 2.5. Note nodes that belonged to modules with insignificant modularity are excluded, including nodes from the Module 3 in the *Egocentric* task, and nodes from Module 2 in the Allocentric task.

Table 2.2 Eigenvector Centrality Hubs of the Egocentric and Allocentric Networks

ROI Name	*Network*	*MNI-x*	*MNI-y*	*MNI-z*	*EGO EVC*
LH_ExStr_1	VisCent	-26	-77	-14	2
LH_ExStrSup_2	VisPeri	-7	-87	28	2
LH_PC_3	DorsAttnB	-31	-46	63	1
RH_ExStrSup_2	VisPeri	11	-74	26	1
RH_SPL_4	DorsAttnA	26	-61	58	1

ROI Name	*Network*	*MNI-x*	*MNI-y*	*MNI-z*	*ALLO EVC*
LH_ExStr_1	VisCent	-26	-77	-14	1
LH_ExStrInf_2	VisPeri	-10	-67	-4	2
LH_ExStrSup_2	VisPeri	-7	-87	28	2
LH_PC_2	DorsAttnB	-41	-35	47	1
LH_PC_3	DorsAttnB	-31	-46	63	2
LH_pCun_2	ContC	-6	-60	57	1
LH_SomMotA_6	SomMotA	-20	-11	68	1
RH_FEF_1	DorsAttnB	59	-16	34	1
RH_PFCd_1	ContA	26	7	58	1
RH_PFCl_1	SalVentAttnB	30	48	27	1
RH_SomMotA_6	SomMotA	33	-21	65	1
RH_StriCal_1	VisPeri	9	-75	9	2

Note: EVC: Eigenvector Centrality; LH_ExStr_1: Left Hemisphere Extrastriate 1; LH_ExStrInf_2: Left Hemisphere Extrastriate Inferior 2; LH_ExStrSup_2: Left Hemisphere Extrastriate Superior 2; LH_PC_2: Left Hemisphere Parietal Cortex 2; LH_PC_3: Left Hemisphere Parietal Cortex 3; LH_pCun_2: Left Hemisphere Precuneus 2; LH_SomMotA_6: Left Hemisphere Somatomotor Area 6; RH_FEF_1: Right Hemisphere Frontal Eye Fields 1; RH_PFCd_1: Right Hemisphere Prefrontal Cortex Dorsal 1; RH_PFCl_1: Right Hemisphere Prefrontal Cortex Lateral 1; RH_SomMotA_6: Right Hemisphere Somatomotor Area 6; RH_StriCal_1: Right Hemisphere Striate Calcarine 1; VisCent: Visual Central; VisPeri: Visual Periphery; DorsAttnB: Dorsal Attention B; ContC: Control C; SomMotA: Somatomotor A ContA: Control A; SalVentAttnB: Salience Ventral Attention B. A value of 2 in the last column indicates $p<0.01$ and value of 1 indicates $p<0.05$.

Global Hubs. **Figure 2.8** depicts significant betweenness centrality hubs within all the Egocentric (**A**) and Allocentric (**B**) modules. Betweenness centrality is a critical measure in graph theory, representing the nodes that serve as key connectors between distinct modules, thereby facilitating information flow across the network. In the Egocentric network, hubs with the highest betweenness centrality were relatively fewer and more widely distributed across different modules.

In contrast, the Allocentric network exhibited additional betweenness centrality hubs, predominantly within the temporal (purple) module, with the notable exception of the extrastriate visual cortex (ExStr), part of the inferior occipital / superior parietal / somatomotor (red) module. The Allocentric hubs within the temporal module were concentrated in the ventral occipital cortex, including the inferior extrastriate cortex (ExInf) and the striate calcarine (StriCal), as well as in the temporoparietal (TempPar) and paraoccipital visual cortices (ParOcc), and extended to the prefrontal cortex (Table 2.3). In short, it appears that additional hubs were recruited for both local and global functional connectivity.

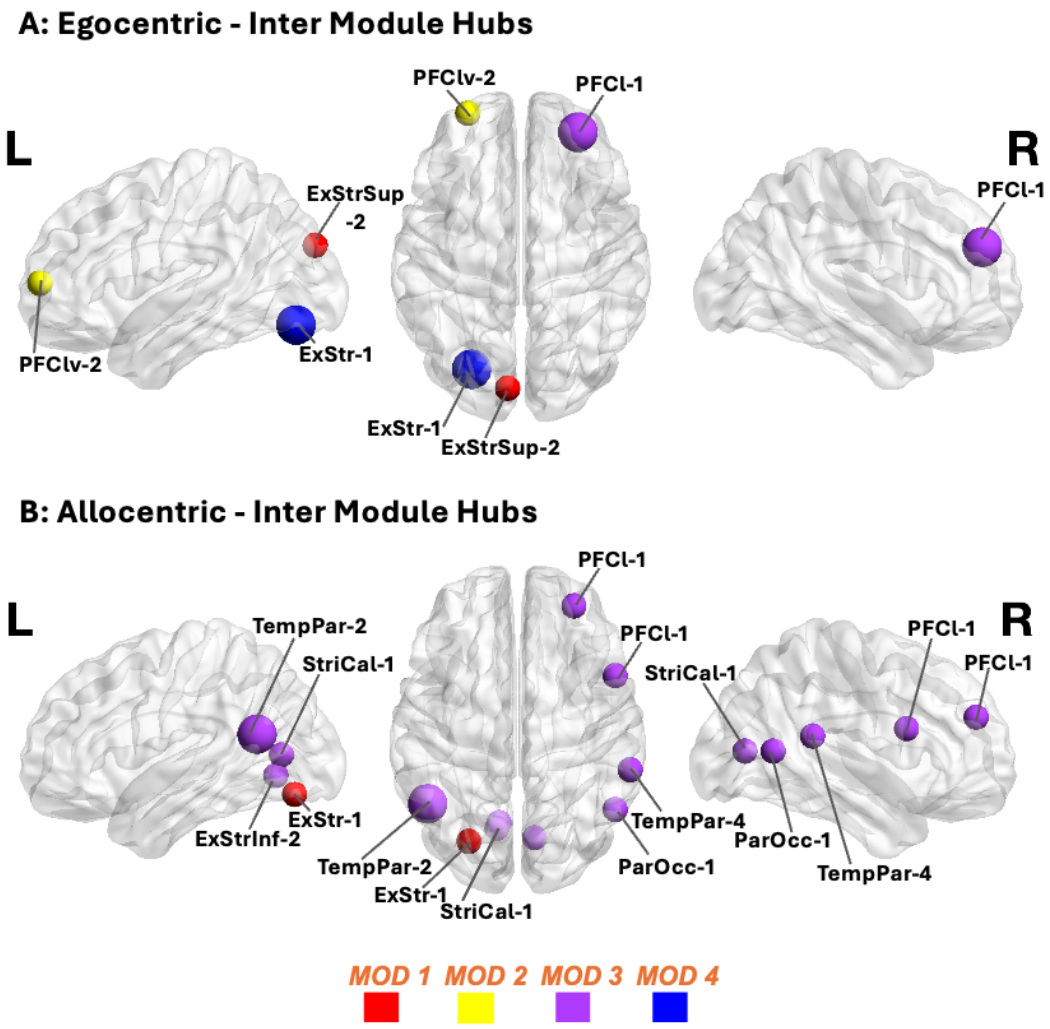


Figure 2.8 Betweenness Centrality Hubs.

A: Egocentric **B:** Allocentric hubs with significant betweenness centrality are shown. See Table 2.3 for definitions of acronyms, their coordinates, and correspondence to functional areas. The node sizes are scaled according to significance-based importance ($p<0.01$ larger nodes, $p<0.05$ smaller nodes), whereas the color scheme is based on the same modularity conventions of Figures 2.4 & 2.5. Nodes from modules with insignificant modularity were not excluded from analysis, as their connectivity role could still contribute to network integration.

Table 2.3 Betweenness Centrality Hubs of the Egocentric and Allocentric Networks

ROI Name	*Network*	*MNI-x*	*MNI-y*	*MNI-z*	*EGO BTW*
LH_ExStr_1	VisCent	-26	-77	-14	2
LH_ExStrSup_2	VisPeri	-7	-87	28	1
LH_PFClv_2	ContB	-28	58	8	1
RH_PFCl_1	SalVentAttnB	30	48	27	2

ROI Name	*Network*	*MNI-x*	*MNI-y*	*MNI-z*	*ALLO BTW*
LH_ExStr_1	VisCent	-26	-77	-14	1
LH_ExStrInf_2	VisPeri	-10	-67	-4	1
LH_StriCal_1	VisPeri	-11	-70	7	1
LH_TempPar_2	TempPar	-48	-57	18	2
RH_ParOcc_1	DorsAttnA	52	-60	9	1
RH_PFCl_1	SalVentAttnB	30	48	27	1
RH_PFCl_1	ContA	52	11	21	1
RH_StriCal_1	VisPeri	9	-75	9	1
RH_TempPar_4	TempPar	60	-39	17	1

Note: BTW: Betweness Centrality; LH_PFClv_2: Left Hemisphere Prefrontal Cortex Lateral Ventral 2; RH_PFCl_1: Right Hemisphere Prefrontal Cortex Lateral 1; LH_TempPar_2: Left Hemisphere Temporal Parietal 2; RH_ParOcc_1: Right Hemisphere Parietal Occipital 1; RH_TempPar_4: Right Hemisphere Temporal Parietal 4; TempPar: Temporal Parietal; DorsAttnA: Dorsal Attention A. A value of 2 in the last column indicates $p<0.01$ and value of 1 indicates $p<0.05$.

Allocentric vs. Egocentric Hubs. To directly test the influence of task instruction, we compared hubness in all nodes of the allocentric vs. egocentric networks. (Note that nodes that showed significantly different 'hubness' were not necessarily hubs in either individual network). **Figure 2.9** illustrates nodes with significantly increased Eigenvector Centrality (**A**) and Betweenness Centrality (**B**) in the Allocentric network compared to the Egocentric network. As shown in Table 2.4, areas that showed significantly higher Eigenvector centrality in the Allocentric task included the left orbitofrontal cortex (OFC), left parietal operculum (ParOper), and left dorsolateral prefrontal cortex (PFCd), as well as regions in the right hemisphere like the insula (Ins), inferior parietal lobule (IPL), and somatomotor areas (SomMotA_1, SomMotA_4, SomMotA_9). Note that these were distributed across both the 'red' occipital / superior parietal / somatomotor module 1 and the 'purple' temporal module 3. In contrast, only two regions showed significantly increased Betweenness Centrality in the Allocentric task: inferior extrastriate cortex (ExStrInf) and the left temporoparietal junction (TempPar), and these were confined to module 3. Overall, the allocentric network was associated with widespread increases in hubness across all four lobes of cortex.

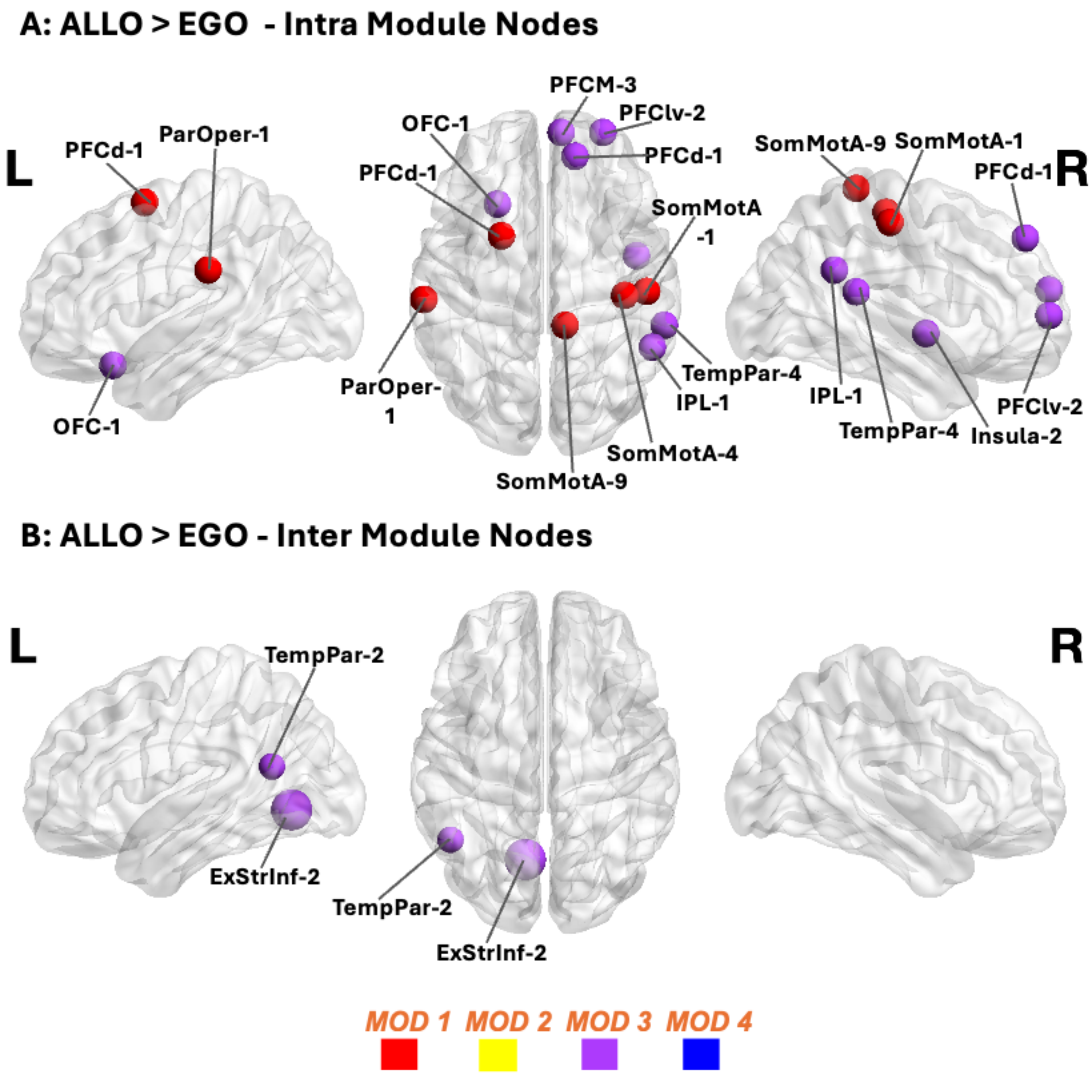


Figure 2.9 Allocentric Inter-task Difference Nodes.

A: Eigenvector Centrality **B:** Betweenness Centrality nodes with significantly higher values in the Allocentric task (ALLO) than the Egocentric task (EGO) are shown. See Table 2.4 for definitions of acronyms, their coordinates, and correspondence to functional areas. The node sizes are scaled according to significance-based importance ($p<0.01$ larger nodes, $p<0.05$ smaller nodes), whereas the color scheme is based on the same modularity conventions of Figures 2.4 & 2.5.

Table 2.4 Allocentric Inter-task Difference Nodes.

ROI Name	*Network*	*MNI-x*	*MNI-y*	*MNI-z*	*ALLO EVC*
LH_OFC_1	LimbicB	-24	22	-20	1
LH_ParOper_1	SalVentAttnA	-61	-26	28	1
LH_PFCd_1	ContA	-22	6	62	1
RH_Ins_2	SalVentAttnA	46	-4	-4	1
RH_IPL_1	DefaultA	54	-50	28	1
RH_PFCD_1	DefaultB	15	46	44	1
RH_PFClv_2	ContB	29	58	5	1
RH_PFCM_3	DefaultA	8	58	18	1
RH_SomMotA_1	SomMotA	51	-22	52	1
RH_SomMotA_4	SomMotA	40	-24	57	1
RH_SomMotA_9	SomMotA	10	-39	69	1
RH_TempPar_4	TempPar	60	-39	17	1
ROI Name	***Network***	***MNI-x***	***MNI-y***	***MNI-z***	***ALLO BTW***
LH_ExStrInf_2	VisPeri	-10	-67	-4	2
LH_TempPar_2	TempPar	-48	-57	18	1

Note: LH_OFC_1: Left Hemisphere Orbitofrontal Cortex 1; LH_ParOper_1: Left Hemisphere Parietal Operculum 1; LH_PFCd_1: Left Hemisphere Prefrontal Cortex Dorsal 1; RH_Ins_2: Right Hemisphere Insula 2; RH_IPL_1: Right Hemisphere Inferior Parietal Lobule 1; RH_PFClv_2: Right Hemisphere Prefrontal Cortex Lateral Ventral 2; RH_PFCM_3: Right Hemisphere Prefrontal Cortex Medial 3; RH_SomMotA_1: Right Hemisphere Somatomotor Area 1; RH_SomMotA_4: Right Hemisphere Somatomotor Area 4; RH_SomMotA_9: Right Hemisphere Somatomotor Area 9. A value of 2 in the last column indicates $p<0.01$ and value of 1 indicates $p<0.05$.

2.5.4 Decoding Task from Network Parameters

Finally, to confirm that our networks represent and *predict* meaningful task differences, and determine which parameters were most important, we decoded task (Egocentric vs. Allocentric) pooling all individual trial data across runs and participants. The decoding was done using a cubic support vector machine (SVM) classification algorithm, which was the model with the highest level of accuracy (see methods for details) and 5-fold cross-validation to evaluate the model's performance, which provides a more comprehensive assessment of the model's generalizability across diverse data. Our previous analysis suggested that modularity discriminates task (**Figure 2.4 - 2.6**), whereas global parameters did not (**Figure 2.3**). To test this formally, the following parameters were used initially as input to the SVM model: clustering coefficient, energy, global efficiency, and modularity of the individual modules. For modules that differed between tasks, the module with the highest overlap across tasks, i.e., most shared ROIs, was used to compute modularity. This resulted in 3 modularity parameters for both the original and detrended data.

Overall, this resulted in a high level of accuracy (85.7%) in distinguishing the Egocentric and Allocentric Networks in the original network, **Figure 2.9** (Note that this accuracy was achieved after removing the two least important parameters, clustering coefficient and energy, based on Kruskal-Wallis feature selection method). In **Figure 2.9 A** we presented confusion matrices, including the positive predictive values (PPV) and false discovery rates (FDR), to provide deeper insights into the model's classification outcomes and reliability. The model achieved a PPV of 87.2% in the *Egocentric* network, with an FDR

of 12.8% and a PPV of 84.3% in the *Allocentric* network, with an FDR of 15.7%. Based on this outcome, SVM performance was similar but slightly higher for the *Egocentric* network than the *Allocentric* network, the combination of modularity parameters and efficiency values have better prediction of the *Egocentric* network when using all the data.

In the *detrended* network, the accuracy rose to 87.7% in distinguishing the *Egocentric* and *Allocentric* detrended networks (**Supplementary Figure 2.2**). The model achieved a PPV of 85.1% in the *Egocentric* network, with an FDR of 14.9% and a PPV of 90.8% in the *Allocentric* network, with an FDR of 9.2%. (**Supplementary Figure 2.2 A**). This means that SVM performance improves in the detrended data due to better classification of the *Allocentric* network using the combination of modularity parameters and efficiency.

Figure 2.10 B shows the relative importance the features for classifying *Egocentric* versus *Allocentric* networks in the original dataset, as determined by the Kruskal-Wallis (KW) approach. Modularity was the most important parameter in classifying the two networks (*Egocentric, Allocentric*), specifically the modularity of the inferior-parietal / lateral frontal module (yellow module 2 in **Figure 2.4**) with a KW score of 138.72 and the modularity values of superior temporal / inferior frontal module (purple module 3 in **Figure 2.4**) with a KW score of 107. 85. The superior-occipital-parietal / somatomotor module (red module 1 in **Figure 2.4**) still had some relevant importance (3.00), but efficiency had very little importance in classification (0.73). In contrast, in the detrended network (**Supplementary, Figure 2.2 B**), the superior occipital-parietal / somatomotor module and the superior temporal / inferior frontal module (p) were the most important (KW of 126.51 and 92.08 respectively), but the remaining two predictors still had a high level of

importance, including the occipital-temporal / prefrontal module (b) with a KW of 17.84 and efficiency with a KW of 6.31.

Finally, **Figure 2.10 C** uses scatter plots to visualize the distribution of data points for the Egocentric (blue) and Allocentric (orange) networks, and to qualitatively assess how well the model separated these classes. Each point provides the two most important features derived from **Figure 2.10 B**, plotting the modularity values of inferior-parietal-lateral frontal module 2 vs the modularity values of superior temporal / inferior frontal module. Correct classifications are shown as dots, whereas incorrect classification are shown as crosses. The *Egocentric* and *Allocentric* form clusters that appear to separate along a diagonal axis with a negative slope, with the Allocentric datapoints clustered at the upper left corner of the scatterplot, which is characterized by higher modularity in the superior temporal / inferior frontal module (y-axis) and lower modularity in the inferior parietal / lateral frontal module 2, with little overlap. Most of the classifications were correct in the egocentric (266 correct vs. 39 mistakes) and Allocentric (279 correct vs. 52 mistakes). Overall, this analysis confirms that 1) our GTA parameters have both descriptive and predictive value for the associated behaviour, and 2) that modularity had the biggest influence in discriminating the two different tasks in this dataset.

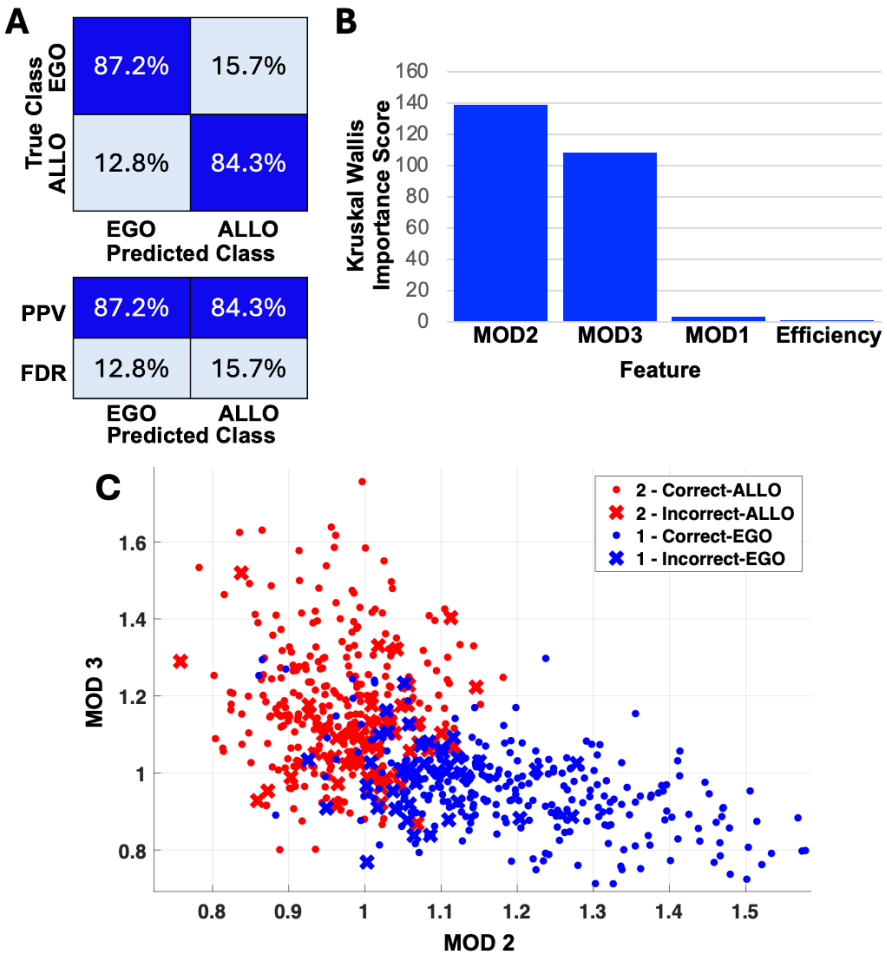


Figure 2.10 Classification Analysis.

Performance of the SVM classifier in distinguishing between the Egocentric and Allocentric networks in the original network (**A**) The confusion matrix (top panel -) comparing the percentage of data points in the four categories shown, top row: data points with a true and predicted class of *Egocentric* (EGO (top left cell), data points with a true class of *Egocentric* (EGO) and predicted class of *Allocentric (ALLO)* (top left cell), and the corresponding categories for the Allocentric task in the second row. The bottom panel table shows the PPV and FDR of the *Egocentric* network (EGO, left column) and the *Allocentric* network (ALLO, right column). (**B**) Importance scores of the features classifying Egocentric and Allocentric networks in the original dataset, as determined by the Kruskal-Wallis approach. (**C**) Scatter plot of distribution of datapoints predicted across two dimensions: (modularity score of module 2 [MOD 2] vs modularity score of module 3 [MOD 3) out of the total four classifier dimensions. Correct classifications are shown as dots whereas misclassifications are shown as crosses. The two networks being classified, *Egocentric and* Allocentric are shown in blue and red, respectively.

The overall statistical model (with all candidate predictors) demonstrated good explanatory power of constant error (R^2=.65, RMSE = 1.41, MAE = 1.12). However, after stepwise reduction, only MOD2 and MOD3 contributed significantly to constant error, depending on task (**Figure 2.11 A**). **Figure 2.11 A1** shows the relationship between MOD2 (yellow module in **Figure 2.4**) and constant error in the *Allocentric* condition (regression coefficient β = –7.57, p = 0.014). Similarly, **Figure 2.11 A2** shows the relationship between MOD3 (purple) and the *Egocentric* condition (β = –6.17, p = 0.015). Note that both of these coefficients (i.e., slopes in the figure) were negative, signifying a reduction of constant reach errors with increased modularity in modules 2 and 3.

The full statistical model provided an even better fit to variable errors (R^2=.69, RMSE = 0.40, MAE = 0.29). In this case, MOD 1 (red module) and 3 and *energy* (synchronization) survived stepwise reduction (**Figure 2.11 B**). **Figure 2.11 B1** shows the relationship MOD1 and variable error in both the *Egocentric* condition (β = –7.93, p = 0.015) and *Allocentric* (β = –4.36, p = 0.033) conditions. **Figure 2.11 B2** shows the relationship between MOD3 (purple) for the *Egocentric* condition (β = –6.17, p = 0.016). **Figure 2.11 B3** shows that Energy was also a significant predictor for the *Allocentric* condition (β = –11.92, p = 0.006). Again, all three of these coefficients were negative, meaning that increased modularity and energy were associated with lower variable reach errors.

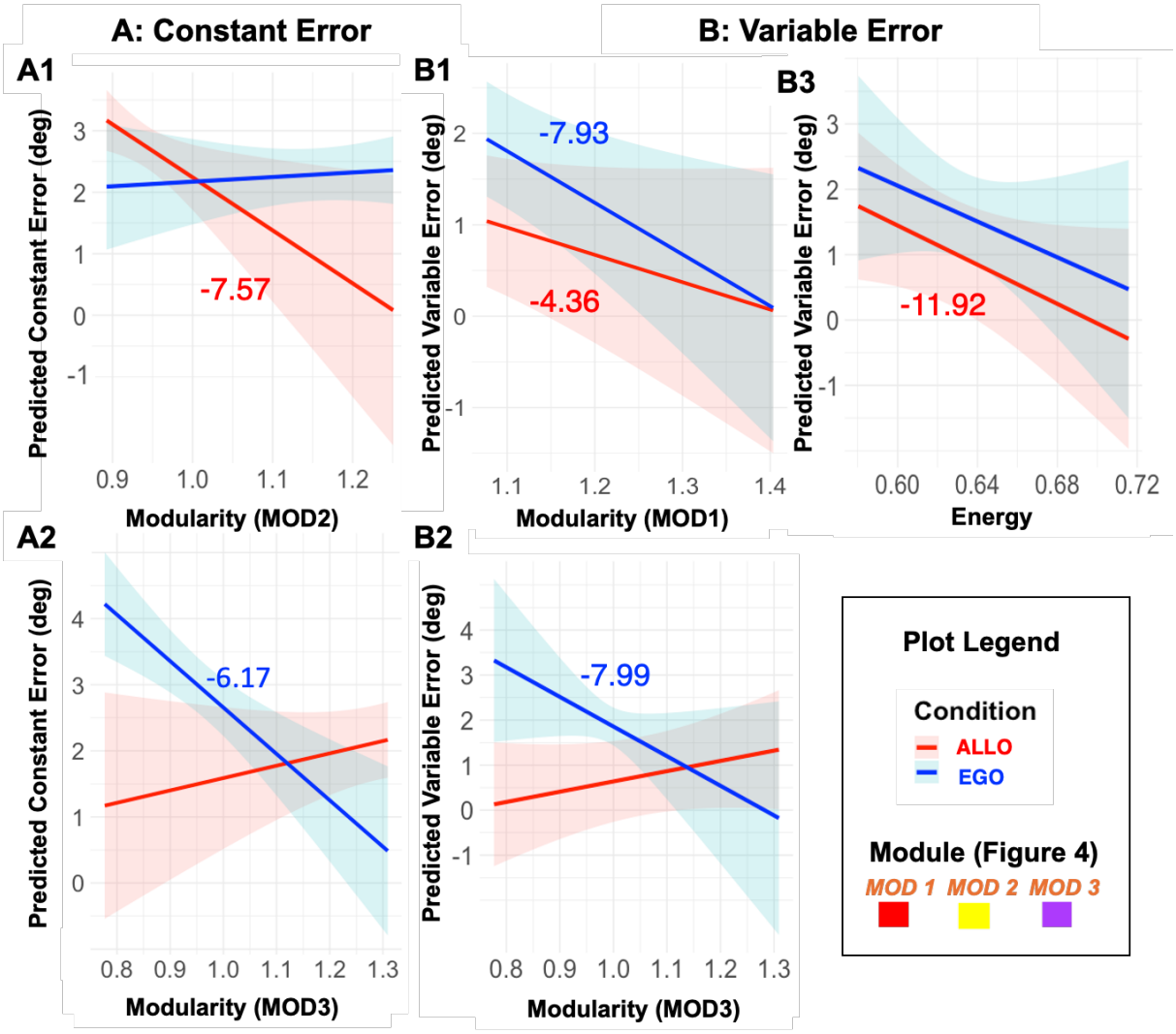


Figure 2.11 Influence of Network Predictors on Behaviour by Condition.

Predicted values from a multiple linear model are shown for each significant network predictor of the **A: Constant** Error and **B: Variable Error**. Each plot shows the linear relationship for both tasks (EGO Blue and ALLO red), the numeric β values of significant relationships (color-coded by task) and 95% confidence intervals. Only predictors with statistically significant effects in the final model, on at least one task, were included in the figure.

2.6 Discussion

The present study examined the influence global activation trends related to planning and task instruction (egocentric vs. allocentric reach) on the integration of target and landmark information into the cortical reach network—through the application of graph theoretical analysis (GTA) on fMRI data (Chen et al. 2014). Importantly, there was no difference in the stimuli presented in these tasks, but only the instruction to ignore or use landmarks for coding reach location (Musa et al. 2024). We hypothesized that the *Allocentric* instruction would induce greater global network connectivity, specifically through the integration of dorsal and ventral visual pathways and recruitment of additional Hubs. In addition, we explored the role of global activation trends in interregional cortical communication, by removing these trends from our analysis. Our results suggest that global activation trends related to reach planning reduced global synchrony while enhancing clustering in a reduced number of modules. Further, whereas the egocentric instruction resulted in four functional cortical modules with Hubs clustered in visual and sensorimotor cortex, the allocentric instruction resulted in the conjoining of nodes in ventral visual cortex with the 'dorsal stream' module 1, and the recruitment of additional hubs in ventral-posterior and frontal cortex areas associated with allocentric coding and ego-allocentric integration respectively. Finally, our decoding results confirmed that modularity, especially in modules 2 and 3, was the most important parameter for distinguishing the influence of task instruction on network properties, whereas modules 1-3 and energy were significant predictors for behavioural errors. These findings suggest that functional network properties are important for understanding the influence of task instruction on the use of sensory stimuli for visuospatial and motor processing.

2.6.1 Influence of Global Trends on Network 'Connectivity'

Planning and execution of reaches result not only in the recruitment of sensorimotor cortex, but also in progressive, widespread cortical activation (Medendorp et al., 2003; Cappadocia et al., 2017), including reactivation of early visual cortex (Gallivan & Culham, 2015; Blohm et al., 2019; Velji-Ibrahim et al., 2022; Monaco et al., 2024). While specific sensorimotor recruitment and sensory reactivation have been well studied, broader activation trends are often ignored or dismissed as non-specific arousal, preparatory set, or artifacts of cumulative BOLD activation.

An important exception to this is the work by Harms & Melcher (2003), who introduced the OSORU model (Onset, Sustain, Offset, Ramp, Undershoot) to capture temporal components of BOLD activity. In particular, they identified ramping activity, a within-trial linear increase in BOLD signal as a meaningful signal associated with cognitive processes such as expectation and preparation. Supporting this, Duff et al. (2007) showed that in the context of motor sequence learning ramp slope directions varied systematically across a symmetric network including SMA, sensorimotor cortex, cingulate, insula, and inferior frontal and temporal regions. Moreover, ramping increased across sessions of motor learning, while sustained responses decreased, supporting the notion that such trends are functionally relevant and not merely artifacts. Our data did not reflect all components of the OSORU model and did not show any obvious long-term drift, but we consistently observed widespread ramping activity within trials.

Based on this observation, we hypothesized that removing such trends might reduce global (intermodular) communication and emphasize more local processes. When global

trends were removed from the BOLD signal, we observed significant changes in network parameters, particularly global synchrony, which is thought to be an important mechanism for 'binding' of oscillating signals between different regions (Singer, 1993, 1999; Miller et al., 2012; Blohm et al., 2019). While our fMRI data cannot support or contradict those specific mechanism, they are consistent with the general notion that task trends play a role in maintaining large-scale network synchronization and align with the hypothesis that global BOLD trends reflect long-range communication across brain regions, which can influence local network dynamics (Smith et al., 2012). Removing task trends also increased global clustering, and reduced modularity, reduced number of modules in the Allocentric network and decreased integration of regions traditionally involved in dorsal and ventral stream processing (Figure 2.4). The latter highlights the importance of baseline brain activity in maintaining network integrity across brain regions (Raichle et al., 2001). Finally, detrending improved task classification based on modularity. These results suggest that removal of such trends is a useful tool to identify task-specific functional segregation.

2.6.2 Global Network Parameters, Task, and Behaviour

We found that global network features, such as clustering coefficient, global efficiency, and energy, were not particularly discriminative for the task conditions. This suggests that global connectivity measures may be too coarse to capture the subtle, task-specific differences in network organization that underlie spatial goal encoding. In contrast, cross-validated decoding methods demonstrated that task-specific differences could be reliably predicted using features derived from network modularity, even when global parameters

showed no significant task-related differences. Finally, network modularity (in modules 1-3) provided the largest contribution to predicting behavioural errors, although increased energy (synchrony) was also associated with decreased errors in the allocentric task.

These findings are consistent with previous studies that suggested network modularity—an intermediate-level feature that reflects the segregation of brain regions into functionally specialized clusters—is a more sensitive marker for distinguishing between cognitive states (Bassett & Sporns, 2017). These findings emphasize the importance of examining the relationship between network modularity and task, as it provides a more nuanced understanding of brain function than broad global parameters alone. In the following sections we examine the influence of task instruction on our network modules and hubs.

2.6.3 The Egocentric Network

Egocentric Modules. As noted above, modularity was the principal factor in determining the influence of task instruction on our functional networks. The egocentric instruction resulted in four primary modules (at the standard 1.0 resolution threshold), suggesting that the brain uses specialized clusters of regions for processing sensory information for action (Figure 2.4). The superior occipital-parietal / somatomotor module (1) clearly corresponds to the dorsal visual stream and areas involved in sensorimotor transformations (Andersen & Buneo, 2002; Iacoboni, 2006; Gallivan & Culham, 2015; Vesia & Crawford, 2012; Monaco et al., 2024). It is noteworthy that increased modularity in this module was associated with decreased variability in reach behaviour, whereas disruptions within this module lead to increased variability (e.g. Vesia et al. 2010).

The inferior parietal / lateral frontal module (2) includes areas with high level spatial processing and top-down instructions (Silver & Kastner, 2009; Peers et al., 2005). The superior temporal / inferior frontal module (3) appears to span auditory cortex and insula, so might be involved in multisensory processing of the instruction (Bamiou et al., 2003; Foxe et al., 2002). The inferior occipital-temporal / prefrontal module (4) incorporates elements of the ventral visual stream (Conway, 2018; Kravitz et al, 2011, 2013) and hippocampus, which are involved in configurational computations and spatial memory (Poucet, 1993) and communicate with frontal cortex for object recognition, and the storage and retrieval of spatial memory configurations in the presence of cues (Kar et al., 2019; Kar & DiCarolo, 2021; Zorzo et al., 2021).

Egocentric Hubs. Local hubs (Figure 2.7A) were primarily located in posterior regions, such as the superior parietal lobule and post-central cortex, which are integral for visuomotor processing (Moro et al., 2017). These hubs likely serve as critical nodes for integrating sensorimotor signals (Vesia & Crawford, 2012). These hubs tended to overlap with BOLD activation areas in the occipital and parietal cortex, suggesting an integral role in the circuitry for sensorimotor transformation. Global hubs (Figure 2.8A) likely play a role in coordinating activity across the different Egocentric network modules described above. These included regions such as the ventral extrastriate cortex, superior extrastriate cortex, and prefrontal cortex—areas known to support visual processing and decision-making in visuomotor tasks (Goodale & Milner, 1992; Pelli et al., 2006).

2.6.4 Changes Observed in the Allocentric Network

Overall, the Allocentric task produced a more integrated network with fewer modules, but more hubs compared to the Egocentric task. A major change observed in the Allocentric task, compared to Egocentric, was a reduction from four to three modules (at the standard 1.0 resolution factor). In part this was due to a conjoining of the ventral occipital (module 4) and dorsal visual pathways (module 1), which are typically thought to support egocentric vs. allocentric functions respectively (Goodale & Milner, 1992). This integration is consistent with the computational need to 1) compute configurational information in the ventral stream, i.e. target relative to landmark (Chen et al. 2014; 2020), and 2) incorporate this information into visuomotor processes typically associated with the dorsal stream.

However, it is equally important that the more anterior temporal portions of egocentric module 4 joined module 3 in the allocentric task, including areas such as auditory cortex and insula. The appears to be consistent with the need for high-level sensory integration in this task, such as relating the instruction to specific visual configurations. Further, our classification analysis (Fig. 10) showed that modules 3 and 2 -conjoining temporal and inferior parietal cortex to prefrontal cortex, were most important for discriminating task. This likely relates to the more linguistic and conceptual aspects of understanding the task, and the role of prefrontal cortex in cognitive control of action (Miller, 2000; Ridderinkhof et al, 2004). Consistent with this interpretation, some regions within these modules (frontal cortex, temporal-parietal junction) have been also implicated in egocentric / allocentric switching in a spatial memory task (Orti et al. 2024).

A direct comparison of ‘hubness’ between tasks (Figure 2.9) revealed widespread increases in the Allocentric task (Figure 2.9), especially in Eigenvector Centrality. These changes spanned nodes within previously reported networks including the LimbicB, SalVentAttnA, ContA, DefaultA, DefaultB, SomMotA, TempPar, and VisPeri (Schaefer et al., 2018). In general, the allocentric ‘Hubs’ that showed increased Eigenvector and Betweenness Centrality (Figure 2.9) were areas that are integral to visual processing and spatial awareness, particularly in the context of landmark-based navigation (Bremmer et al., 2001; Grefkes & Fink, 2005). These findings align with previous research suggesting that the Allocentric task places higher demands on cognitive control and requires greater interaction between sensory, memory, and motor networks (McNamara & Shelton, 2000).

The specific Eigenvector hubs for the Allocentric task (Fig. 7B) also correspond to areas in the control, salience, and dorsal attention networks (Schaefer et al., 2018). The presence of additional Eigenvector hubs in extrastriate cortex, especially the inferior areas, seems consistent with the increased visual complexity of this task. We also observed an increased recruitment of hubs in parietal cortex. Likewise, Ruotolo et al. (2019) showed that allocentric spatial judgments, specifically involving two vertical bars at the same distance and side relative to a horizontal bar, recruited dorsal regions including the supramarginal gyrus and inferior frontal gyrus (triangular part). These areas likely reflect the active use of a precise coordinate system to remember target positions rather than categorical spatial relations. Although their task was purely perceptual and ours involved delayed reaches, our analysis of the delay phase isolates similar encoding demands, suggesting shared network features supporting allocentric representation.

We also observed an increased recruitment of frontal cortex hubs in the allocentric task. Some of these regions (e.g., frontal eye fields) have been shown to play a role in egocentric-allocentric integration (Chen et al., 2018; Bharmauria et al., 2020, 2021; Schutz et al., 2023), consistent with the increased communication (dorsal-ventral modularity, betweenness hubs) observed in our allocentric reach task (Bharmauria et al., 2025). The presence of additional prefrontal hubs could also reflect the need for increased top-down cognitive demands of the Allocentric task, likely involving executive control, attentional allocation, and memory (Desimone & Duncan, 1995). This modulatory role might explain why more frontal hubs tended to align less with BOLD activation, whereas the posterior hubs were integral within the visual response to stimuli.

2.6.5 Lateralization

While examining hemispheric asymmetry in the networks, we found that both the Egocentric and Allocentric networks exhibited substantial bilateral symmetry in terms of modularity. This contrasts with prior research that has reported hemispheric lateralization in spatial processing in more perceptual / cognitive tasks. Ruotolo et al. (2019) found right-hemisphere dominance for egocentric tasks and left-hemisphere engagement for allocentric processing. Similarly, Tomou et al. (2025) reported lateralized visual modularity in a task that involved multiple feature judgements, but these lateral modules joined when transsaccadic remapping necessitated bilateral communication. Likewise, the bilateral distribution organization observed in the current study might suggest a need for interhemispheric communication when overt actions are required.

Most of our network hubs were also bilateral, but some lateralization was observed in Allocentric network hubs was observed. Specifically, left hemisphere hubs were associated with the orbitofrontal cortex (OFC), parietal operculum (ParOper), and dorsolateral prefrontal cortex (PFCd), while the right hemisphere showed significant involvement of the insula (Ins), inferior parietal lobule (IPL), and somatomotor areas (SomMotA). The left hemisphere regions are primarily associated with decision-making and motor planning (Heekeren et al., 2006), while right hemisphere regions are involved in spatial memory (Ferber et al., 2020), sensory integration and spatial processing.

2.6.6 Possible Physiological Basis of Network

The BOLD signals observed in this study reflect large-scale population-level neural activity, likely driven by synaptic inputs from various brain regions (Logothetis et al., 2001). Numerous physiological studies have observed configurational information (feature vs. feature, object vs. object) in the ventral visual stream, including areas possibly corresponding to ExStr_1 and ExStrInf_2 in our study (Kravitz et al., 2013). Fewer studies have examined target-landmark interactions for action, it has been shown that target and landmark signals coexist and interact to produce landmark-centred codes in frontal and supplementary cortex (Schutz et al., 2023). Further Bharmauria et al. (2020, 2021) showed that landmark shifts in these areas are detected in the memory responses and integrate in the motor responses of these structures. Finally, Taghizadeh et al. (2024) found evidence for both egocentric and allocentric coding in dorsal stream reach areas of monkey cortex, corresponding to our areas PC_3, SomMotA_1, and SomMotA_4. These studies suggest that our networks reflect real physiological processes and conversely our

results suggest that simultaneous physiological recordings over a broad range of areas are likely necessary to fully understand how these signals are integrated at a cellular level.

2.6.7 Relationship to Sensorimotor Transformation Models

As noted in the Introduction above, the dorsal visual stream / parietofrontal reach network is generally thought to provide the egocentric transformations for action (Goodale & Milner, 1992; Andersen & Buneo, 2002). More recent experiments have divided this into both 'bottom-up' and 'top-down' aspects (Blohm et al., 2019; Gallivan et al., 2013; Monaco et al., 2020). The bottom-up transformation from vision to movement is thought to include postural 'gain' modulations, e.g., from eye and hand position signals, to convert signals from gaze-centred to shoulder-centered coordinates for reach (Andersen & Buneo, 2002; Blohm & Crawford, 2009; Chang and Snyder, 2010). One of the well-known top-down influences is the use of efference saccade signals from the gaze system to spatially update gaze-centered reach goals at the level of parietal cortex (Batista et al. 1999; Henriques et al. 1998; Medendorp et al. 2003). Behavioural studies suggest that this information is re-integrated with allocentric cues after the updating process (Byrne et al. 2010b), suggesting a model in which ego-allocentric integration occurs just before the conversion of gaze-to-motor coordinates (Chen & Crawford, 2020). Although this integration is normally a weighted process (Byrne & Crawford 2010; Fiehler et al., 2014), the current and previous studies (Chen et al. 2018) suggest that instruction can modulate this process to full ego-centric or allocentric weighting in the dorsal stream, through modulations of the functional connectivity with the ventral stream. Thus, our results

remain consistent with the notion of the dorsal stream as the default sensorimotor transformation, but allow room for it to be modulated by other inputs.

2.6.8 General Implications

The findings from this study suggest that the modular organization of brain networks, particularly in terms of how regions segregate and integrate information, plays a critical role in supporting complex cognitive behaviours such as spatial goal encoding. Specifically, we find that task-related instructions can have a profound influence on modularity and hubness, likely influencing the way the brain processes sensory information (which was otherwise equalized in our two tasks). Further, it appears that widespread activation attributed to recurrent motor signals (Blohm et al. 2019) may play a complementary role in integrating these signals across cortex when it is time for action. These results could have broad implications for understanding how brain signals are organized to handle other types of complex, goal-directed behaviours. Furthermore, the ability to decode task-specific brain networks based on modularity measures suggests that event-related connectivity analysis could serve as a powerful tool for clinical diagnostics. For example, disruptions in the modular structure of brain networks may be indicative of neurological disorders that affect cognitive function, such as Alzheimer's disease or schizophrenia (Bassett et al., 2011) or explain why visual landmarks benefit movement initiation for Parkinsons’s patients (Russo et al., 2022).

Our findings can also be contextualized within classic and contemporary models of spatial cognition and embodiment. Galati et al. (2000) and Burgess (2006) proposed hierarchical and distributed mechanisms by which sensory input is transformed into spatial

representations across egocentric and allocentric frames, while Wolbers and Hegarty (2010) emphasized the flexible integration of these frames based on task demands.

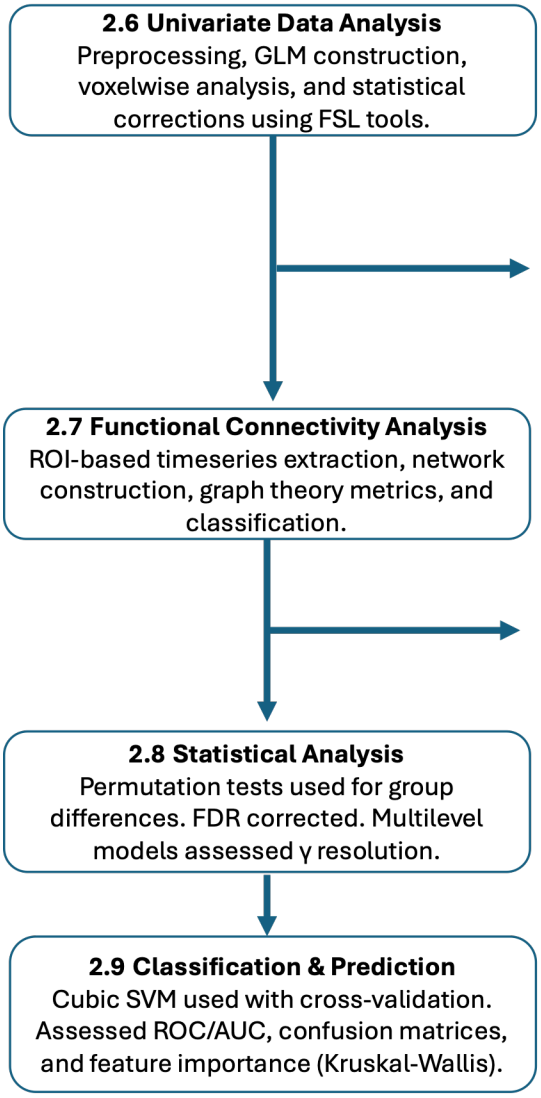
2.6.9 Conclusions

In conclusion, we have identified complementary mechanisms for segregating and integrating networks in response to task instructions: 1) topological segregation of similar signals into functional modules for visually-evoked movements, 2) integration across modules for specific task (such as the dorsoventral and posterior-anterior integration of modules observed in our allocentric task), 3) recruitment of specialized hubs for specific task requirements, and 4) promotion of global synchrony through the overall activation trends that emerge during movement planning. Although these results emerge from a specific dataset, we suggest that they would likely generalize to other complex visually guided behaviours, and that they would degrade during disease processes.

2.7 Funding

This work was funded by the Canadian Institutes for Health Research [grant number MOP-68812] and the Vision: Science to Applications (VISTA) Program [grant number 102001171]. L. Musa and A. H. Ghaderi were supported by VISTA. J.D. Crawford was supported by a Canada Research Chair, Canada First Research Excellence fund [grant number 101035774].

2.8 Supplementary Figures and Tables

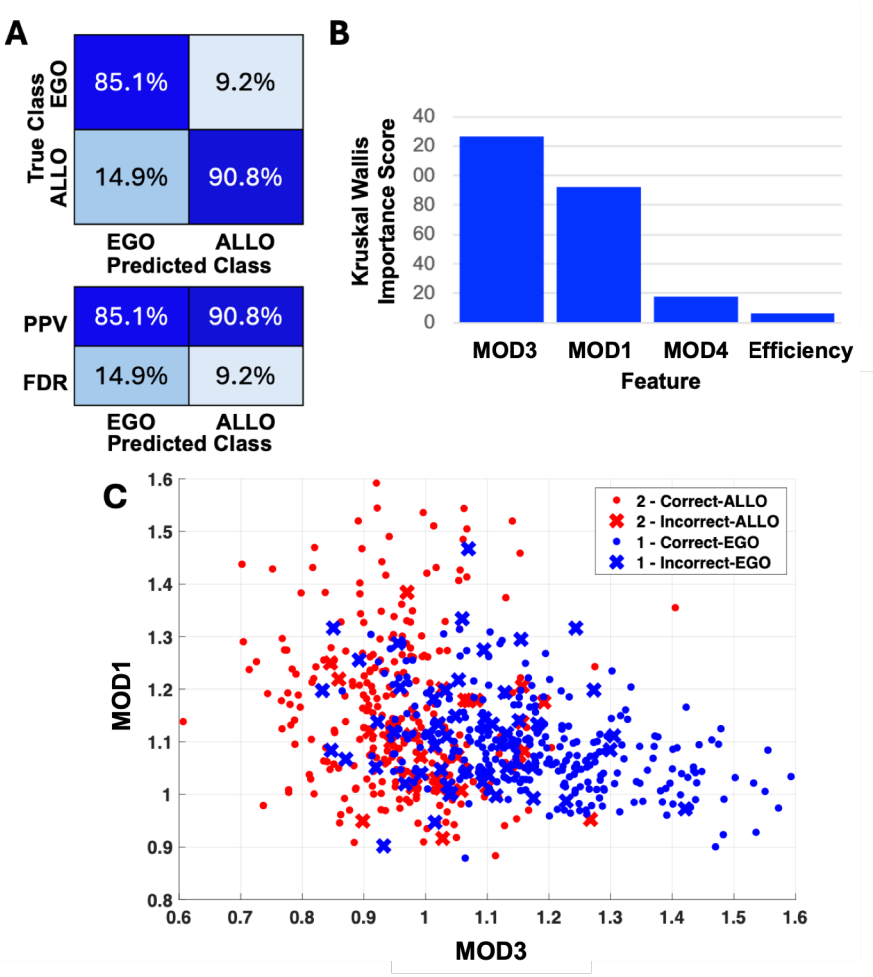


Subsection	Title	Description
2.6.1	Preprocessing	Performed in FSL. Included slice timing correction, motion correction (MCFLIRT), high-pass filtering, co-registration (FLIRT), MNI normalization, and 6-mm FWHM spatial smoothing.
2.6.2	GLM Construction	Constructed using FSL's FEAT with task-specific predictors. Included 6 motion regressors. EGOCENTRIC and ALLOCENTRIC tasks modeled.
2.6.3	Voxelwise Analysis	Group-level mixed-effects analysis (FLAME). Contrasts included EGOCENTRIC vs. baseline, ALLOCENTRIC vs. baseline, directional comparisons.
2.6.4	Statistical Corrections	Used cluster-based correction (randomise, 1000 permutations) and Bonferroni correction ($p<0.0167$).

Subsection	Title	Description
2.7.1	ROIs and Time Series	200 ROIs from Schaefer-Yeo atlas. Extracted contrast-reduced timeseries using fslmeants and custom MATLAB scripts.
2.7.2	Detrending	Linear trend removed using MATLAB's detrend function to isolate dynamic fluctuations.
2.7.3	Network Analysis	Correlation matrices formed adjacency matrices to assess signal sharing among ROIs.
2.7.4	Graph Theory Analysis	Assessed clustering coefficient, global efficiency, energy, modularity, and hubness.
2.7.4.1	Global Network Topology	Measured CC and EF to evaluate segregation and integration.
2.7.4.2	Global Network Dynamics	Energy (E) used to assess synchronization stability.
2.7.4.3	Mesoscale Network Topology	Measured modularity using Newman's algorithm and self-developed functions.
2.7.4.4	Local Network Topology	Measured Eigenvector and Betweenness Centrality. Hubs identified via LASSO regression.
2.7.4.5	Null Normalization	Used null models to normalize graph metrics (CC, EF, E).

Supplementary Figure 2.1 Influence of Network Predictors on Behaviour by Condition.

A summary of the methodological pipeline is shown. Numbering follows the numbering in the methods section.



Supplementary Figure 2.2 Classification Analysis.

Performance of the SVM classifier in distinguishing between the Egocentric and Allocentric networks in the detrended network (A) The confusion matrix (top panel table) comparing the percentage of data points in the four categories shown, top row: data points with a true and predicted class of Egocentric (EGO (top left cell), data points with a true class of Egocentric (EGO) and predicted class of Allocentric (ALLO) (top left cell), and the corresponding categories for the Allocentric task in the second row. The bottom panel table shows the PPV and FDR of the Egocentric network (EGO, left column) and the Allocentric network (ALLO, right column). (B) Importance scores of the features classifying Egocentric and Allocentric networks in the original dataset, as determined by the Kruskal-Wallis approach. (C) Scatter plot of distribution of datapoints predicted across two dimensions: (modularity score of module 3 [MOD3] vs modularity score of module 1 [MOD1]) out of the total four classifier dimensions. Correct classifications are shown as dots whereas misclassifications are shown as crosses. The two networks being classified, Egocentric and Allocentric are shown in blue and red, respectively.

3 CHAPTER THREE

3.1 Transcranial Magnetic Stimulation Differentiates Egocentric vs. Allocentric Network Hubs for Memory-Guided Reach

Lina Musa[1-3], Gaelle Nsamba Luabeya[1,2,5], Brando Sheldrick[1-3], Ali Rezaei[1-3], Saihong Sun[1-2], Xiaogang Yan[1-2], Michael Vesia[6], J. D. Crawford[1-5]

Affiliations: [1]Centre for Integrative and Applied Neuroscience (CIAN); [2]Centre for Vision Research, York University, Toronto, Canada; Departments of [3]Psychology, [4]Kinesiology & Health Sciences and [5]Biology, York University, Toronto, ON, Canada; [6]University of Michigan School of Kinesiology, Ann Arbor, Michigan, U.S.

Publication status:

Available as a preprint on bioRxiv:

https://www.biorxiv.org/content/10.64898/2026.07.29.741451v1

Ethics Approval: *Use of brief trains of repetitive transcranial magnetic stimulation (rTMS) to temporarily disrupt cortical function related to spatial memory and eye-hand coordination. Certificate #: e2019-248*

3.2 Abstract

Previous patient and imaging studies suggest that dorsal and ventral visual stream mechanisms contribute selectively to egocentric (eye-centred) and allocentric (landmark-centred) goal-directed behaviours, respectively. However, causal evidence for this ego-allocentric dissociation in healthy brains is lacking. Based on a recent neuroimaging study, we hypothesized that perturbations to dorsal stream network hubs would disrupt both egocentric and allocentric reaches, whereas perturbations to ventral hubs would affect only allocentric reaches. Sixteen participants viewed a briefly presented target in the presence of a landmark that later shifted after a memory interval. Participants were instructed to 1) ignore the landmark and reach toward / opposite the original target location (egocentric task) or 2) reach toward the target's location fixed relative to the shifted landmark (allocentric task). Transcranial magnetic stimulation (TMS) was applied during the memory period, spanning the landmark shift, at two occipital sites, based on the network hub coordinates from our previous study and individual brain anatomy. As predicted, superior occipital TMS impaired reaction time, accuracy, and precision in both tasks, whereas inferior occipital TMS only impaired allocentric performance. Further, spatial asymmetries in the resulting error patterns were influenced by TMS site and task: superior occipital TMS influenced asymmetries more strongly in the egocentric task, whereas inferior occipital TMS only influenced spatial asymmetries in the allocentric task. Finally, a functional network analysis revealed a widespread influence of TMS on network-behaviour relations and another dissociation: greater influence of superior occipital TMS on the egocentric task and of inferior occipital TMS on the allocentric task. These results establish specific causal relationships between occipital hubs, widespread

cortical networks, and reach behaviour, confirming a default dorsal egocentric transformation for visually aimed reaches, and a role for the ventral stream for landmark-centred actions.

Key Words: Allocentric coding; Egocentric coding; Memory-guided reaching; Transcranial magnetic stimulation (TMS); Network neuroscience

3.3 Introduction

Successful interactions with our surroundings depend on the ability to encode, retain, and transform spatial information into goal-directed actions. Visual target locations can be represented either in egocentric (relative to the observer) or allocentric (relative to visual landmarks) frames of reference (Crawford et al., 2011; Byrne et al., 2010; Soechting & Flanders, 1992). These mechanisms can be dissociated by instructing participants to rely on one cue or the other (e.g., Chen et al., 2014; Musa et al., 2024). Using such tasks, human neuroimaging / neuropsychology experiments suggest that activity / damage within different cortical 'streams' correlates differentially with egocentric vs. landmark-centred aiming movements (Chen et al., 2014; Goodale & Haffenden, 1998; Musa et al., 2025; Schenk & McIntosh, 2010). However, direct causal evidence for this dissociation in healthy individuals has not been established.

The idea that the visual system is divided into two streams was originally based on the spatial tuning of neurons recorded in animals (Ungerleider and Mishkin 1982) but was later refined by neuropsychological experiments in humans (Goodale & Milner, 1992; Milner & Goodale, 2006). Specifically, damage to the 'dorsal stream' (from occipital cortex through posterior parietal cortex) is associated with deficits in egocentric, action-oriented transformations, whereas damage to the ventral stream (from occipital to temporal cortex) is associated with deficits in object- and landmark-centered representations for perception (Goodale & Milner, 1992; Milner & Goodale, 2006; Schenk & McIntosh, 2010). More recent neuroimaging studies confirmed a dorsal-ventral / ego-allocentric dissociation and localized these processes to specific anatomic sites. Specifically, dorsal occipital / parietal

cortex is activated and spatially tuned for egocentric reaches, whereas inferior occipital / temporal cortex is activated and tuned for landmark centred reaches (Chen et al. 2014; Neggers et al., 2008).

Under natural conditions, ego- and allocentric cues are combined for optimal behaviour (Byrne & Crawford, 2010), with the weighting dependent on various factors, including visual conditions (Fiehler et al., 2014; Klinghammer et al., 2015) and memory delay (Chen et al. 2011; Goodale et al., 2005). This suggests that some mechanism flexibly integrates ventral / allocentric signals into the dorsal parietal-frontal stream, where egocentric transformations from gaze-centered visual signals to body-centred motor commands predominate (Andersen & Buneo, 2002; Blohm et al. 2009). Neuroimaging and physiological experiments suggest this could occur as early as parietal or as late as prefrontal cortex (Bharmauria et al. 2025; Chen et al. 2018).

Recently, Musa et al. (2025) analyzed functional connectivity (temporal correlations in brain activity) using the same dataset recorded by Chen et al. (2014), employing graph theory (Sporns, 2011). We identified two ‘hubs’ (nodes with highly distributed, strong inter-node correlations) within the visual peripheral network (Musa et al., 2025): a superior occipital hub for both the egocentric and allocentric reaching, and an inferior occipital hub for allocentric reaching. Further, modularity analysis revealed that dorsal and ventral stream modules (clusters of correlated nodes) were separated during egocentric reaches, but joined during landmark-centred reaches, suggesting task-dependent ventral-dorsal integration (Musa et al. 2025).

Overall, these findings suggest that the dorsal visual stream provides a default egocentric transformation for visually guided action, and the ventral stream provides allocentric information to augment this transformation by stabilizing 'noisy' egocentric signals (Bharmauria et al. 2025; Chen et al. 2011). But again, direct causal evidence to link these observations to the spatial deficits observed in patient populations is lacking. One potential approach is to transiently perturb ongoing neural processes with transcranial magnetic stimulation (TMS). For instance, TMS over known parietal 'reach regions' has been shown to reduce egocentric precision and accuracy in memory-guided reaches (Striemer et al. 2011; Vesia et al. 2006, 2008, 2010). One previous TMS study showed that stimulation of both the ventral and dorsal streams can influence movement time in an allocentric reach task (Adam et al., 2016). However, to our knowledge, no previous TMS study has provided the dissociation necessary to directly establish causal evidence for the dorsal / ventral segregation of egocentric / allocentric coding of reach targets.

We tested this question by applying online TMS to MRI-localized occipital hubs identified in our previous study (Musa et al. 2025) during the memory interval before reaches, using a previously reported psychophysical paradigm (Musa et al. 2024). Based on the observation that allocentric information is integrated into dorsal stream mechanisms (Bharmauria et al. 2025; Chen et al. 2018; Musa et al. 2024), we predicted that superior occipital stimulation would affect both egocentric- and allocentric-based reaching, inferior occipital stimulation would selectively impair only allocentric performance, and that these effects would likely interact with asymmetries observed in the control data (Musa et al. 2024). In addition, we performed a network behaviour analysis to determine TMS site influences, based on the modularity of subnetworks derived from individual resting state

MRI data and reach errors. Consistent with our hypothesis, superior occipital stimulation perturbed behaviour in both tasks, inferior stimulation only perturbed behaviour in the allocentric task, and further dissociations between dorsal and ventral spatial coding merged in detailed behavioural asymmetries and cross-participant modularity–behaviour correlations.

3.4 Materials and Methods

3.4.1 Participants

Sixteen individuals (8 males, 8 females; ages 22–34 years) were recruited based on an a priori power analysis (See Sample Size Analysis below.) and provided informed consent to participate in this study. All participants were right-handed, had normal or corrected-to-normal vision, and reported no history of neurological disorders, including epilepsy. Participants met standard safety criteria for transcranial magnetic stimulation (Rossi et al., 2021). No participant data were excluded from analysis. All received monetary compensation for their time. The experimental procedures were approved by the York Human Participants Review Subcommittee (Certificate #: e2019-248) and were conducted in accordance with the tenets of the Declaration of Helsinki.

3.4.2 Experimental Design

The experiment was conducted across three sessions: one MRI session followed by two TMS sessions scheduled 3 days to 1 week apart. Each session included a control block (no stimulation; 72 trials) with EGO and ALLO trials pseudo randomly interleaved as in Musa et al. (2024), followed by a TMS block (72 trials) using the same task structure. The

stimulated brain region was counterbalanced across days. Stimulation sites (Figure 3.6A) were selected based on functional hubs identified in Musa et al. (2025): ExstrSup-2, a superior occipital hub shared by both EGO and ALLO reaching, and ExstrInf-2, an inferior occipital hub preferentially associated with ALLO reaching.

3.4.3 Experimental Setup for TMS and Behavioural Recordings

Participants performed a delayed reach-to-touch task under egocentric (EGO) and allocentric (ALLO) instructions, with sensory and motor demands identical to those of Musa et al. (2024). The full experimental setup is shown in Figure 3.6. Participants were seated in a darkened room with their heads stabilized using a personalized bite bar. The right hand rested on a button box that served as both the starting position and pacing control. A customized ring with a 3 × 3 array of infrared-emitting diodes (IREDs) was attached to the right index finger, and three-dimensional hand position was recorded using two OptoTrak 3020 tracking systems (Northern Digital, Waterloo, ON, Canada). Eye position was monitored monocularly (right eye) using an EyeLink II infrared eye-tracking system (SR Research, Ottawa, ON, Canada) mounted on the bite-bar stand. Visual stimuli were presented on an LED display panel positioned approximately 50 cm from the eyes and aligned with the participant's right shoulder, ensuring stimuli were centered within the comfortable mechanical workspace of the right arm. Occasional illumination was provided during breaks to prevent dark adaptation.

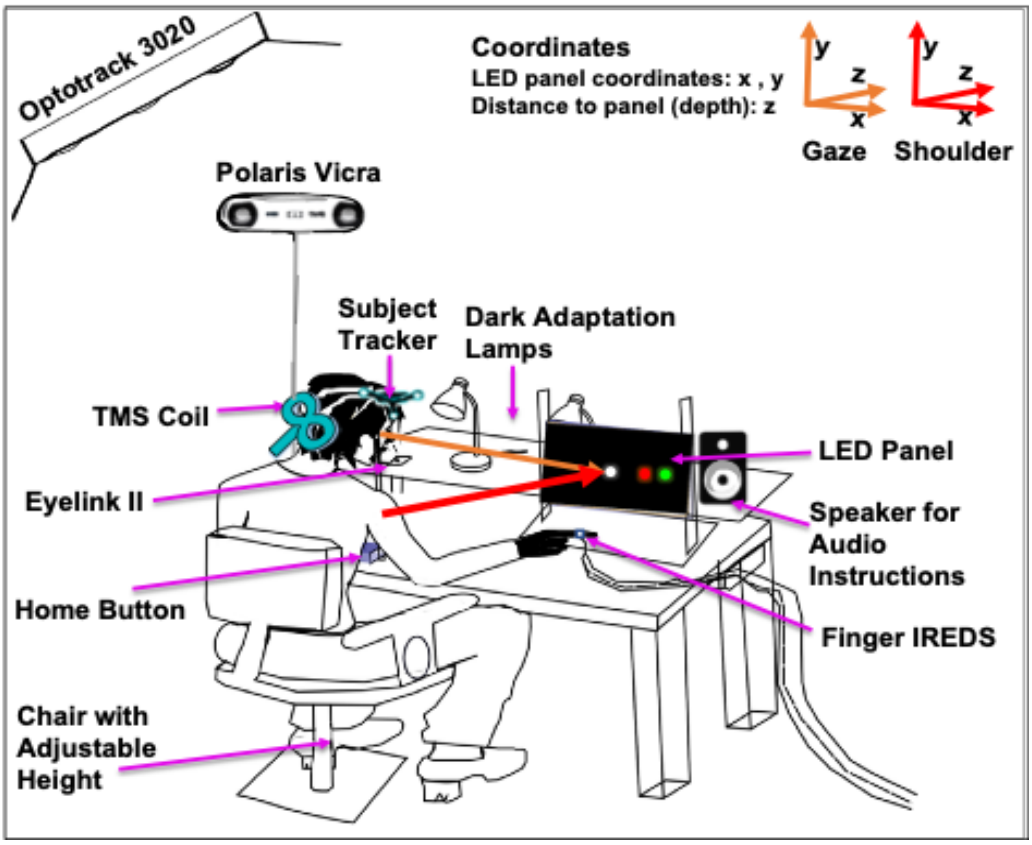


Figure 3.1 Experimental Setup.

Sixteen participants performed a delayed reach-to-touch task under EGO (relative to self) and ALLO (relative to a visual landmark) instructions, with a similar setup to Musa et al., 2024. Participants were seated in an adjustable chair facing an LED panel that presented visual targets. Right index finger position was recorded using infrared markers (finger IREDs) tracked by a motion capture system (Optotrak 3020). Eye position was monitored with an Eyelink II eye tracker. Participants began each trial with their hand on a home button that also controlled the experiment's pace and executed reaching movements toward targets displayed on the LED panel. Lamps controlled ambient lighting conditions to prevent dark adaptation, and speakers delivered auditory instructions to guide participants during the task. The LED panel was shifted to the right shoulder and coordinate systems were aligned with the center of the LED panel (x–y position on the panel and z depth), with reference frames illustrated for gaze-centered and shoulder-centered coordinates. A TMS coil was positioned over the participant's head during the stimulation conditions and neuronavigated using a subject tracker attached to the head and a Polaris Vicra camera. TMS (triple-pulse, 1 Hz, 110% resting motor threshold) was applied during the delay + planning period to dorsal / ventral hubs.

3.4.4 Task Paradigm

The behavioural paradigm is illustrated in Figure 1B and described in the accompanying text of the Results section. As described in Musa et al. (2024), each trial consisted of fixation, brief presentation of a visual target (green LED) and landmark (red LED), followed by a memory delay and a reach-to-touch response. Participants received auditory instructions at trial onset specifying whether to reach based on the remembered target location relative to themselves (EGO) or relative to the landmark (ALLO). In a subset of trials, participants performed mirror-opposite ("anti-reach") responses, as described previously (Cappadocia et al., 2017; Gail & Andersen, 2006).

3.4.5 Transcranial Magnetic Stimulation and Neuronavigation

TMS was delivered using a Magstim Rapid^2 stimulator (MagStim, Whitland, UK) and a 70-mm Air Film Coil (air-cooled figure-of-eight coil). Subject-specific functional parcellations derived from resting-state fMRI were used to precisely localize the centroid coordinates of Schaefer atlas parcels corresponding to ExstrSup-2 and ExstrInf-2 for stimulation (Schaefer et al., 2018). For simplicity, the current dissertation refers to these TMS targets as SupOcc-TMS and InfOcc-TMS, reflecting their assignment to the superior occipito-parietal and inferior occipito-temporal modules, respectively, in the network analysis of Musa et al. (2025). These coordinates were individualized for each participant by coregistering the T1-weighted anatomical scan using Brainsight neuronavigation software (Version 2.1.5; Rogue Research, Montreal, Canada) for real-time neuronavigation and accurate coil positioning during the TMS session.

During TMS Blocks, three 1 Hz biphasic single pulses were delivered at suprathreshold (110% of visible resting motor threshold [vRMT]) during the memory delay period (Fig. 3.1B), spanning the second appearance of the landmark. vRMT was defined as the minimum stimulation intensity required for visible contraction of the first dorsal interosseous in 5 of 10 consecutive trials. The final stimulation intensity was adjusted with consideration of the known differences between visually determined and EMG-based motor thresholds and the associated safety implications of the visual observation method (Westin et al., 2014). This protocol was designed to perturb memory and planning signals as well as the integration of the landmark information preceding movement onset, while minimizing sensory side effects and muscle discomfort.

3.4.6 Behavioural Data Acquisition and Analysis

Finger and eye position data were analyzed offline using custom MATLAB scripts (R2019a). Reach endpoints were converted from OptoTrak (Northern Digital Inc [NDI]) coordinates into screen and visual coordinates using participant-specific calibration mappings. Movement onset and offset were defined using velocity-based thresholds. Endpoint variability was quantified using 95% confidence ellipses, and accuracy was assessed via horizontal overshoot error relative to the expected reach goal. Supplementary Figure 3.4 illustrates the timing of events for an example participant.

3.4.7 MRI Data Acquisition

3.4.7.1 Structural Imaging

High-resolution T1-weighted anatomical images were acquired for each participant and used for cortical reconstruction, neuronavigation, and functional coregistration.

3.4.7.2 Retinotopic Mapping

Participants completed retinotopic population receptive field (pRF) mapping to confirm the retinotopic organization of occipital cortex and to visualize stimulation targets relative to visual field representations. These maps were generated using a sweeping bar stimulus from the Human Connectome Project (HCP) visual stimulus set. The bar traversed the visual field in multiple orientations while participants maintained central fixation and performed a fixation task to ensure attentional engagement. pRF mapping followed established methods (Benson et al., 2018; Dumoulin & Wandell, 2008; Wandell et al., 2007). Voxel-wise responses were modeled using a two-dimensional Gaussian pRF model to estimate preferred visual field location and receptive field size. Retinotopic maps and stimulation sites projected onto the cortical surface are shown in Figure 3.1A.

3.4.7.3 Resting-State fMRI (Multi-Echo)

Participants also completed multi-echo resting-state fMRI scans. Data were denoised using multi-echo independent component analysis (ME-ICA) to separate BOLD and non-BOLD signal components, improving signal quality for individual-level functional parcellation (Kundu et al., 2013).

3.4.8 Individualized Functional Parcellation (GPIP)

Individual T1-weighted anatomical images were processed using the recon-all pipeline in FreeSurfer v6.0.1. Preprocessed and denoised resting-state functional data were coregistered to the anatomical images using bbregister and resampled to the fsaverage5 surface using mri_vol2surf with trilinear interpolation. Surface-based smoothing was applied using a 6-mm full-width at half-maximum kernel with mri_surf2surf. Functional time series were normalized to zero mean and unit variance.

Group Prior Individual Parcellation (GPIP; Chong et al., 2017) was used to generate subject-specific functional parcellations. GPIP was initialized using the 200-parcel, 17-network Schaefer atlas (Schaefer et al., 2018), ensuring a common labeling scheme across participants while allowing parcel boundaries to adapt to individual functional connectivity patterns. Parcel homogeneity was computed at each GPIP iteration as the mean pairwise correlation between vertices within each parcel, averaged across parcels. Homogeneity values increased and plateaued prior to the final iteration, indicating stable individualized parcellations. These subject-specific Schaefer parcels were used to localize SupOcc-TMS and InfOcc-TMS targets to guide neuronavigation.

3.4.9 Network Modularity Analysis

For each participant, we segregated our imaging data into 8 subdivisions, by simplifying the Schaefer-Yeo 17-network subdivisions (Figure 3.5 A), which included the Control, Default, Dorsal Attention, Limbic, Visual, Somato-Motor, Salience Ventral Attention and Temporo-parietal Networks. We first computed inter-regional (parcel) associations of our

resting state BOLD time series data and then used graph theoretical analysis to compute the modularity of each network subdivision (grouping together regions of interest into their respective network subdivision). Then we used variations of modularity across participants as a predictor for differences in their behaviour during TMS stimulation, using the spatial behavioural variables described above.

3.4.10 Statistical Analysis

Linear mixed-effects models were used to analyze accuracy, reaching variability, and reaction time as a function of task (EGO/ALLO) and stimulation condition (control, SupOcc-TMS, InfOcc-TMS), including all interactions. Spatial asymmetries were analyzed by computing difference scores for visual field (LEFT − RIGHT) and reaching direction (OPPOSITE − SAME), which were subsequently analyzed using separate linear mixed-effects models. Models were fitted using the lme4 package in R (R Core Team, 2025), with participant included as a random intercept. Estimated marginal means and post hoc pairwise contrasts were computed using the emmeans package, and contrast p-values reported were adjusted for multiple comparisons using the Benjamini–Hochberg false discovery rate procedure.

3.4.11 Sample Size Analysis

Sample size was estimated using the simulation-based approach described by Green and MacLeod (2016) and implemented in the simr package in R, which performs power analyses for linear mixed-effects models fitted with the lme4 package. Consistent with the approach reported by Musa et al. (2024), power was estimated using Monte Carlo

simulations based on a pilot dataset comprising three participants and 576 observations across task (EGO/ALLO), stimulation site, and stimulation (control vs. TMS) conditions. A linear mixed-effects model was fitted to the pilot data to estimate the fixed effects and variance components. The estimated effect of interest ($\beta = 0.74$) was then used as the basis for the power simulations. Sample size was iteratively increased using simr until the estimated statistical power reached 85%, yielding a required sample size of 15 participants.

3.5 Results

3.5.1 Overview of Experimental Paradigm

Based on an *a priori* power analysis, 16 participants performed each stage of the experiment (see Methods for details). Each series of experiments (Figure 3.1) began with an MRI session designed to localize TMS targets and establish functional network modularity. Figure 3.1A shows the two stimulation sites in the left inferior (ExtrInf-2) and superior (ExtrSup-2) extrastriate occipital cortex (i.e., contralateral to the right hand used in the reach task) (Schaefer et al., 2018), superimposed on group-average population receptive field maps. In our previous functional network analysis, these were identified as important hubs in an inferior occipital-temporal and superior occipital-parietal module, respectively (Musa et al. 2025). Henceforth we refer to these as the inferior occipital (InfOcc-TMS) and superior occipital (SupOcc-TMS) stimulation sites.

During behavioural / TMS experiments (Figure 3.1B), participants were instructed at the start of each trial to either ‘reach to target’ (EGO task) or ‘reach relative to cue’ (ALLO

task). Participants then fixated a white dot while a landmark (red) and target (green) briefly appeared within a horizontal stimulus array (encoding phase). Fixation subsequently shifted to the centre to dissociate egocentric and allocentric reference frames, followed by a visual mask. This was followed by the memory delay, during which the landmark re-appeared at a different horizontal position in the same or opposite visual field.

Finally, an auditory instruction cued a reach with the right index finger to touch the remembered target location. In the ALLO task, the instruction was simply: ‘reach’ This could result in reaches toward the same visual field (ALLO-SAME task) or opposite visual field (ALLO-OPP task) as the original target, depending on where the landmark reappeared. To balance this, we used two instructions in the EGO task: toward the “Target” (EGO-SAME task) or “Opposite” (EGO-OPP task). Note that visual stimuli were the same in both tasks, only the instructions were different. Stimulation trials were the same, except three TMS pulses were applied at 1 Hz during the memory delay, spanning landmark re-appearance.

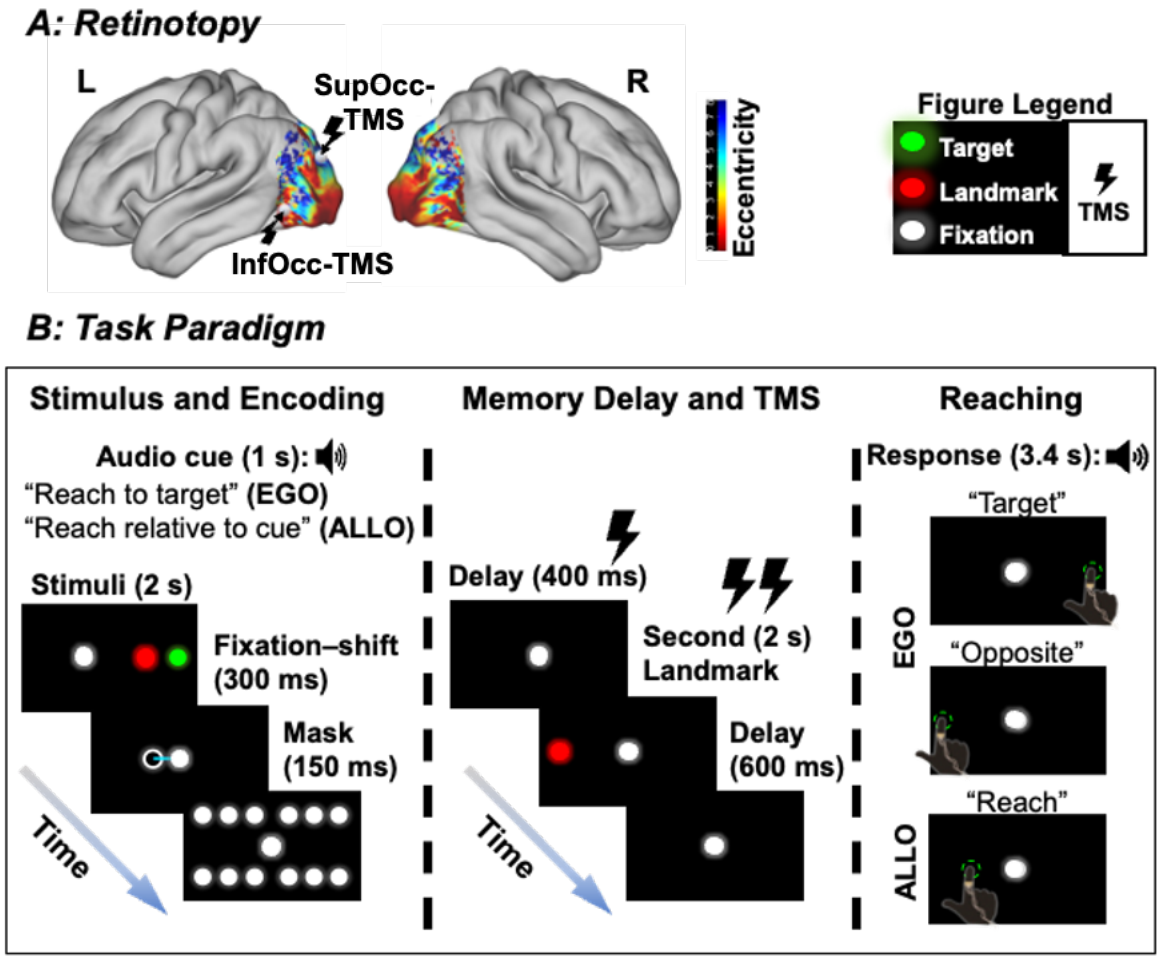


Figure 3.2 Stimulation Site and Experimental Paradigm.

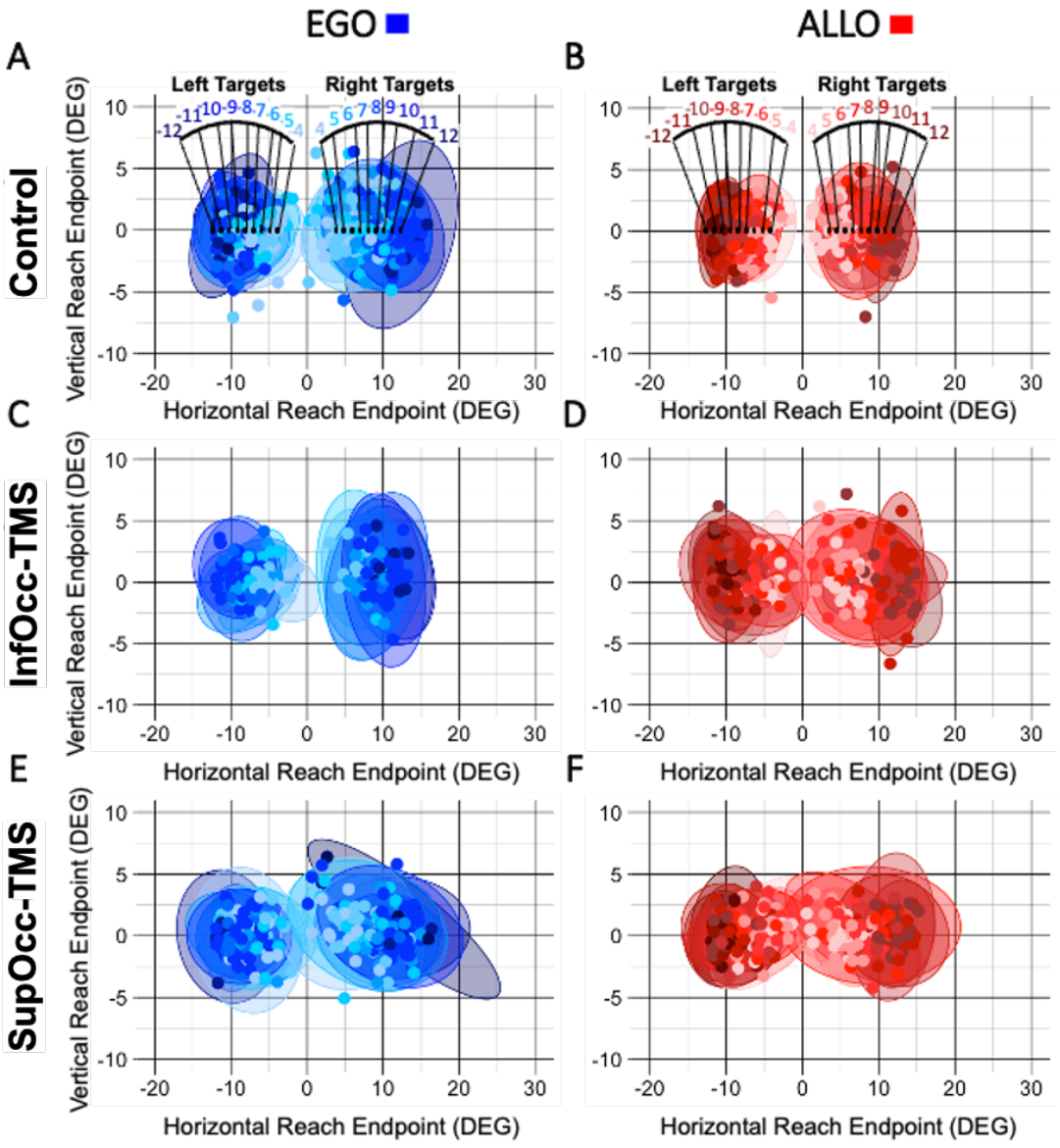
A – TMS sites (SupOcc-TMS and InfOcc-TMS) superimposed on group-average Population Receptive Field Model maps of target eccentricity (N = 16) are shown on the left and right lateral cortex. Colors indicate eccentricity according to the color scale, showing central (red) to peripheral (blue) eccentricity. **B –** Experimental paradigm summarized across three task epochs. **Stimulus and encoding:** Participants fixated a white dot while a landmark (red dot) and target (green dot) briefly appeared. Fixation then shifted to the center to dissociate egocentric (EGO) and allocentric (ALLO) reference frames, followed by a mask. **Memory delay and TMS:** TMS (three pulses at 1 Hz) was delivered during the first delay and when the landmark reappeared at a different position. **Reaching:** An auditory cue instructed participants to reach and touch with their right index finger the remembered target location according to either the EGO instructions ("Target"/"Opposite") or ALLO instructions ("Reach").

3.5.2 Reach Endpoint Errors

Figure 3.2 illustrates how we quantified reach errors. The top two panels show target locations (black dots labeled -12º to +12º). All panels show the corresponding participant average reach end-point positions per target location (coloured dots), and 95% confidence ellipses fit to the reach data, averaged across participants. The centres of these ellipses correspond to the mean constant error for each target and their area corresponds to the mean variable error.

Figure 3.2 panels A and B illustrate the control condition for EGO (blue) and ALLO (red) tasks, respectively. Reach distributions clustered around the correct target locations, i.e., ellipses shift from left to right along with the targets. Further, the EGO ellipses are visibly larger (mean 18.64 ± 5.25 deg²) than the ALLO ellipses (15.92 ± 5.05 deg²). This replicates our previous finding that an allocentric instruction leads to more precise overall performance in memory-guided reaching tasks (Musa et al., 2024).

Reach performance looks generally similar during TMS trials (Figure 3.2 C-F) but with subtle differences that are already evident in the raw data. For example, the allocentric advantage observed in control trials (Figure 3.2 B) appears to be lost during both InfOcc-TMS (Figure 3.2 D) and SupOcc-TMS trials (Figure 3.2 F). These and other observations are documented and quantified more extensively in the following sections and figures.



.

Figure 3.3 Average Reach Endpoint Ellipses.

Average 95 % confidence ellipses (2D reach endpoint variability) at each target location are shown for EGO (blue) and ALLO (red) tasks and across stimulation conditions: **A,B –** Control data, including target positions in visual angle degrees as black dots numbered 4 - 12 relative to central fixation right and left (negative values relative to fixation) visual fields. **C,D –** InfOcc-TMS, and **E,F –** SupOcc-TMS. Small, filled circles are individual participant average reach endpoints. Light-to-dark colors represent data for targets running central to peripheral. SAME / OPP side trials are pooled in this dataset.

3.5.3 Influence of TMS in the Spatial Domain: Variable and Constant Error

Our hypothesis predicts that SupOcc-TMS will impair both egocentric and allocentric pointing (because they share a common sensorimotor mechanism), whereas InfOcc-TMS will affect only allocentric reaching. Figure 3.3 A and B compare spatial performance in our different experimental conditions by providing the distributions of variable error (mean ellipse areas) and constant error (mean absolute error) across participants, including both LEFT/RIGHT field and SAME/OPP reaching for ALLO and EGO conditions.

First, we examined the influence of TMS on variable errors relative to control performance (Figure 3.3 A). A mixed-effects model revealed a significant interaction between stimulation site and task condition (interaction: $t = 6.21$, $p = 5.4 \times 10^{-10}$), indicating that the effect of TMS differed between EGO and ALLO trials. Follow-up one-tailed pairwise t-tests for increased error of the interaction effect (adjusted for multiple comparisons) showed that SupOcc-TMS increased reach variability in both EGO (Δ 9.52 deg^2; $t = 10.62$, $p < 1 \times 10^{-16}$) and ALLO trials (Δ 4.89 deg^2; $t = 4.66$, $p = 1.79 \times 10^{-6}$) relative to control. In contrast, InfOcc-TMS stimulation produced a selective effect, with no reliable change in EGO trials ($t = 1.21$, $p = 0.12$), but a significant increase in ALLO variability (Δ 3.57 deg^2; $t = 3.08$, $p = 1.06 \times 10^{-3}$).

Next, we quantified constant error as the mean absolute reach error between the goal and the actual reach (Figure 3.3 B). A mixed-effects model again revealed a significant interaction between stimulation site and condition ($t = 7.48$, $p = 8.9 \times 10^{-13}$), indicating differential TMS effects across tasks. In the control condition, mean error was higher for EGO trials (2.02°) than ALLO trials (1.07°), replicating Musa et al. (2024). SupOcc-TMS

increased constant error in both EGO (Δ 0.87°; $t = 5.63$, $p < 1 \times 10^{-16}$) and ALLO trials (Δ 1.19°; $t = 11.92$, $p < 1 \times 10^{-16}$). In contrast, behaviour during InfOcc-TMS stimulation showed no significant increase in EGO trials (Δ −0.77°; $t = -3.95$, $p = 0.99$) while increasing error in ALLO trials (Δ 1.27°; $t = 6.56$, $p < 2 \times 10^{-16}$).

In summary, the influence of TMS in the spatial domain depended on both stimulation site and task: TMS over superior occipital cortex influenced spatial reach errors in both tasks, but TMS over inferior occipital cortex only affected the ALLO task.

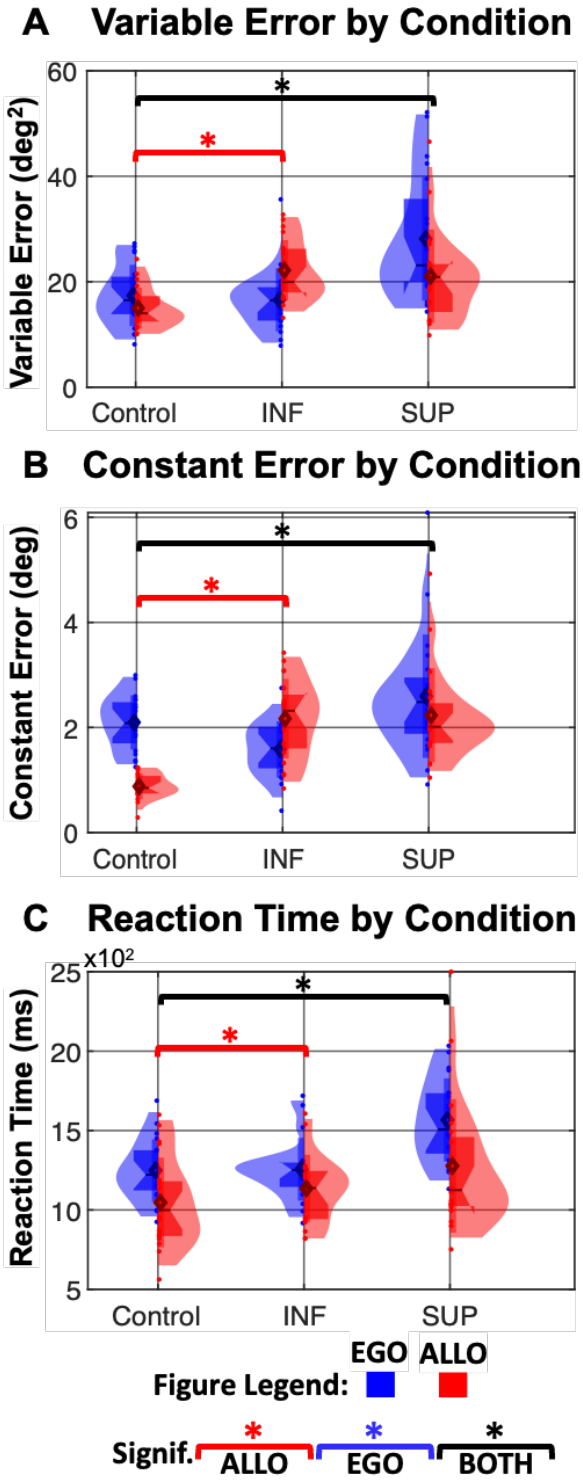


Figure 3.4 Influence of TMS in the Spatial and Temporal Domains. Violin plots showing the distribution of (top) **A –** Variable Error (deg²), (middle) **B –** Constant Error (deg), (bottom) **C –** Reaction Time (ms), for EGO (blue) and ALLO (red) conditions across Control, InfOcc-TMS (INF), and SupOcc-TMS (SUP) conditions. Horizontal lines indicate significant differences ($p < 0.05$), color coded by condition. LEFT / RIGHT field and SAME / OPPOSITE reaching trials are pooled in these datasets but are separated in Supplementary Figure 1.

3.5.4 Influence of TMS in the Temporal Domain: Reaction Time

Assuming that our TMS pulses interfered with motor planning, our hypothesis remains similar for reaction time: deficits in both tasks during SupOcc-TMS, but only the ALLO task during InfOcc-TMS. Temporal results are shown on the bottom panel of Figure 3.3 C. A mixed-effects model revealed a significant interaction between stimulation site and task condition ($t = 5.84$, $p = 4.7 \times 10^{-9}$), indicating that the effect of TMS differed between EGO and ALLO trials. In the control condition, reaction times were longer for EGO trials (mean: 1211 ms) than for ALLO trials (1017 ms), replicating findings from Musa et al. (2024). Follow-up one-tailed pairwise contrasts testing an increase in reaction time showed that SupOcc-TMS significantly prolonged reaction times in both EGO (Δ 359 ms; $t = 6.29$, $p < 1 \times 10^{-16}$) and ALLO trials (Δ 373 ms; $t = 6.91$, $p < 1 \times 10^{-16}$). In contrast, InfOcc-TMS increased reaction times in ALLO trials (Δ 76.3 ms; $t = 3.08$, $p = 0.0011$), but did not reliably affect EGO trials ($t = 1.02$, $p = 0.16$).

In summary, the influence of TMS in the temporal domain depended on both stimulation site and task. TMS over superior occipital cortex influenced reaction time in both tasks, but TMS over inferior occipital cortex only affected the ALLO task. Taken together with our spatial results (Figure 3.3 A,B), these results support our hypothesis that the superior occipital hub is part of the default sensorimotor transformation for reach, whereas the inferior occipital hub is only engaged for allocentric processing.

3.5.5 Spatial Asymmetries: Visual Field and SAME vs. OPPOSITE Reaching

The reach system tends to show contralateral preference for both hand and visual field (Andersen et al., 1985; Chang et al., 2008). Based on this, we expected that 1) left TMS would have the most influence for reaches in the right visual field, 2) this effect would be greater in the ALLO task during InfOcc-TMS, and 3) less task-dependent during SupOcc-Stim. Consistent with this, we found an interaction between task, stimulation site, and visual field asymmetries (Figure 4A/B; $t = 3.99$, $p = 6.8 \times 10^{-5}$). Inferior stimulation increased RIGHT > LEFT asymmetry for both variable error (Figure 4A, $\Delta = 2.93°$; $t = 3.72$, $p = 2 \times 10^{-4}$) and constant error (Figure 4B, $\Delta = 2.27°$; $t = 6.56$, $p = 5 \times 10^{-11}$) in the ALLO task (red), with no (or decreased) asymmetry in the EGO task. Superior stimulation increased variable error in the EGO task (Figure 4A, $\Delta = 1.98°$; $t = 4.56$, $p = 5 \times 10^{-6}$) and constant error in both tasks (Figure 4B, ALLO task: $\Delta = 1.24°$; $t = 2.56$, $p = 0.01$; EGO task: $\Delta = 2.06°$; $t = 4.01$, $p = 6 \times 10^{-5}$).

In our previous study, we found that egocentric reach performance was less accurate and precise when the movement goal appeared in the opposite visual field to the target, whereas the presence of a landmark in the ALLO task largely nullified this effect (Musa et al. 2024). This was confirmed in our control data (Figure 3.4 C/D). If TMS affects this OPPOSITE > SAME error pattern, our hypothesis would predict this influence to be task dependent: inferior occipital stimulation for the ALLO task, superior occipital stimulation for both tasks. Consistent with this, we found a significant interaction between TMS stimulation site and task in these data (Figure 4 C/D; $t = 5.84$, $p = 4.7 \times 10^{-9}$). InfOcc-TMS re-introduced OPPOSITE-SAME asymmetries in the ALLO task for variable (Figure

3.4C; Δ = 3.23°; t = 2.83, p = 0.0046) and constant (Figure 3.4D; Δ = 1.19°; t = 2.07, p = 0.038) errors, whereas superior stimulation exacerbated the pre-existing egocentric asymmetries for variable error in the EGO task (Figure 3.4C; Δ = 6.93°; t = 2.83, p = 0.0046) and constant error (Figure 3.4D; Δ = 1.45°; t = 2.03, p = 0.042).

In summary, the influence of TMS on visual field and same-opposite goal asymmetries was site-dependent and generally consistent with our hypothesis: inferior occipital stimulation affected both variable and absolute errors in the ALLO task, whereas superior stimulation affected variable errors in the EGO task and constant errors in both tasks. Moreover, TMS tended to exacerbate errors associated with dissociating the movement goal from the target, either negating the advantage of a landmark (during inferior stimulation) or magnifying control errors (during superior stimulation). Finally, similar TMS asymmetries were also observed in reaction time (Supplementary Figure 3.2).

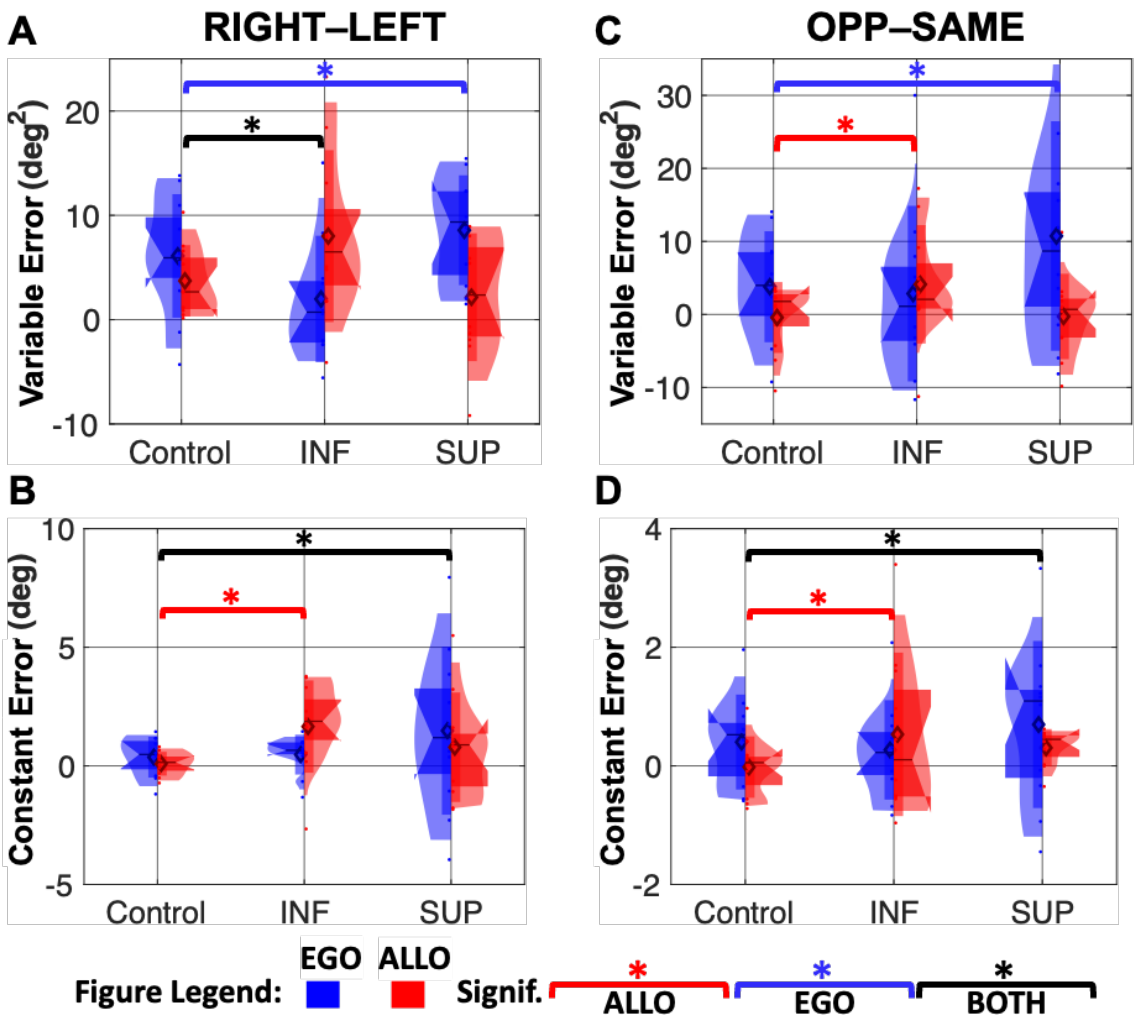


Figure 3.5 Lateralization of Response.

The average **Precision** and **Accuracy** compared for **A,B –** OPPOSITE-SAME target-movement mappings and **C,D –** RIGHT-LEFT visual field lateralization for EGO (blue) and ALLO (red) conditions across Control, TMS InfOcc-TMS, and TMS SupOcc-TMS conditions. Horizontal lines indicate significant differences ($p < 0.05$), color coded by condition.

3.5.6 Network Analysis: Modularity Predicts Behavioural Changes Induced by TMS

It is thought that TMS has an influence well beyond local networks (Beynel et al., 2020; Hallet et al., 2017). To test the relationship between TMS site, regional network properties, and behaviour, we performed a functional network analysis based on our resting state MRI data (Standage et al., 2025). Specifically, we segregated the imaging data of each participant into 8 bilateral network subdivisions (Figure 3.5 A), corresponding to the Control, Default, Dorsal Attention, Limbic, Visual, Somato-Motor, Salience Ventral Attention and Temporo-Parietal Networks (Schaefer et al., 2018). We then used graph theory analysis to compute the modularity of each subdivision (the degree to which network nodes tend to cluster into correlated communities). We found that, across participants, the modularity score for most of the brain subdivisions listed above were significantly correlated to both constant and variable behavioural errors measured in our control data (Supplementary Figure 3.3).

We then tested if modularity predicts TMS-induced errors (i.e., TMS - control error), the cortical distribution of this influence, and its dependence on TMS site. Figure 3.5 B/C show the results of this analysis for variable (B) and constant (C) error parameters. Each radial datapoint represents the relationship (regression slope) of TMS-induced errors as a function of modularity across 16 participants, computed for each of the 8 brain subdivisions. Both error measures show that 1) modularity predicts TMS-induced error across a broad range of cortical subnetworks (with strongest associations in the Visual, Temporo-Parietal, Control and Salience Ventral Attention networks), and 2)

although significant modularity-behaviour influences were present during stimulation of both sites and tasks, InfOcc-TMS had more influence in the ALLO task (red) and SupOcc-TMS had more influence in the EGO task (blue). Taken together with our other results, this suggests that (although the dorsal stream participates in both tasks), its intrinsic network organization is primarily egocentric.

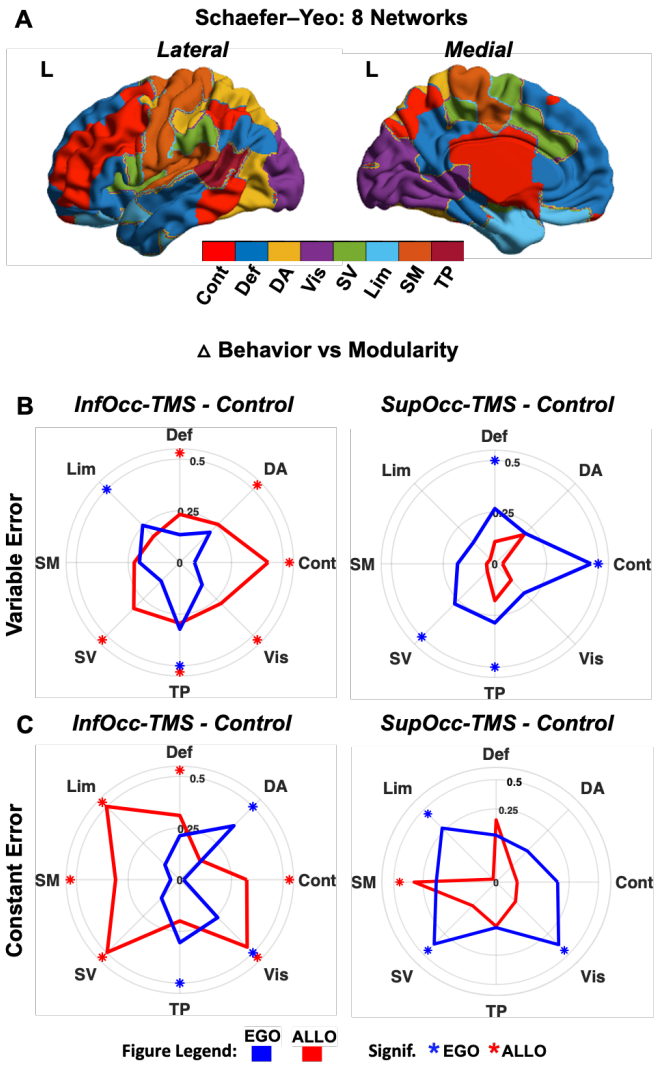


Figure 3.6 Association of Network Modularity with Behaviour.

A – Schaefer-Yeo 8 network parcellation (collapsed from 17 networks to 8 unique networks) is color-coded by network and overlaid on the left medial and lateral cortex. The 8 parcellations are: Control (Cont), Default (Def), Dorsal Attention (DA), Limbic (Lim), Visual (Vis), Somato-motor (SM), Salience Ventral Attention (SV) and Temporo-parietal (TP) Networks. The *four lower panels* **(B, C)** show the relationship between modularity and TMS-induced **B –** variable and **C –** absolute errors in the 8 networks described above, plotted radially. The *left column* plots InfOcc-TMS data and the *right column* plots SupOcc-TMS data, during the EGO (blue) and ALLO (red) tasks. Each datapoint represents the relationship (slope) between modularity and TMS-induced errors across 16 participants (quantified as the absolute value of the TMS induced error vs modularity linear association), computed using standardized regression coefficients. Asterisks indicate statistical significance.

3.6 Discussion

The present study used transcranial magnetic stimulation (TMS) to investigate the causal role of extrastriate visual cortex in egocentric (EGO) and allocentric (ALLO) memory-guided reaching. We hypothesized that superior occipital stimulation would affect both egocentric- and allocentric-based reaching, whereas inferior occipital stimulation would selectively impair allocentric performance. Consistent with our hypotheses, stimulation of the superior occipital cortex disrupted performance (accuracy, precision, and reaction time) in both EGO and ALLO conditions, whereas stimulation of the inferior occipital cortex produced selective impairments that were strongest in the ALLO condition. TMS also had more specific effects, i.e., tending to affect movements to contralateral space and target-goal dissociations (in the OPPOSITE condition), in the predicted site and task-dependent manner. Finally, a double dissociation between superior / EGO vs. inferior / ALLO emerged in the widespread relationship between occipital stimulation, cortical modularity, and behavioural errors. Together, these findings consistently show a causal dissociation between the contributions of inferior and superior occipital cortex to spatial behaviour.

3.6.1 Behaviour in the Control Task Replicates Previous Observations

Even in the absence of TMS, the instruction to use EGO vs. ALLO cues influenced reaching behaviour. ALLO reaching was more precise and accurate than EGO reaching, as reflected by smaller endpoint variability and lower absolute error. Reaction times were also faster in the ALLO condition, indicating more efficient movement planning when landmark information was available. These findings replicate the results of our previous

behavioural study (Musa et al., 2024) and support the idea that allocentric landmarks help stabilize spatial behaviour in the presence of spatial uncertainty and 'noisy' internal egocentric signals during memory delays (Burgess, 2006; Byrne et al., 2007 Chen et al., 2011).

3.6.2 TMS Causally Dissociates Visual Streams and Spatial Behaviour

As noted in the introduction, neuropsychological, neuroimaging, and neurophysiological data suggest that the ventral visual stream is associated with allocentric spatial processes but ultimately must influence behaviour through a primarily egocentric dorsal stream (Chen et al. 2014, 2018; Bharmauria et al. 2025; Goodale & Haffenden, 1998; Musa et al. 2025; Schenk & McIntosh, 2010). However, causal evidence for this dissociation in healthy humans was lacking until now. This led us to hypothesize that inferior occipital TMS would selectively influence landmark-guided reaching, whereas superior occipital TMS would influence both allocentric and egocentric reaching. Overall, our TMS results (selective disruption of reach precision, accuracy, and reaction time) support this prediction. By design, the timing of our TMS pulses (during the memory interval preceding action), suggests that these errors arise from disruptions of spatial memory and planning (Vesia et al. 2010), as opposed to feedback control during execution (Breveglieri et al. 2024; Striemer et al. 2011).

These results are consistent with the numerous studies which suggest transformation from gaze-centred visual signals to somatotopic motor signals through the dorsal occipital-parietal-frontal pathway (Andersen et al., 1997; Andersen & Buneo, 2002; Culham & Valyear, 2006; Goodale & Milner, 1992) in contrast to configurational (feature

relative to feature, object relative to object) processing in the ventral stream (Goodale & Milner, 1992; Kravitz et al., 2011; Milner & Goodale, 2006). However, this distinction is not absolute: allocentric relationships (such as target-relative-to-landmark) must ultimately be represented in some sensory frame (such as the eye) and be converted into muscle coordinates to influence behaviour. Behavioural studies suggest that this transformation occurs at the first opportunity, possibly to benefit readiness for action (Chen et al. 2010). This is likely why allocentric cues influence the dorsal stream (Chen et al. 2018), even extending to single-cell codes in frontal cortex (Schutz et al. 2023).

Occipital TMS Influences Spatial Asymmetries in a Site-Specific Manner

Focal TMS in the visuomotor reach network is known to have more influence on the contralateral visual field and limb (Bestmann et al., 2013; Koch et al., 2008; Vesia et al., 2006, 2008, 2010) and has been shown to disrupt the stability of location when eye movements dissociate the target from the movement goal (Morris et al. 2007; Müller et al. 2018), especially when the goal is updated into the stimulated hemifield (Malik et al. 2015). A similar spatial updating process occurs in 'anti-reaching' tasks, like the EGO-OPPOSITE task used here (Crawford et al., 2011; Gail & Andersen, 2006; Munoz & Everling, 2004). As noted above, these processes are known to benefit from the stabilizing influence of visual landmarks (Byrne et al. 2010; Musa et al. 2024).

Our TMS results show that the stimulation site interacts with these spatial asymmetries in a site-dependent manner consistent with our main hypothesis: first, we observed that inferior occipital stimulation had more contralateral influence in the ALLO task, whereas superior stimulation was more task-independent. Second, we observed that inferior

stimulation tends to ‘undo’ the benefit of landmarks in the OPPOSITE task, whereas superior stimulation tends to exacerbate the normal errors.

3.6.3 Implications for Cortical Network Organization

Our findings support a network perspective of visual function in two ways. First, our stimulation sites were derived from a specific inferior occipital hub (for the ALLO task) and superior occipital hub (for both the EGO and ALLO tasks) derived in our previous functional network study (Musa et al., 2025). The current results thus provide causal evidence to support the previous study. Second, the new network analysis here establishes a relationship between occipital TMS site, modularity throughout the cortex (based on resting state data), and behavioural errors.

The latter analysis provided several useful observations. First, our control results (Supplementary Figure 3.3) support the notion that modularity provides a useful biomarker for linking intrinsic network properties to task and behaviour (Musa et al., 2025; Standage et al., 2025; Tomou et al. 2025). Second, we found that modularity throughout the brain predicted TMS-induced behavioural errors, perhaps through increased susceptibility to TMS, or by reducing intermodular communication (Alstott et al., 2009; Bullmore & Sporns, 2012; Sporns, 2013). Third, these effects were site dependent in a manner generally supportive of our dorsal-ventral hypothesis. However, the dissociation was stronger than expected (there was a double dissociation — stronger inferior site predictions in the ALLO task, stronger superior site prediction in the EGO task), perhaps because this network-based analysis better reflected the internal organization of the dorsal-ventral streams than overt behaviour alone. Finally, this analysis gives general

causal credence to the motion that functional network parameters provide real interpretive power for understanding brain-behaviour relationships (Alstott et al., 2009; Bestmann & Feredoes, 2013; Braun et al., 2012; Bullmore & Sporns, 2012; Sporns, 2011; Freud et al., 2018).

3.6.4 Potential Clinical Implications

The selective impairment of allocentric processing following inferior occipital stimulation has potential clinical relevance. It is well established that dorsal stream damage produces egocentric deficits, whereas ventral stream damage affects landmark-based spatial abilities (Aguirre & D'Esposito, 1999; Bohbot et al., 2004; Goodale & Haffenden, 1998; Maguire et al., 1998; Schenk & McIntosh, 2010). Our results, which show both regional specializations with widespread network influence, provide causal support for the notion that rehabilitation strategies could leverage alternative networks when default spatial mechanisms are compromised (Schenk & McIntosh, 2010). For example, training on the use of allocentric cues may augment or even bypass egocentric mechanisms that have become ‘noisy’ due to damage, disease or normal ageing (Musa et al. 2025). Further, the interaction between hub location and network organization may inform individualized clinical neuromodulation.

3.6.5 Conclusions

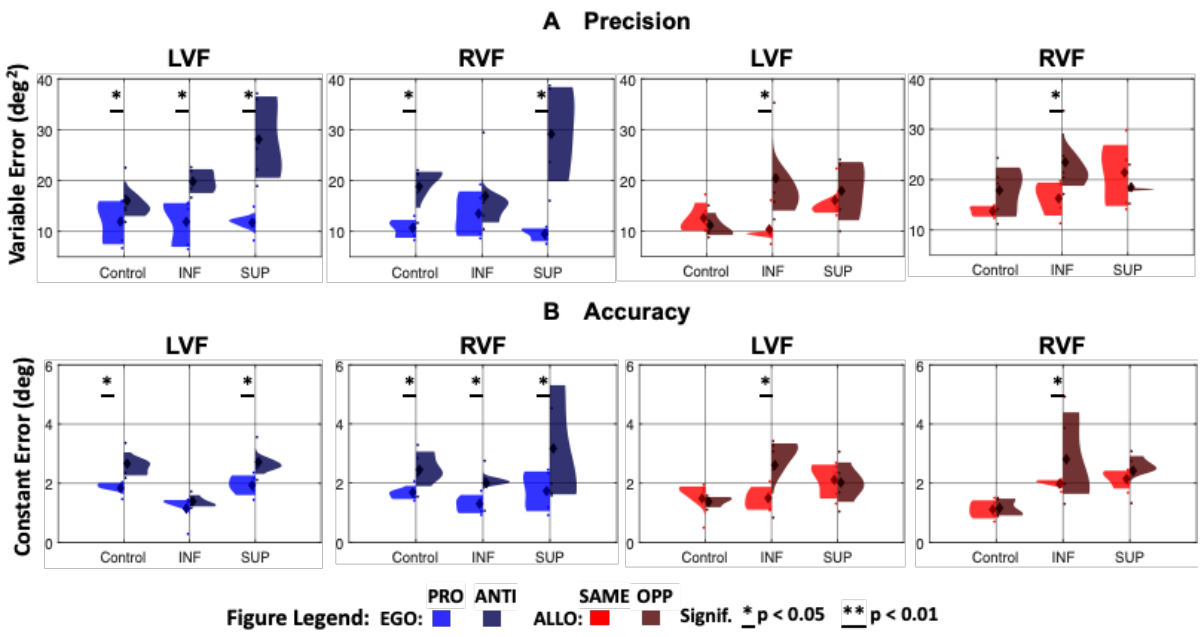
This study demonstrates that occipital visual regions make causal and dissociable contributions to memory-guided reaching. Inferior occipital cortex preferentially supports allocentric representations, whereas superior occipital cortex likely integrates allocentric

information but fundamentally supports the default egocentric transformations for action. Critically, the behavioural impact of focal disruption is shaped by large-scale network organization. These findings provide a framework linking global network topology, local cortical specializations, and spatial behaviour.

3.6.6 Funding

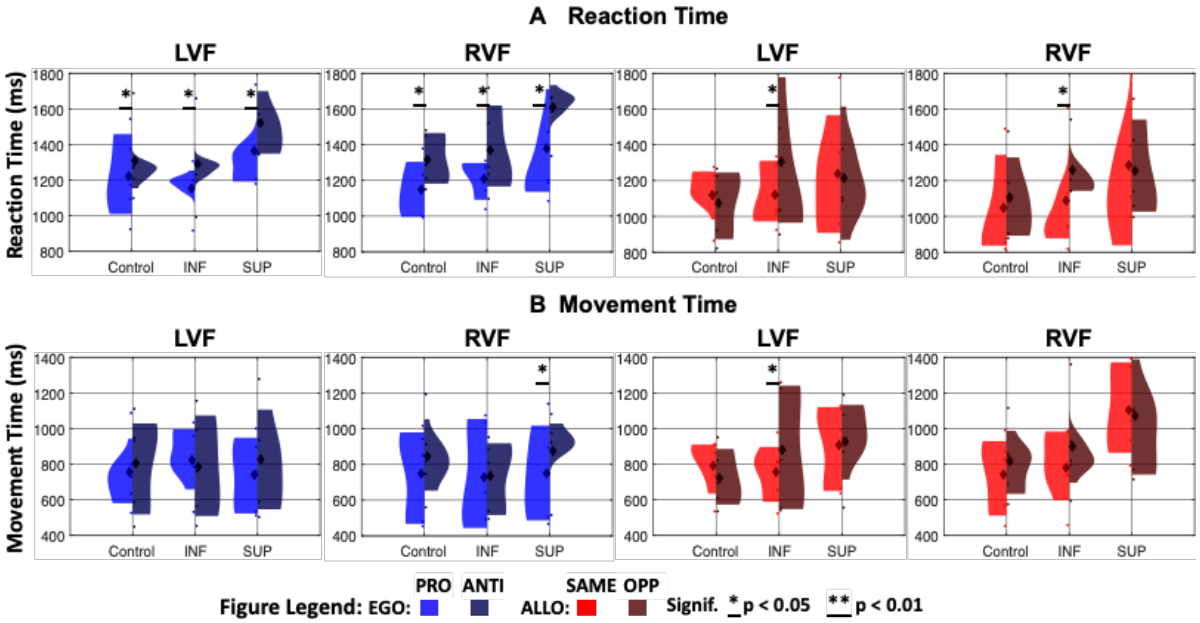
This work was funded by the Canadian Institutes for Health Research [grant number MOP-68812] and the Vision: Science to Applications (VISTA) Program [grant number 102001171]. L. Musa was supported by VISTA. J.D. Crawford was supported by a Canada Research Chair, Canada First Research Excellence fund [grant number 101035774].

3.7 Supplementary Materials



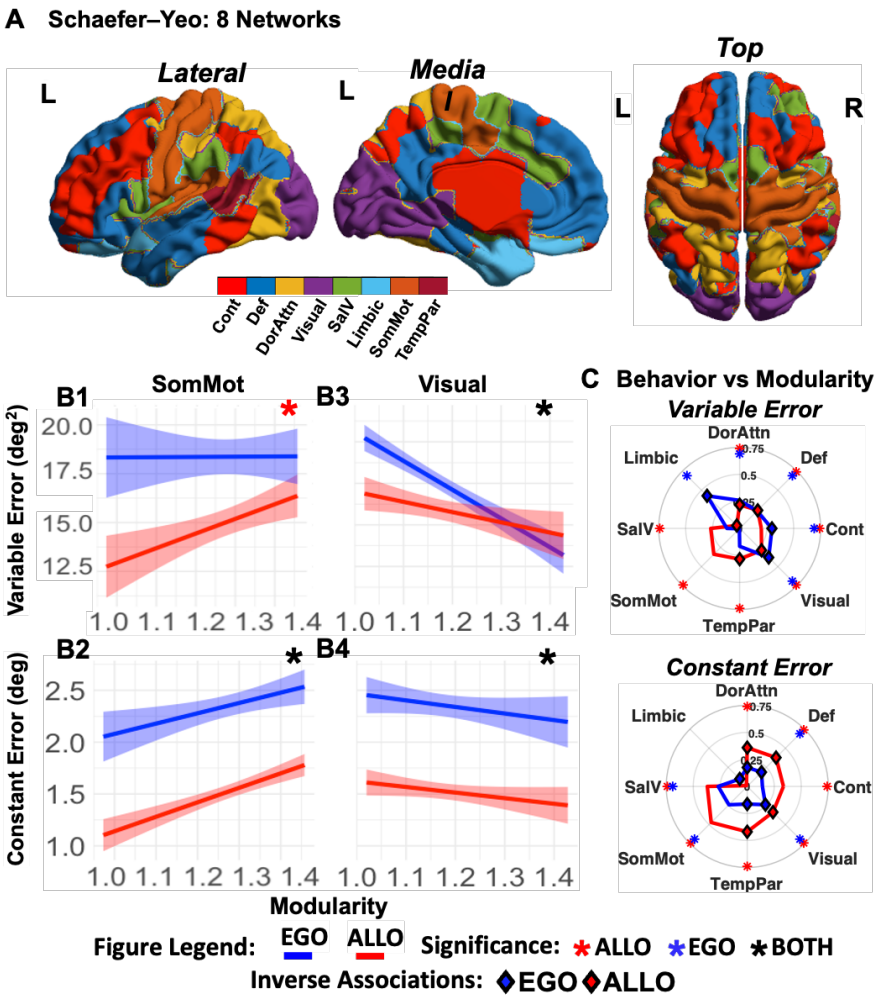
Supplementary Figure 3.1 Reach Accuracy and Precision Across Target-Movement Mappings.

Violin plots show the distribution of **A – Precision:** Variable Error (deg²) and **B – Accuracy:** Constant Error (deg) for EGO (left panels) SAME/OPP reaching (blue/dark blue) and ALLO (right panels) SAME/OPP second landmark relative to first landmark positions (red/dark red) conditions across Control, InfOcc-TMS, and SupOcc-TMS conditions. Left visual field (LVF) and right visual field (RVF) reaches are shown separately for both spatial updating conditions. Horizontal lines indicate significant differences ($p < 0.05$).



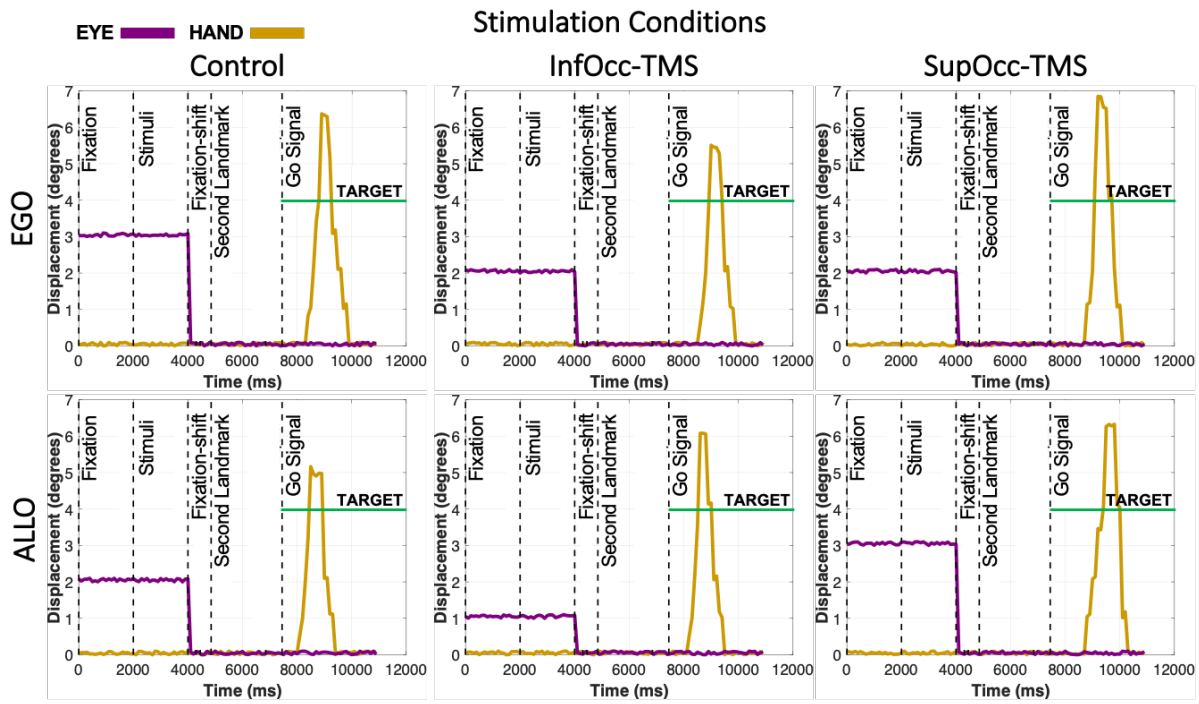
Supplementary Figure 3.2 Reaction Time and Movement Time Across Target-Movement Mappings.

Violin plots show the distribution of **A – Reaction Time:** Time between Go signal and finger movement onset (ms) **B – Movement Time:** Time between index finger movement onset and stabilization on screen (ms) for EGO (left panels) SAME/OPP reaching (blue/dark blue) and ALLO (right panels) SAME/OPP second landmark relative to first landmark positions (red/dark red) conditions across Control, InfOcc-TMS, and SupOcc-TMS conditions. Left visual field (LVF) and right visual field (RVF) reaches are shown separately for both spatial updating conditions. Horizontal lines indicate significant differences ($p < 0.05$).



Supplementary Figure 3.3 Modularity Correlates to Behavioural Errors in Control Data.

A – Schaefer-Yeo 8 network parcellation (collapsed from 17 networks to 8 unique networks) is color-coded by network and overlaid on the left lateral cortex. The 8 parcellations are: Control (Cont), Default (Def), Dorsal Attention (DorAttn), Limbic, Visual (Vis), Somato-motor (SomMot), Salience Ventral Attention (SalV) and Temporo-parietal (TempPar) Networks. **B –** The regression plots (line of best fit and 95% confidence interval) on the left show the association between Modularity and Behaviour in the SomMot network (**B1,B2**) and the Visual network (**B3,B4**). Variable Error is shown on the top panels and Constant Error is shown on the bottom panels, for EGO and ALLO conditions in blue and red. and **C –** The two plots in left panel show the relationship between modularity, and variable (top) and constant (bottom) errors for the *Control* condition in the 8 networks described above, plotted radially**.** Inverse (Negative) associations are indicated by diamond connectors and significant associations are marked in the plot by asterisks, color-coded by condition (blue – EGO, red – ALLO).



Supplementary Figure 3.4 Timing of events.

Six example trials from one participant are shown for a target position of 4° under the EGO (top panels) and ALLO (bottom panels) spatial conditions, and for the control and two TMS stimulation conditions. Hand position (purple) and eye position (yellow) are plotted as a function of time. Vertical dashed lines mark the onset of key task events: fixation point appearance (Fixation), target and landmark presentation (Stimuli), and fixation shift to the center of the LED panel (Fixation Shift) during the **Stimulus and Encoding** phase (see Fig. 3.1 for a description of the task phases and events); landmark reappearance (Second Landmark) during the **Memory Delay and TMS** phase; and the onset of the auditory instruction (Go Signal) during the **Response** phase. The horizontal green dashed line indicates the physical location of the reach target.

4 CHAPTER FOUR

GENERAL DISCUSSION

4.1 Summary

My studies represent a comprehensive investigation into the neural mechanisms underlying allocentric and egocentric coding of spatial targets for memory-guided reaching movements, employing complementary methodologies that span functional neuroimaging, graph theoretical network analysis, and causal manipulation via transcranial magnetic stimulation (TMS). Together, these investigations advance our understanding of how the brain encodes, integrates, and transforms spatial information depending on the reference frame demanded by task instruction.

The first major line of work used fMRI combined with graph theoretical analysis (GTA) to examine how task instruction (egocentric vs. allocentric) and global activation trends related to reach planning shape the integration of target and landmark information into the cortical reach network. Critically, the visual stimuli were held constant across conditions, with only the instruction to ignore or use landmarks differing between tasks (Chen et al., 2014; Musa et al., 2024). This design isolated the influence of top-down instruction on network organization. The results demonstrated that the allocentric instruction induced a more integrated network characterized by fewer modules but more hubs, including the conjoining of ventral visual cortex with the dorsal stream into a single module and the recruitment of additional hubs in ventral-posterior and frontal cortical areas associated with allocentric coding and ego-allocentric integration. In contrast, the egocentric instruction produced four functional modules with hubs

clustered in visual and sensorimotor cortex. Importantly, decoding analyses confirmed that modularity, particularly in modules 2 and 3, was the most discriminative parameter for distinguishing task instruction, while modules 1–3 and network energy were significant predictors of behavioural error.

The second line of work used TMS to establish the causal contributions of extrastriate visual cortex to egocentric and allocentric reaching. Stimulation of superior occipital cortex disrupted performance in both reference frames, whereas inferior occipital stimulation produced selective impairments strongest in the allocentric condition. These effects manifested as increased endpoint variability, reduced accuracy, and prolonged reaction times. Crucially, individual differences in network modularity predicted susceptibility to TMS-induced disruption, demonstrating that large-scale network topology not only correlates with behaviour but actively modulates the consequences of focal cortical perturbation.

Taken together, these findings are consistent with theories of functional specialization in the dorsal and ventral visual streams (Goodale & Milner, 1992; Milner & Goodale, 2008), indicating that both streams contribute to spatial coding for movement, but in fundamentally different ways. The dorsal stream provides the default egocentric sensorimotor transformation, while the ventral stream supplies configurational, landmark-based allocentric representations that can be flexibly integrated into action depending on task demands.

These findings carry important translational implications. If "egocentric" dorsal regions are compromised by stroke or neurodegeneration, intact "allocentric" ventral

mechanisms might still support action. Rehabilitation strategies designed to enhance reliance on allocentric, landmark-based information could reinforce recovery (Schenk & McIntosh, 2010), and may be particularly valuable for elderly individuals with degraded egocentric function during normal ageing (Colombo et al., 2017; Ruggiero et al., 2016).

4.2 The Role of Network Modularity in Spatial Goal Encoding

A central and novel contribution of my work is the demonstration that network modularity, an intermediate-level topological feature reflecting the segregation of brain regions into functionally specialized clusters, is the most sensitive marker for distinguishing how task instruction influences spatial coding. Whereas coarse global measures such as clustering coefficient, global efficiency, and energy were poorly discriminative of task condition, modularity reliably predicted both task instruction and behavioural error. This finding aligns with the broader principle that modularity provides a more nuanced window into cognitive state than global connectivity parameters alone (Bassett & Sporns, 2017; Sporns & Betzel, 2016).

The principle that the brain balances functional segregation and integration to support complex behaviour is now well established (Bertolero et al., 2015; Cohen & D'Esposito, 2016; Shine et al., 2019; Sporns, 2013). My results extend this principle to the domain of visuospatial motor control by showing that task instruction can profoundly reorganize the modular architecture of the reach network. The egocentric instruction favoured a segregated organization with specialized modules for dorsal-stream sensorimotor transformation, high-level spatial processing, multisensory integration, and ventral-stream configurational processing. The allocentric instruction, by contrast, drove

integration, most notably the conjoining of dorsal and ventral visual pathways, reflecting the computational need to compute target-relative-to-landmark configurations in the ventral stream and then incorporate these into dorsal-stream visuomotor processes (Chen et al., 2014; Chen & Crawford, 2020).

This interpretation is reinforced by recent work demonstrating that flexible reconfiguration of brain network modularity supports adaptive behaviour across changing task demands (Finc et al., 2020). The finding that modularity also predicts behavioural error suggests that the efficiency of this segregation-integration balance has direct functional consequences for the precision of memory-guided action. An interesting connection here is to the broader literature on the "network neuroscience theory" of intelligence (Barbey, 2018), which posits that the dynamic capacity to reconfigure from modular to integrated states underlies flexible cognition. My finding that an allocentric instruction, arguably the more computationally demanding reference-frame transformation, drives integration is precisely the kind of "difficult-to-easy" trajectory described by Finc et al. (2020), in which network integration scales with cognitive demand before segregating again as a task becomes automatic. This positions reference-frame selection as a model system for studying instruction-driven network reconfiguration more generally.

4.3 Global Activation Trends and Large-Scale Network Communication

An important and often overlooked aspect of my findings concerns the functional role of widespread global activation trends. Planning and execution of reaches recruit not only sensorimotor cortex but also produce progressive, widespread cortical activation

(Cappadocia et al., 2017; Medendorp et al., 2003), including reactivation of early visual cortex (Gallivan & Culham, 2015; Monaco et al., 2024; Velji-Ibrahim et al., 2022). Such trends are frequently dismissed as non-specific arousal, preparatory set, or BOLD artifacts.

Building on the foundational work of Harms and Melcher (2003), who introduced the OSORU model and identified ramping activity as a functionally meaningful signal, and Duff et al. (2007), who showed systematic ramp-slope organization across motor learning, I consistently observed widespread within-trial ramping activity. Removing these global trends significantly altered network parameters—particularly global synchrony, a candidate mechanism for binding oscillatory signals across regions (Blohm et al., 2019; Fries, 2015; Singer, 1999). Detrending also increased global clustering, reduced modularity and the number of modules, and decreased dorsal-ventral integration, while paradoxically improving task classification based on modularity.

These results are consistent with the notion that global BOLD trends reflect long-range communication that influences local network dynamics (Smith et al., 2012). My demonstration that detrending the signal sharpens task-specific modular structure offers a reconciliation: the global component and the task-specific modular component are dissociable but co-existing signals, and their separation is informative rather than merely a cleaning step. Methodologically, my work establishes that removing such trends is a useful tool to reveal task-specific functional segregation. Theoretically, it suggests that recurrent motor-related activation (Blohm et al., 2019) may play a complementary role in promoting global synchrony to integrate spatial signals across

cortex when it is time for action. This recurrent-activation account also resonates with predictive-processing frameworks (Friston, 2010; Keller & Mrsic-Flogel, 2018), in which feedback reactivation of early visual cortex during the delay period could represent a top-down "reconstruction" of the spatial goal—a mechanism that would naturally produce both the early-visual reactivation I observed and the ramping signals that promote integration.

4.4 Causal Evidence and the Convergence of Correlational and Interventional Methods

A particular strength of my thesis is the integration of correlational network analysis with causal TMS manipulation. While the fMRI/GTA work identified the topological signatures of egocentric and allocentric coding, the TMS work established the causal necessity of specific extrastriate regions and, crucially, demonstrated that network topology modulates the behavioural consequences of focal perturbation.

The TMS results provide direct causal evidence for functional specialization within extrastriate occipital cortex: superior occipital stimulation disrupted both reference frames, consistent with a role in reference-frame-general transformations and sensorimotor coordination (Goodale & Milner, 1992; Vesia & Crawford, 2012), whereas inferior occipital stimulation selectively impaired allocentric performance, consistent with ventral-stream contributions to landmark-centered processing (Chen et al., 2014; Milner & Goodale, 2008). This dissociation refines longstanding models by localizing reference-frame-dependent computations within the extrastriate cortex.

Most importantly, the finding that resting-state network modularity predicted TMS-induced disruption provides a mechanistic account of why focal stimulation produces variable effects across individuals and tasks. Theoretically, when a high-centrality hub is stimulated, segregated networks should confine the perturbation locally, while integrated networks should propagate it more widely. Consistent with this, inferior occipital stimulation effects were predominantly predicted by large-scale modularity in the allocentric task, whereas superior occipital effects were predicted by modularity in the egocentric task—suggesting that allocentric hubness in superior occipital cortex may depend on localized interactions with specific ventral-dorsal hub areas rather than large-scale (including dorsal stream) propagation (Musa et al., 2025). This extends prior correlational work by demonstrating that network topology not only predicts behaviour but actively shapes causal perturbation effects (Braun et al., 2012; Freud et al., 2018; Sporns, 2011). This finding speaks directly to the emerging field of "network-controllability" theory (Gu et al., 2015; Pasqualetti et al., 2014), which formalizes how the topological role of a stimulated node determines whether energy injected at that node drives the brain into nearby (easy) or distant (difficult) states. My result that modularity predicts perturbation spread is an empirical, behaviourally-anchored validation of the controllability prediction that integrative hubs in low-modularity configurations are more efficient at broadcasting their influence. It also aligns with the broader "lesion-network mapping" programme (Fox, 2018), in which the behavioural consequence of damage or stimulation is better predicted by the connectivity profile of the targeted site than by its location alone—a principle my data extend from structural

lesions to transient TMS perturbation and from group averages to individual differences in modularity.

4.5 Relationship to Sensorimotor Transformation Models

The dorsal visual stream / parietofrontal reach network is generally thought to provide egocentric transformations for action (Goodale & Milner, 1992; Andersen & Buneo, 2002). More recent frameworks distinguish bottom-up and top-down components (Blohm et al., 2019; Gallivan et al., 2013; Monaco et al., 2024). The bottom-up transformation converts gaze-centered to shoulder-centered coordinates through postural gain modulation (Blohm & Crawford, 2009; Chang & Snyder, 2010), while a well-characterized top-down influence is the use of efference saccade signals to spatially update gaze-centered reach goals in parietal cortex (Medendorp et al., 2003).

My findings refine this model. Behavioural work suggests that allocentric cues are re-integrated after gaze updating, implying that ego-allocentric integration occurs just before the gaze-to-motor conversion (Byrne & Crawford, 2010; Chen & Crawford, 2020). While this integration is normally a weighted process (Byrne & Crawford, 2010; Fiehler et al., 2014), my results, together with prior work (Chen et al., 2018), indicate that instruction can modulate this weighting toward full egocentric or allocentric reliance through changes in functional connectivity between dorsal and ventral streams. Thus, my work preserves the notion of the dorsal stream as the default sensorimotor transformer while demonstrating that it is flexibly modulated by ventral-stream and frontal inputs according to task demands. This weighted-integration picture can be cast formally in Bayesian terms: the relative reliability of egocentric versus allocentric cues

determines their optimal weighting (Byrne & Crawford, 2010), and instruction can be understood as a top-down prior that re-scales these weights. My network results provide a candidate neural implementation for such a prior—namely, instruction-dependent modulation of dorsal-ventral functional coupling—linking the cue-combination literature (Ernst & Banks, 2002) to large-scale connectivity. It is notable that landmark reliability and stability govern whether allocentric cues are used at all (Fiehler et al., 2014; Klinghammer et al., 2017), suggesting that the instruction effect I observed and the stimulus-reliability effects in those studies may converge on the same dorsal-ventral gating mechanism.

4.6 Possible Physiological Basis of the Networks

The BOLD signals and network properties I observed reflect large-scale, population-level neural activity driven by synaptic inputs across brain regions (Logothetis, 2008). My network findings are grounded in a growing body of single-neuron evidence. Configurational information (feature-vs-feature, object-vs-object) is encoded in the ventral stream (Kravitz et al., 2013), corresponding to extrastriate regions in my analyses. Target-landmark interactions producing landmark-centered codes have been demonstrated in frontal and supplementary cortex (Bharmauria et al., 2020, 2021; Schütz et al., 2023), and both egocentric and allocentric codes coexist in dorsal-stream reach areas of monkey cortex (Taghizadeh et al., 2024), corresponding to parietal and somatomotor nodes in my networks. These convergences suggest that my network-level results reflect genuine physiological processes, and conversely that simultaneous recordings across broad cortical territories will ultimately be required to understand how these signals are integrated at the cellular level. The coexistence of egocentric and

allocentric codes within the same dorsal-stream populations (Taghizadeh et al., 2024) is especially significant for interpreting my modularity findings: it implies that the dorsal-ventral "integration" I detect at the network scale need not require wholesale rewiring, but could be implemented by a relative gain change on already-present mixed-selectivity neurons. Mixed selectivity is now recognized as a computational substrate for flexible, context-dependent behaviour (Fusi et al., 2016; Rigotti et al., 2013), and instruction-dependent reweighting of such neurons offers a parsimonious cellular bridge between the single-unit and network levels of my account.

4.7 Lateralization

My network analyses revealed substantial bilateral symmetry in modularity for both egocentric and allocentric tasks, contrasting with perceptual studies reporting hemispheric lateralization—right-hemisphere dominance for egocentric and left-hemisphere engagement for allocentric processing (Galati et al., 2000; Ruotolo et al., 2019). The bilateral organization in my reaching paradigms may reflect the need for interhemispheric communication when overt actions are required, paralleling findings that lateralized visual modules can join when bilateral communication becomes necessary (Tomou et al., 2025).

Some lateralization did emerge in allocentric network hubs: left-hemisphere hubs included orbitofrontal cortex, parietal operculum, and dorsolateral prefrontal cortex (associated with decision-making and motor planning; Heekeren et al., 2008), while right-hemisphere hubs included insula, inferior parietal lobule, and somatomotor areas (associated with spatial memory and sensory integration; Ferber et al., 2020). This

pattern suggests that while the overall modular architecture is bilateral for action, finer hub-level asymmetries persist along functional lines. The discrepancy between bilateral reach networks and lateralized perceptual findings may itself be informative about the perception-action distinction at the heart of the two-streams model. Whereas perceptual spatial judgments can be lateralized to whichever hemisphere is specialized for the relevant reference frame, the demand to specify and execute a movement of a particular limb imposes a contralateral motor constraint that necessarily engages both hemispheres, recruiting the well-documented right-hemisphere bias for spatial attention (Corbetta & Shulman, 2011) alongside left-hemisphere praxis and planning circuits. In this light, the bilaterality I observe is not a failure to replicate lateralization but a signature of the action requirement transforming a lateralizable perceptual representation into an obligatorily bilateral motor plan.

4.8 Limitations

Several limitations should be considered when interpreting the present findings. First, fMRI measures neural signals indirectly through BOLD and cannot determine the precise neuronal mechanisms or directionality of communication between cortical regions. Thus, interpretations of dorsal–ventral stream interactions would benefit from complementary approaches with greater temporal resolution, such as EEG/MEG or electrophysiological recordings.

Second, graph theoretical analyses depend on methodological choices, including parcellation, thresholding, and community detection approaches. Although the findings were robust within the current framework, future studies should test their reproducibility

across alternative network construction methods and independent datasets. Third, while TMS provided causal evidence for the contribution of extrastriate regions, stimulation effects likely extend beyond the targeted site through connected networks. Concurrent neuroimaging or multimodal approaches could further characterize how perturbations propagate across functional networks.

The generalizability of these findings is also limited by the use of healthy young adults. Future work should examine whether similar network mechanisms apply across ageing and neurological populations where spatial processing may be altered. Finally, the controlled laboratory tasks used here isolated reference-frame-dependent processing but may not fully capture the complexity of natural behaviour. Studies using more dynamic and ecologically valid environments will be important for determining how these principles extend to real-world goal-directed actions.

Despite these limitations, the convergence of behavioural, network, and causal evidence provides strong support for a framework in which large-scale network organization shapes spatial coding and visuomotor control.

4.9 General Implications and Clinical Relevance

Collectively, my findings demonstrate that the modular organization of brain networks plays a critical role in supporting spatial goal encoding, and that task instruction profoundly influences modularity and hubness even when sensory stimuli are held constant. The ability to decode task-specific networks from modularity, and to predict TMS-induced behavioural disruption from network topology, suggests that event-related and individualized connectivity analysis could serve as a powerful clinical tool.

Disruptions in modular structure are implicated in neurological and psychiatric disorders affecting cognition (Bassett & Bullmore, 2009; Gratton et al., 2018) and may help explain why visual landmarks benefit movement initiation in Parkinson's disease (Russo et al., 2022).

The selective impairment of allocentric processing following inferior occipital TMS, alongside preserved egocentric performance, has clear clinical relevance. Patients with ventral or occipital damage frequently show landmark-based spatial memory deficits while retaining egocentric abilities; my results provide causal support for this dissociation and suggest rehabilitation could leverage intact egocentric mechanisms when allocentric processing is compromised, or vice versa (Schenk & McIntosh, 2010). More broadly, the dependence of TMS effects on hub location and network organization argues for individualized, connectivity-informed approaches to neuromodulation. These findings can be situated within classic and contemporary models of spatial cognition that emphasize hierarchical, distributed, and flexibly integrated egocentric and allocentric representations (Burgess, 2008; Galati et al., 2000; Wolbers & Hegarty, 2010).

4.10 Future Directions

Several promising avenues emerge from this work. First, the relationship between specific network hubs and behaviour could be probed more deeply by combining TMS with diffusion tensor imaging (DTI) to relate the structural connectivity of perturbed hubs to the spread of stimulation effects, directly testing the hypothesis that integrative versus segregative topology governs perturbation propagation. Second, given my evidence for effector-dependent allocentric mechanisms, future work should test whether the network

reorganization and ego-allocentric integration principles identified for reaching also govern saccadic eye movements, using parallel behavioural and fMRI/GTA designs. Third, the temporal dynamics of network reconfiguration could be examined using EEG/MEG or chronometric TMS to determine when during the delay and response phases dorsal-ventral integration occurs. Fourth, extending these paradigms to clinical populations, including stroke, Parkinson's disease, and early Alzheimer's disease, would test whether disease-related degradation of modularity predicts spatial deficits and rehabilitation potential. Finally, computational modelling that links global activation trends, synchrony, and modular dynamics could clarify the mechanistic relationship between recurrent motor-related activation and large-scale network integration during goal-directed action.

4.11 Conclusions

In conclusion, this thesis has identified complementary mechanisms by which the brain segregates and integrates networks in response to task instruction during memory-guided reaching: (1) topological segregation of similar signals into functional modules for visually-evoked movement; (2) integration across modules for specific task demands, such as the dorsoventral and posterior-anterior integration observed in the allocentric task; (3) recruitment of specialized hubs for particular task requirements; and (4) promotion of global synchrony through activation trends emerging during movement planning. The TMS findings provide causal confirmation that extrastriate occipital regions make dissociable contributions to egocentric and allocentric reaching—superior occipital cortex supporting reference-frame-general transformations and inferior occipital cortex preferentially supporting allocentric representations—and that the behavioural

impact of focal disruption is shaped by large-scale network organization. Together, these results provide a unified framework linking cortical specialization, network topology, and spatial behaviour, with broad implications for understanding goal-directed action in health and its degradation in disease.

5 References

Adam, J. J., Bovend'Eerdt, T. J. H., Schuhmann, T., & Sack, A. T. (2016). Allocentric coding in ventral and dorsal routes during real-time reaching: Evidence from imaging-guided multi-site brain stimulation. *Behavioural Brain Research, 300*, 143–149.

Aguirre, G. K., & D'Esposito, M. (1999). Topographical disorientation: A synthesis and taxonomy. *Brain, 122*(9), 1613–1628.

Alstott, J., Breakspear, M., Hagmann, P., Cammoun, L., & Sporns, O. (2009). Modeling the impact of lesions in the human brain. *PLOS Computational Biology, 5*(6), e1000408.

Andersen, R. A., & Buneo, C. A. (2002). Intentional maps in posterior parietal cortex. *Annual Review of Neuroscience, 25*, 189–220.

Andersen, R. A., & Cui, H. (2009). Intention, action planning, and decision making in parietal-frontal circuits. *Neuron, 63*(5), 568–583.

Andersen, R. A., Essick, G. K., & Siegel, R. M. (1985). Encoding of spatial location by posterior parietal neurons. *Science, 230*(4724), 456–458.

Andersen, R. A., Snyder, L. H., Bradley, D. C., & Xing, J. (1997). Multimodal representation of space in the posterior parietal cortex and its use in planning movements. *Annual Review of Neuroscience, 20*, 303–330.

Baltaretu, B. R., Monaco, S., Velji-Ibrahim, J., Luabeya, G. N., & Crawford, J. D. (2020). Parietal cortex integrates saccade and object orientation signals to update grasp plans. *Journal of Neuroscience, 40*(23), 4525–4535.

Bamiou, D. E., Musiek, F. E., & Luxon, L. M. (2003). The insula (Island of Reil) and its role in auditory processing: Literature review. *Brain Research Reviews, 42*(2), 143–154.

Barbey, A. K. (2018). Network neuroscience theory of human intelligence. *Trends in Cognitive Sciences, 22*(1), 8–20.

Bassett, D. S., & Bullmore, E. T. (2009). Human brain networks in health and disease. *Current Opinion in Neurology, 22*(4), 340–347.

Bassett, D. S., & Sporns, O. (2017). Network neuroscience. *Nature Neuroscience, 20*(3), 353–364.

Bassett, D. S., Wymbs, N. F., Porter, M. A., Mucha, P. J., Carlson, J. M., & Grafton, S. T. (2011). Dynamic reconfiguration of human brain networks during learning. *Proceedings of the National Academy of Sciences, 108*(18), 7641–7646.

Batista, A. P., Buneo, C. A., Snyder, L. H., & Andersen, R. A. (1999). Reach plans in eye-centered coordinates. *Science, 285*(5425), 257–260.

Benson, N. C., Jamison, K. W., Arcaro, M. J., Vu, A. T., Glasser, M. F., Coalson, T. S., et al. (2018). The Human Connectome Project 7 Tesla retinotopy dataset: Description and population receptive field analysis. *Journal of Vision, 18*(13), 23.

Bertolero, M. A., Yeo, B. T. T., & D'Esposito, M. (2015). The modular and integrative functional architecture of the human brain. *Proceedings of the National Academy of Sciences, 112*(49), E6798–E6807.

Bestmann, S., & Feredoes, E. (2013). Combined neurostimulation and neuroimaging in cognitive neuroscience: Past, present, and future. *Nature Reviews Neuroscience, 14*, 222–232.

Beynel, L., Davis, S. W., Crowell, C. A., Hilbig, S. A., Lim, S., Nguyen, D., et al. (2020). Effects of repetitive transcranial magnetic stimulation on resting-state connectivity: A systematic review. *Neuroscience & Biobehavioural Reviews, 108*, 262–272.

Bharmauria, V., Sajad, A., Li, J., Yan, X., Wang, H., & Crawford, J. D. (2020). Integration of eye-centered and landmark-centered codes in frontal eye field gaze responses. *Cerebral Cortex, 30*(9), 4995–5013.

Bharmauria, V., Sajad, A., Yan, X., Wang, H., & Crawford, J. D. (2021). Spatiotemporal coding in the macaque supplementary eye fields: Landmark influence in the target-to-gaze transformation. *ENeuro, 8*(1).

Bharmauria, V., Seo, S., & Crawford, J. D. (2025). Neural integration of egocentric and allocentric visual cues in the gaze system. *Journal of Neurophysiology, 133*(1), 109–120.

Blohm, G., Alikhanian, H., Gaetz, W., Goltz, H. C., DeSouza, J. F., Cheyne, D. O., & Crawford, J. D. (2019). Neuromagnetic signatures of the spatiotemporal transformation for manual pointing. *NeuroImage, 197*, 306–319.

Blohm, G., & Crawford, J. D. (2009). Fields of gain in the brain. *Neuron, 64*(5), 598–600.

Blohm, G., Keith, G. P., & Crawford, J. D. (2009). Decoding the cortical transformations for visually guided reaching in 3D space. *Cerebral Cortex, 19*(6), 1372–1393.

Blondel, V. D., Guillaume, J. L., Lambiotte, R., & Lefebvre, E. (2008). Fast unfolding of communities in large networks. *Journal of Statistical Mechanics: Theory and Experiment, 2008*(10), P10008.

Bohbot, V. D., Iaria, G., & Petrides, M. (2004). Hippocampal function and spatial memory: Evidence from functional neuroimaging in healthy participants and performance of patients with medial temporal lobe resections. *Neuropsychology, 18*(3), 418–425.

Bonacich, P. (1972). Factoring and weighting approaches to status scores and clique identification. *Journal of Mathematical Sociology, 2*(1), 113–120.

Bonacich, P. (2007). Some unique properties of eigenvector centrality. *Social Networks, 29*(4), 555–564.

Born, R. T., & Bradley, D. C. (2005). Structure and function of visual area MT. *Annual Review of Neuroscience, 28*, 157–189.

Braun, U., Plichta, M. M., Esslinger, C., Sauer, C., Haddad, L., Grimm, O., ... Meyer-Lindenberg, A. (2012). Test–retest reliability of resting-state connectivity network characteristics using fMRI and graph theoretical measures. *NeuroImage, 59*(2), 1404–1412.

Breakspear, M. (2017). Dynamic models of large-scale brain activity. *Nature Neuroscience, 20*(3), 340–352.

Bremmer, F., Schlack, A., Duhamel, J. R., Graf, W., & Fink, G. R. (2001). Space coding in primate posterior parietal cortex. *NeuroImage, 14*(1), S46-S51.

Bressler, S. L., & Menon, V. (2010). Large-scale brain networks in cognition: Emerging methods and principles. *Trends in Cognitive Sciences, 14*(6), 277–290.

Breveglieri, R., Borgomaneri, S., Bosco, A., Filippini, M., De Vitis, M., Tessari, A., et al. (2024). RTMS over the human medial parietal cortex impairs online reaching corrections. *Brain Structure and Function, 229*(2), 297–310.

Bridgeman, B., Peery, S., & Anand, S. (1997). Interaction of cognitive and sensorimotor maps of visual space. *Perception & Psychophysics, 59*, 456–469.

Budisavljevic, S., Dell'Acqua, F., & Castiello, U. (2018). Cross-talk connections underlying dorsal and ventral stream integration during hand actions. *Cortex, 103*, 224–239.

Bullmore, E., & Sporns, O. (2009). Complex brain networks: Graph theoretical analysis of structural and functional systems. *Nature Reviews Neuroscience, 10*, 186–198.

Bullmore, E., & Sporns, O. (2012). The economy of brain network organization. *Nature Reviews Neuroscience, 13*(5), 336–349.

Buneo, C. A., & Andersen, R. A. (2006). The posterior parietal cortex: Sensorimotor interface for the planning and control of goal-directed movements. *Neuropsychologia, 44*(13), 2594–2606.

Burgess, N. (2006). Spatial memory: How egocentric and allocentric combine. *Trends in Cognitive Sciences, 10*(12), 551–557.

Byrne, P. A., Becker, S., & Burgess, N. (2007). Remembering the past and imagining the future: A neural model of spatial memory and imagery. *Psychological Review, 114*(2), 340–375.

Byrne, P. A., Cappadocia, D. C., & Crawford, J. D. (2010). Interactions between gaze-centered and allocentric representations of reach target location in the presence of spatial updating. *Vision Research, 50*(24), 2661–2670.

Byrne, P. A., & Crawford, J. D. (2010). Cue reliability and a landmark stability heuristic determine relative weighting between egocentric and allocentric visual

information in memory-guided reach. *Journal of Neurophysiology, 103*(6), 3054–3069.

Cappadocia, D. C., Monaco, S., Chen, Y., Blohm, G., & Crawford, J. D. (2017). Temporal evolution of target representation, movement direction planning, and reach execution in occipital–parietal–frontal cortex: An fMRI study. *Cerebral Cortex, 27*(11), 5242–5260.

Chang, S. W., Dickinson, A. R., & Snyder, L. H. (2008). The hierarchy of reach planning processes in the posterior parietal cortex. *Journal of Neuroscience, 28*(40), 10131–10142.

Chang, S. W., & Snyder, L. H. (2010). Idiosyncratic and systematic aspects of spatial representations in the macaque parietal cortex. *Proceedings of the National Academy of Sciences, 107*(17), 7951–7956.

Chen, Y., Byrne, P., & Crawford, J. D. (2011). Time course of allocentric decay, egocentric decay, and allocentric-to-egocentric conversion in memory-guided reach. *Neuropsychologia, 49*(1), 49–60.

Chen, Y., & Crawford, J. D. (2020). Allocentric representations for target memory and reaching in human cortex. *Annuals of the New York Academy of Sciences, 1464*(1), 142–155.

Chen, Y., Monaco, S., Byrne, P., Yan, X., Henriques, D. Y. P., & Crawford, J. D. (2014). Allocentric versus egocentric representation of remembered reach targets in human cortex. *Journal of Neuroscience, 34*(37), 12515–12526.

Chen, Y., Monaco, S., & Crawford, J. D. (2018). Neural substrates for allocentric-to-egocentric conversion of remembered reach targets in humans. *European Journal of Neuroscience, 47*(8), 901–917.

Chong, M., Bhushan, C., Joshi, A. A., Choi, S., Haldar, J. P., Shattuck, D. W., et al. (2017). Individual parcellation of resting fMRI with a group functional connectivity prior. *NeuroImage, 156*, 87–100.

Cisek, P. (2005). Neural representations of motor plans, desired trajectories, and controlled objects. *Cognitive Processing, 6*(1), 15–24.

Cohen, J. R., & D'Esposito, M. (2016). The segregation and integration of distinct brain networks and their relationship to cognition. *Journal of Neuroscience, 36*(48), 12083–12094.

Cohen, Y. E., & Andersen, R. A. (2002). A common reference frame for movement plans in the posterior parietal cortex. *Nature Reviews Neuroscience, 3*, 553–562.

Colby, C. L. (1998). Action-oriented spatial reference frames in parietal cortex. *Neuron, 20*(1), 15–24.

Colombo, D., Serino, S., Tuena, C., Pedroli, E., Dakanalis, A., Cipresso, P., & Riva, G. (2017). Egocentric and allocentric spatial reference frames in aging: A systematic review. *Neuroscience & Biobehavioural Reviews, 80*, 605–621.

Committeri, G., Galati, G., Paradis, A. L., Pizzamiglio, L., Berthoz, A., & LeBihan, D. (2004). Reference frames for spatial cognition: Different brain areas are involved in viewer-, object-, and landmark-centered judgments about object location. *Journal of Cognitive Neuroscience, 16*(9), 1517–1535.

Connolly, J. D., Goodale, M. A., Desouza, J. F. X., & Menon, R. S. (2000). A comparison of frontoparietal fMRI activation during anti-saccades and memory-guided saccades. *NeuroImage, 12*(5), 554–562.

Conway, B. R. (2018). The organization and operation of inferior temporal cortex. *Annual Review of Vision Science, 4*(1), 381–402.

Corbetta, M., & Shulman, G. L. (2011). Spatial neglect and attention networks. *Annual Review of Neuroscience, 34*, 569–599.

Crawford, J. D., Henriques, D. Y., & Medendorp, W. P. (2011). Three-dimensional transformations for goal-directed action. *Annual Review of Neuroscience, 34*(1), 309–331.

Crawford, J. D., Medendorp, W. P., & Marotta, J. J. (2004). Spatial transformations for eye-hand coordination. *Journal of Neurophysiology, 92*(1), 10–19.

Culham, J. C., Cavina-Pratesi, C., & Singhal, A. (2006). The role of posterior parietal cortex in visuomotor control. *Neuropsychologia, 44*(13), 2611–2621.

Culham, J. C., & Kanwisher, N. G. (2001). Neuroimaging of cognitive functions in human parietal cortex. *Current Opinion in Neurobiology, 11*(2), 157–163.

Culham, J. C., & Valyear, K. F. (2006). Human parietal cortex in action. *Current Opinion in Neurobiology, 16*(2), 205–212.

Desimone, R., & Duncan, J. (1995). Neural mechanisms of selective visual attention. *Annual Review of Neuroscience, 18*(1), 193–222.

Desmurget, M., Epstein, C. M., Turner, R. S., Prablanc, C., Alexander, G. E., & Grafton, S. T. (1999). Role of the posterior parietal cortex in updating reaching movements. *Science, 286*(5441), 161–164.

Diedrichsen, J., Werner, S., Schmidt, T., & Trommershäuser, J. (2004). Immediate spatial distortions of pointing movements induced by visual landmarks. *Perception & Psychophysics, 66*(1), 89–103.

Duff, E., Xiong, J., Wang, B., Cunnington, R., Fox, P., & Egan, G. (2007). Complex spatio-temporal dynamics of fMRI BOLD: A study of motor learning. *NeuroImage, 34*(1), 156–168.

Dumoulin, S. O., & Wandell, B. A. (2008). Population receptive field estimates in human visual cortex. *NeuroImage, 39*(2), 647–660.

Ellison, A., & Cowey, A. (2009). Differential and co-involvement of areas of the temporal and parietal streams in visual tasks. *Neuropsychologia, 47*(6), 1609–1614.

Ernst, M. O., & Banks, M. S. (2002). Humans integrate visual and haptic information in a statistically optimal fashion. *Nature, 415*(6870), 429–433.

Felleman, D. J., & Van Essen, D. C. (1991). Distributed hierarchical processing in the primate cerebral cortex. *Cerebral Cortex, 1*(1), 1–47.

Ferber, S., Ruppel, J., & Danckert, J. (2020). Visual working memory deficits following right brain damage. *Brain and Cognition, 142*, 105566.

Fiehler, K., Wolf, C., Klinghammer, M., & Blohm, G. (2014). Integration of egocentric and allocentric information during memory-guided reaching to images of a natural environment. *Frontiers in Human Neuroscience, 8*, 636.

Filimon, F. (2010). Human cortical control of hand movements: From observation to action. *Annual Review of Neuroscience, 33*, 233–259.

Finc, K., Bonna, K., He, X., Lydon-Staley, D. M., Kühn, S., Duch, W., & Bassett, D. S. (2020). Dynamic reconfiguration of functional brain networks during working memory training. *Nature Communications, 11*, Article 2435.

Finn, E. S., Poldrack, R. A., & Shine, J. M. (2023). Functional neuroimaging as a catalyst for integrated neuroscience. *Nature, 623*(7986), 263–273.

Fortunato, S. (2010). Community detection in graphs. *Physics Reports, 486*(3–5), 75–174.

Foxe, J. J., Wylie, G. R., Martinez, A., Schroeder, C. E., Javitt, D. C., Guilfoyle, D., ... Murray, M. M. (2002). Auditory-somatosensory multisensory processing in auditory association cortex: An fMRI study. *Journal of Neurophysiology, 88*(1), 540–543.

Fox, M. D. (2018). Mapping symptoms to brain networks with the human connectome. *The New England Journal of Medicine, 379*(23), 2237–2245.

Freeman, L. C. (1977). A set of measures of centrality based on betweenness. *Sociometry*, 35–41.

Freud, E., Macdonald, S. N., Chen, J., Quinlan, D. J., Goodale, M. A., & Culham, J. C. (2018). Getting a grip on reality: Grasping movements directed to real objects and images rely on dissociable neural representations. *Cortex, 98*, 34–48.

Freud, E., Plaut, D. C., & Behrmann, M. (2017). “What” is happening in the dorsal visual pathway. *Trends in Cognitive Sciences, 21*(6), 413–426.

Freud, E., Plaut, D. C., & Behrmann, M. (2018). ‘What’ is happening in the dorsal visual pathway. *Trends in Cognitive Sciences, 22*(9), 773–784.

Fries, P. (2015). Rhythms for cognition: Communication through coherence. *Neuron, 88*(1), 220–235.

Friston, K. J., Jezzard, P., & Turner, R. (1994). Analysis of functional MRI time-series. *Human Brain Mapping, 1*(2), 153–171.

FSLeyes Documentation. (2024). *FEAT mode—FSLeyes user guide*. FMRIB, University of Oxford. https://git.fmrib.ox.ac.uk/fsl/fsleyes/fsleyes/-/blob/main/userdoc/feat_mode.rst

Fusi, S., Miller, E. K., & Rigotti, M. (2016). Why neurons mix: High-dimensionality for higher cognition. *Current Opinion in Neurobiology, 37*, 66–74.

Gail, A., & Andersen, R. A. (2006). Neural dynamics in monkey parietal reach region reflect context-specific sensorimotor transformations. *Journal of Neuroscience, 26*(37), 9376–9384.

Gail, A., Klaes, C., & Westendorff, S. (2009). Implementation of spatial transformations in parietal cortex. *Neuron, 64*(5), 634–646.

Galati, G., Lobel, E., Vallar, G., Berthoz, A., Pizzamiglio, L., & Le Bihan, D. (2000). The neural basis of egocentric and allocentric coding of space in humans: A functional magnetic resonance study. *Experimental Brain Research, 133*, 156–164.

Gallivan, J. P., & Culham, J. C. (2015). Neural coding within human brain areas involved in actions. *Current opinion in neurobiology, 33*, 141–149.

Gallivan, J. P., McLean, D. A., Flanagan, J. R., & Culham, J. C. (2013). Where one hand meets the other: Limb-specific and action-dependent movement plans

decoded from preparatory signals in single human frontoparietal brain areas. *Journal of Neuroscience, 33*(5), 1991–2008.

Georgopoulos, A. P., Kalaska, J. F., Caminiti, R., & Massey, J. T. (1982). On the relations between the direction of two-dimensional arm movements and cell discharge. *Journal of Neuroscience, 2*(11), 1527–1537.

Ghaderi, A. H., Baltaretu, B. R., Andevari, M. N., Bharmauria, V., & Balci, F. (2020). Synchrony and complexity in state-related EEG networks: An application of spectral graph theory. *Neural Computation, 32*(12), 2422–2454.

Ghaderi, A. H., Brown, E. C., Clark, D. L., Ramasubbu, R., Kiss, Z. H., & Protzner, A. B. (2023). Functional brain network features specify DBS outcome for patients with treatment resistant depression. *Molecular Psychiatry, 28*(9), 3888–3899.

Ghaderi, A. H., Taghizadeh, S., & Nazari, M. A. (2025). Altered visual network modularity and communication in ADHD subtypes: Classification via source-localized EEG modules. *Biomedical Signal Processing and Control, 106*, 107755.

Ghaderi, A., Niemeier, M., & Crawford, J. D. (2023). Saccades alter cortical network modularity and decrease lateralization in a visual perception task. *Journal of Vision, 23*(9), 5510–5510.

Glasser, M. F., et al. (2016). A multi-modal parcellation of human cerebral cortex. *Nature, 536*, 171–178.

Gnadt, J. W., & Andersen, R. A. (1988). Memory related motor planning activity in posterior parietal cortex. *Experimental Brain Research, 70*, 216–220.

Goodale, M. A., & Haffenden, A. (1998). Frames of reference for perception and action in the human visual system. *Neuroscience & Biobehavioural Reviews, 22*(2), 161–172.

Goodale, M. A., Króliczak, G., & Westwood, D. A. (2005). Dual routes to action: Contributions of the dorsal and ventral streams to adaptive behaviour. *Progress in Brain Research, 149*, 269–283.

Goodale, M. A., & Milner, A. D. (1992). Separate visual pathways for perception and action. *Trends in Neurosciences, 15*(1), 20–25. https://doi.org/10.1016/0166-2236(92)90344-8

Goodale, M. A., Milner, A. D., Jakobson, L. S., & Carey, D. P. (1991). A neurological dissociation between perceiving objects and grasping them. *Nature, 349*(6305), 154–156. https://doi.org/10.1038/349154a0

Good, B. H., De Montjoye, Y. A., & Clauset, A. (2010). Performance of modularity maximization in practical contexts. *Physical Review E—Statistical, Nonlinear, and Soft Matter Physics, 81*(4), 046106.

Gratton, C., Kraus, B. T., Greene, D. J., Gordon, E. M., Laumann, T. O., Nelson, S. M., & Petersen, S. E. (2018). Defining individual-specific functional neuroanatomy for precision neuroscience. *Nature Neuroscience, 21*(11), 1649–1659.

Green, P., & MacLeod, C. J. (2016). Simr: An R package for power analysis of generalized linear mixed models by simulation. *Methods in Ecology and Evolution, 7*(4), 493–498.

Grefkes, C., & Fink, G. R. (2005). The functional organization of the intraparietal sulcus in humans and monkeys. *Journal of Anatomy, 207*(1), 3–17.

Grol, M. J., Majdandžić, J., Stephan, K. E., et al. (2007). Parieto-frontal connectivity during reaching. *Journal of Neuroscience, 27*(45), 11869–11878.

Gu, S., Pasqualetti, F., Cieslak, M., Telesford, Q. K., Yu, A. B., Kahn, A. E., Medaglia, J. D., Vettel, J. M., Miller, M. B., Grafton, S. T., & Bassett, D. S. (2015). Controllability of structural brain networks. *Nature Communications, 6*, Article 8414.

Hallett, M. (2007). Transcranial magnetic stimulation: A primer. *Neuron, 55*(2), 187–199.

Hallett, M., Di Lazzaro, V., Ziemann, U., et al. (2017). Contribution of transcranial magnetic stimulation to assessment of brain connectivity and networks. *Clinical Neurophysiology, 128*(11), 2125–2139.

Harms, M. P., & Melcher, J. R. (2003). Detection and quantification of a wide range of fMRI temporal responses using a physiologically-motivated basis set. *Human Brain Mapping, 20*(3), 168–183.

Hay, L., & Redon, C. (1999). Accuracy of spatial memory for reaching movements. *Experimental Brain Research, 129*, 223–232.

Heekeren, H. R., Marrett, S., Ruff, D. A., Bandettini, P. A., & Ungerleider, L. G. (2006). Involvement of human left dorsolateral prefrontal cortex in perceptual decision making is independent of response modality. *Proceedings of the National Academy of Sciences, 103*(26), 10023–10028.

Henriques, D. Y., Klier, E. M., Smith, M. A., Lowy, D., & Crawford, J. D. (1998). Gaze-centered remapping of remembered visual space in an open-loop pointing task. *Journal of Neuroscience, 18*(4), 1583–1594.

Henriques, D. Y. P., & Crawford, J. D. (2000). Direction-dependent distortions of remembered visual space. *Experimental Brain Research, 132*, 179–194.

Honey, C. J., Thivierge, J. P., & Sporns, O. (2010). Can structure predict function in the human brain?. *NeuroImage, 52*(3), 766–776.

Huang, S., De Brigard, F., Cabeza, R., & Davis, S. W. (2024). Connectivity analyses for task-based fMRI. *Physics of Life Reviews, 49*, 139–156.

Iacoboni, M. (2006). Visuo-motor integration and control in the human posterior parietal cortex: Evidence from TMS and fMRI. *Neuropsychologia, 44*(13), 2691–2699.

Kar, K., & DiCarlo, J. J. (2021). Fast recurrent processing via ventrolateral prefrontal cortex is needed by the primate ventral stream for robust core visual object recognition. *Neuron, 109*(1), 164–176.

Kar, K., Kubilius, J., Schmidt, K., Issa, E. B., & DiCarlo, J. J. (2019). Evidence that recurrent circuits are critical to the ventral stream's execution of core object recognition behaviour. *Nature Neuroscience, 22*(6), 974–983.

Keller, G. B., & Mrsic-Flogel, T. D. (2018). Predictive processing: A canonical cortical computation. *Neuron, 100*(2), 424–435.

Khan, A. Z., Pisella, L., & Blohm, G. (2013). Causal evidence for posterior parietal cortex involvement in visual-to-motor transformations of reach targets. *Cortex, 49*(9), 2439–2448.

Klatzky, R. L. (1998). Allocentric and egocentric spatial representations. In *Spatial cognition*. Springer.

Klinghammer, M., Blohm, G., & Fiehler, K. (2015). Contextual factors determine the use of allocentric information for reaching in a naturalistic scene. *Journal of Vision, 15*(13), 24.

Koch, G., Del Olmo, M. F., Cheeran, B., Schippling, S., Caltagirone, C., Driver, J., & Rothwell, J. C. (2008). Functional interplay between posterior parietal and ipsilateral motor cortex revealed by twin-coil transcranial magnetic stimulation during reach planning toward contralateral space. *Journal of Neuroscience, 28*(23), 5944–5953.

Kravitz, D. J., Saleem, K. S., Baker, C. I., & Mishkin, M. (2011). A new neural framework for visuospatial processing. *Nature Reviews Neuroscience, 12*(4), 217–230.

Kravitz, D. J., Saleem, K. S., Baker, C. I., Ungerleider, L. G., & Mishkin, M. (2013). The ventral visual pathway: An expanded neural framework for the processing of object quality. *Trends in Cognitive Sciences, 17*(1), 26–49.

Körding, K. P., & Wolpert, D. M. (2004). Bayesian integration in sensorimotor learning. *Nature, 427*, 244–247.

Krigolson, O. E., & Heath, M. (2004). Internal representations of spatial targets during reaching. *Experimental Brain Research, 156*, 237–247.

Kundu, P., Brenowitz, N. D., Voon, V., Worbe, Y., Vértes, P. E., Inati, S. J., et al. (2013). Integrated strategy for improving functional connectivity mapping using multiecho fMRI. *Proceedings of the National Academy of Sciences, 110*(40), 16187–16192.

Latora, V., & Marchiori, M. (2001). Efficient behaviour of small-world networks. *Physical Review Letters, 87*(19), 198701.

Lemay, M., Bertram, C. P., & Stelmach, G. E. (2004). Pointing to an allocentric and egocentric remembered target. *Motor Control, 8*(1), 16–32.

Logothetis, N. K., Pauls, J., Augath, M., Trinath, T., & Oeltermann, A. (2001). Neurophysiological investigation of the basis of the fMRI signal. *Nature, 412*(6843), 150–157.

Maguire, E. A., Burgess, N., Donnett, J. G., Frackowiak, R. S. J., Frith, C. D., & O'Keefe, J. (1998). Knowing where and getting there: A human navigation network. *Science, 280*(5365), 921–924.

Malik, P., Dessing, J. C., & Crawford, J. D. (2015). Role of early visual cortex in trans-saccadic memory of object features. *Journal of Vision, 15*(11), 7.

McNamara, T. P., & Shelton, A. L. (2000). Cognitive maps and the hippocampus. *Trends in Cognitive Sciences, 4*(12), 443–448.

Medendorp, W. P., Goltz, H. C., Vilis, T., & Crawford, J. D. (2003). Gaze-centered updating of visual space in human parietal cortex. *Journal of Neuroscience, 23*(15), 6209–6214.

Miller, E. K. (2000). The prefontral cortex and cognitive control. *Nature reviews neuroscience, 1*(1), 59–65.

Miller, K. J., Hermes, D., Honey, C. J., Hebb, A. O., Ramsey, N. F., Knight, R. T., Ojemann, J. G., & Fetz, E. E. (2012). Human motor cortical activity is selectively phase-entrained on underlying rhythms. *PLOS Computational Biology, 8*(9), e1002655.

Milner, A. D., & Goodale, M. A. (2006). *The visual brain in action* (2nd ed.). Oxford University Press.

Milner, A. D., & Goodale, M. A. (2008). Two visual systems re-viewed. *Neuropsychologia, 46*(3), 774–785.

Müller, N. G., Riemer, M., Brandt, L., & Wolbers, T. (2018). Repetitive transcranial magnetic stimulation reveals a causal role of the human precuneus in spatial updating. *Scientific Reports, 8*(1), 10171.

Monaco, S., Menghi, N., & Crawford, J. D. (2024). Action-specific feature processing in the human cortex: An fMRI study. *Neuropsychologia, 194*, 108773.

Moro, S., et al. (2017). Visual and sensorimotor cortex involvement in reaching and grasping. *Neuropsychologia, 105*, 135–145.

Morris, A. P., Chambers, C. D., & Mattingley, J. B. (2007). Parietal stimulation destabilizes spatial updating across saccadic eye movements. *Proceedings of the National Academy of Sciences, 104*(21), 9069–9074.

Munoz, D. P., & Everling, S. (2004). Look away: The anti-saccade task and voluntary control of eye movement. *Nature Reviews Neuroscience, 5*(3), 218–228.

Musa, L., Ghaderi, A., Chen, Y., & Crawford, J. D. (2025). Spatial task instructions and global activation trends influence functional modularity in the cortical reach network. *NeuroImage*, 121460.

Musa, L., Yan, X., & Crawford, J. D. (2024). Instruction alters the influence of allocentric landmarks in a reach task. *Journal of Vision, 24*(7), 17–17.

Nachev, P., Kennard, C., & Husain, M. (2008). Functional role of the supplementary and pre-supplementary motor areas. *Nature Reviews Neuroscience, 9*, 856–869.

Neggers, S. F. W., Van der Lubbe, R. H. J., Ramsey, N. F., & Postma, A. (2006). Interactions between ego- and allocentric neuronal representations of space. *NeuroImage, 31*(1), 320–331.

Newman, M. E. (2006). Modularity and community structure in networks. *Proceedings of the National Academy of Sciences, 103*(23), 8577–8582.

Orti, R., Coello, Y., Ruotolo, F., Vincent, M., Bartolo, A., Iachini, T., & Ruggiero, G. (2024). Cortical correlates of visuospatial switching processes between egocentric and allocentric frames of reference: A fNIRS study. *Brain Topography, 37*, 712–730.

Park, H. J., & Friston, K. (2013). Structural and functional brain networks: From connections to cognition. *Science, 342*(6158), 1238411.

Pascual-Leone, A., Bartres-Faz, D., & Keenan, J. P. (2000). Transcranial magnetic stimulation. *Journal of Neuropsychology, 14*, 125–140.

Peers, P. V., Ludwig, C. J., Rorden, C., Cusack, R., Bonfiglioli, C., Bundesen, C., ... Duncan, J. (2005). Attentional functions of parietal and frontal cortex. *Cerebral Cortex, 15*(10), 1469–1484.

Perenin, M. T., & Vighetto, A. (1988). Optic ataxia: A specific disruption in visuomotor mechanisms. *Brain, 111*, 643–674.

Pisella, L., et al. (2000). An automatic pilot for the hand in human posterior parietal cortex. *Nature Neuroscience, 3*, 729–736.

Poucet, B. (1993). Spatial cognitive maps in animals: New hypotheses on their structure and neural mechanisms. *Psychological review, 100*(2), 163.

Prime, S. L., Tsotsos, L., Keith, G. P., & Crawford, J. D. (2007). Visual memory capacity in transsaccadic integration. *Experimental Brain Research, 180*, 609–628.

Raichle, M. E., MacLeod, A. M., Snyder, A. Z., Powers, W. J., Gusnard, D. A., & Shulman, G. L. (2001). A default mode of brain function. *Proceedings of the National Academy of Sciences, 98*(2), 676–682.

R Core Team (2025). *R: A language and environment for statistical computing*. R Foundation for Statistical Computing.

Ridderinkhof, K. R., Ullsperger, M., Crone, E. A., & Nieuwenhuis, S. (2004). The role of the medial frontal cortex in cognitive control. *Science, 306*(5695), 443–447.

Rigotti, M., Barak, O., Warden, M. R., Wang, X.-J., Daw, N. D., Miller, E. K., & Fusi, S. (2013). The importance of mixed selectivity in complex cognitive tasks. *Nature, 497*(7451), 585–590.

Rizzolatti, G., & Craighero, L. (2004). The mirror-neuron system. *Annual Review of Neuroscience, 27*, 169–192.

Rizzolatti, G., & Matelli, M. (2003). Two different streams form the dorsal visual system. *Experimental Brain Research, 153*, 146–157.

Rossetti, Y., Pisella, L., & Vighetto, A. (2003). Optic ataxia revisited. *Experimental Brain Research, 153*, 171–179.

Rossi, S., Antal, A., Bestmann, S., Bikson, M., Brewer, C., Brockmöller, J., et al. (2021). Safety and recommendations for TMS use in healthy subjects and patient populations, with updates on training, ethical and regulatory issues: Expert guidelines. *Clinical Neurophysiology, 132*(1), 269–306.

Rubinov, M., & Sporns, O. (2010). Complex network measures of brain connectivity uses and interpretations. *NeuroImage, 52*(3), 1059–1069.

Ruggiero, G., D'Errico, O., & Iachini, T. (2016). Development of egocentric and allocentric spatial representations from childhood to elderly age. *Psychological Research, 80*(2), 259–272.

Ruotolo, F., Ruggiero, G., Raemaekers, M., Iachini, T., Van der Ham, I. J. M., Fracasso, A., & Postma, A. (2019). Neural correlates of egocentric and allocentric frames of reference combined with metric and non-metric spatial relations. *Neuroscience, 409*, 235–252.

Russo, Y., Stuart, S., Silva-Batista, C., Brumbach, B., Vannozzi, G., & Mancini, M. (2022). Does visual cueing improve gait initiation in people with Parkinson's disease?. *Human Movement Science, 84*, 102970.

Sack, A. T., et al. (2009). Optimizing functional accuracy of TMS with neuronavigation. *NeuroImage, 47*, 1623–1632.

Saramäki, J., Kivelä, M., Onnela, J. P., Kaski, K., & Kertesz, J. (2007). Generalizations of the clustering coefficient to weighted complex networks. *Physical Review E—Statistical, Nonlinear, and Soft Matter Physics, 75*(2), 027105.

Schaefer, A., Kong, R., Gordon, E. M., Laumann, T. O., Zuo, X. N., Holmes, A. J., ... Yeo, B. T. (2018). Local-global parcellation of the human cerebral cortex from intrinsic functional connectivity MRI. *Cerebral Cortex, 28*(9), 3095–3114.

Schenk, T., & McIntosh, R. D. (2010). Do we have independent visual streams for perception and action?. *Cognitive Neuroscience, 1*(1), 52–62.

Schütz, A., Bharmauria, V., Yan, X., Wang, H., Bremmer, F., & Crawford, J. D. (2023). Integration of landmark and saccade target signals in macaque frontal cortex visual responses. *Communications Biology, 6*(1), 938.

Shadmehr, R., & Krakauer, J. W. (2008). A computational neuroanatomy for motor control. *Experimental Brain Research, 185*, 359–381.

Shine, J. M., Breakspear, M., Bell, P. T., Martens, K. A. E., Shine, R., Koyejo, O., Sporns, O., & Poldrack, R. A. (2019). Human cognition involves the dynamic integration of neural activity and neuromodulatory systems. *Nature Neuroscience, 22*, 289–296.

Silvanto, J., & Pascual-Leone, A. (2008). State-dependency of TMS. *Brain Stimulation, 1*, 50–58.

Silver, M. A., & Kastner, S. (2009). Topographic maps in human frontal and parietal cortex. *Trends in Cognitive Sciences, 13*(11), 488–495.

Singer, W. (1993). Synchronization of cortical activity and its putative role in information processing and learning. *Annual Review of Physiology, 55*(1), 349–374.

Singer, W. (1999). Neuronal synchrony: A versatile code for the definition of relations?. *Neuron, 24*(1), 49–65.

Smith, S. M., Beckmann, C. F., Andersson, J., Auerbach, E. J., Bijsterbosch, J., Douaud, G., ... WU-Minn HCP Consortium. (2013). Resting-state fMRI in the human connectome project. *NeuroImage, 80*, 144–168.

Snyder, L. H., Batista, A. P., & Andersen, R. A. (1997). Coding of intention in the posterior parietal cortex. *Nature, 386*, 167–170.

Soechting, J. F., & Flanders, M. (1992). Moving in three-dimensional space: Frames of reference, vectors, and coordinate systems. *Annual Review of Neuroscience, 15*(1), 167–191.

Sporns, O. (2011). *Networks of the brain*. MIT Press.

Sporns, O. (2011). The human connectome: A complex network. *Annuals of the New York Academy of Sciences, 1224*(1), 109–125.

Sporns, O. (2013). Structure and function of complex brain networks. *Dialogues in Clinical Neuroscience, 15*(3), 247–262.

Sporns, O., & Betzel, R. F. (2016). Modular brain networks. *Annual Review of Psychology, 67*, 613–640.

Sporns, O., Honey, C. J., & Kötter, R. (2007). Identification and classification of hubs in brain networks. *PLOS ONE, 2*(10), e1049.

Sporns, O., Tononi, G., & Kötter, R. (2005). The human connectome: A structural description of the human brain. *PLOS Computational Biology, 1*(4), e42.

Standage, D. I., Gale, D. J., Nashed, J. Y., Flanagan, J. R., & Gallivan, J. P. (2025). Whole-brain modular dynamics at rest predict sensorimotor learning performance. *Network Neuroscience, 9*(2), 631–660.

Striemer, C. L., Chouinard, P. A., & Goodale, M. A. (2011). Programs for action in superior parietal cortex: A triple-pulse TMS investigation. *Neuropsychologia, 49*(9), 2391–2399.

Taghizadeh, B., Fortmann, O., & Gail, A. (2024). Position-and scale-invariant object-centered spatial localization in monkey frontoparietal cortex dynamically adapts to cognitive demand. *Nature Communications, 15*(1), 3357.

Tomou, G., Baltaretu, B. R., Ghaderi, A., & Crawford, J. D. (2025). Saccades influence functional modularity in the human cortical vision network. *Scientific Reports, 15*(1), 10683.

Traag, V. A., Van Dooren, P., & Nesterov, Y. (2011). Narrow scope for resolution-limit-free community detection. *Physical Review E—Statistical, Nonlinear, and Soft Matter Physics, 84*(1), 016114.

Tunik, E., Rice, N. J., Hamilton, A., & Grafton, S. T. (2007). Beyond grasping: Representation of action in human anterior intraparietal sulcus. *NeuroImage, 36*, T77-T86.

Ungerleider, L. G., & Mishkin, M. (1982). Two cortical visual systems. In D. J. Ingle, M. A. Goodale, & R. J. W. Mansfield (Eds.), *Analysis of visual behaviour* (pp. 549–586). MIT Press.

Váša, F., & Mišić, B. (2022). Null models in network neuroscience. *Nature Reviews Neuroscience, 23*(8), 493–504.

van den Heuvel, M. P., & Sporns, O. (2013). Network hubs in the human brain. *Trends in Cognitive Sciences, 17*, 683–696.

Velji-Ibrahim, J., Crawford, J. D., Cattaneo, L., & Monaco, S. (2022). Action planning modulates the representation of object features in human fronto-parietal and occipital cortex. *European Journal of Neuroscience, 56*(6), 4803–4818.

Vesia, M., & Crawford, J. D. (2012). Specialization of reach function in human posterior parietal cortex. *Experimental Brain Research, 221*, 1–18.

Vesia, M., Monteon, J. A., Sergio, L. E., & Crawford, J. D. (2006). Hemispheric asymmetry in memory-guided pointing during single-pulse transcranial magnetic

stimulation of human parietal cortex. *Journal of Neurophysiology, 96*(6), 3016–3027.

Vesia, M., Prime, S. L., Yan, X., Sergio, L. E., & Crawford, J. D. (2006). Specificity of human parietal cortex stimulation for reaching. *Journal of Neuroscience, 26*, 1077–1087.

Vesia, M., Prime, S. L., Yan, X., Sergio, L. E., & Crawford, J. D. (2010). Specificity of human parietal saccade and reach regions during transcranial magnetic stimulation. *Journal of Neuroscience, 30*(39), 13053–13065.

Vesia, M., Yan, X., Henriques, D. Y. P., Sergio, L. E., & Crawford, J. D. (2008). Transcranial magnetic stimulation over human dorsal–lateral posterior parietal cortex disrupts integration of hand position signals into the reach plan. *Journal of Neurophysiology, 100*(4), 2005–2014.

Walsh, V., & Cowey, A. (2000). Transcranial magnetic stimulation and cognitive neuroscience. *Nature Reviews Neuroscience, 1*, 73–79.

Wandell, B. A., Dumoulin, S. O., & Brewer, A. A. (2007). Visual field maps in human cortex. *Neuron, 56*(2), 366–383.

Watts, D. J., & Strogatz, S. H. (1998). Collective dynamics of ‘small-world’networks. *Nature, 393*(6684), 440–442.

Westin, G. G., Bassi, B. D., Lisanby, S. H., & Luber, B. (2014). Determination of motor threshold using visual observation overestimates transcranial magnetic stimulation dosage: Safety implications. *Clinical Neurophysiology, 125*(1), 142–147.

Wise, S. P., Boussaoud, D., Johnson, P. B., & Caminiti, R. (1997). Premotor and parietal cortex: Corticocortical connectivity and motor control. *Annual Review of Neuroscience, 20*, 25–42.

Zaehle, T., Jordan, K., Wüstenberg, T., Baudewig, J., Dechent, P., & Mast, F. W. (2007). The neural basis of the egocentric and allocentric spatial frame of reference. *Brain Research, 1137*, 92–103.

Zeidman, P., Ashburner, J., Barnes, G., Kowalczyk, O., Lambert, C., Litvak, V., Nichols, T. E., Parr, T., Tierney, T. M., & Friston, K. (2025). SPM—30 years and beyond. *Cerebral Cortex, 35*(8), bhaf234.

Zorzo, C., Arias, J. L., & Méndez, M. (2021). Hippocampus and cortex are involved in the retrieval of a spatial memory under full and partial cue availability. *Behavioural Brain Research, 405*, 113204.

6 Appendix A.

TITLE:

CORTICAL NETWORKS FOR CODING EGOCENTRIC VERSUS ALLOCENTRIC REACH GOALS

by **Lina Musa**

a dissertation submitted to the faculty of graduate studies in partial fulfilment of the requirements for the degree of

Doctor of Philosophy

© 2026
Some Rights Reserved.
This work is licensed under a Creative Commons Attribution-Non Commercial-ShareAlike 2.5 Canada Licence

Permission has been granted to: a) YORK UNIVERSITY LIBRARIES to lend or sell copies of this dissertation in paper, microform or electronic formats, and b) LIBRARY AND ARCHIVES CANADA to reproduce, lend, distribute, or sell copies of this dissertation anywhere in the world in microform, paper or electronic formats and to authorize or and to authorize or and procure the reproduction, loan, distribution or sale of copies of this dissertation anywhere in the world in microform, paper or electronic formats.

8 Appendix B.

CORTICAL NETWORKS FOR CODING EGOCENTRIC VERSUS ALLOCENTRIC REACH GOALS

by Lina Musa

By virtue of submitting this document electronically, the author certifies that this is a true electronic equivalent of the copy of the dissertation approved by York University for the award of the degree. No alteration of the content has occurred and if there are any minor variations in formatting, they are as a result of the conversion to Adobe Acrobat format (or similar software application).

Examination Committee members:

1. Dr. J. Douglas Crawford
2. Dr. Jennifer Steeves
3. Dr. Dale Stevens
4. Dr. Shayna Rosenbaum
5. Dr. Denise Henriques
6. Dr. Jason Gallivan

9 Appendix C. Author Contributions

The research presented in this thesis includes collaborative work with contributions from multiple authors. The following summaries describe the contributions of the doctoral candidate and co-authors for each chapter. The doctoral candidate, Lina Musa, was the primary contributor to the conception, analysis, interpretation, visualization, and preparation of the manuscripts presented in this thesis.

9.1 Chapter 2

This chapter is based on collaborative work by Lina Musa, Amirhossein Ghaderi, Ying Chen, and John Douglas Crawford. Lina Musa contributed to the conceptualization of the study, data curation, data analysis, visualization, and preparation of the original manuscript draft. Amirhossein Ghaderi contributed to the conceptualization of the study, analysis, and provided supervision and expertise for the graph theory analyses. Ying Chen contributed to the investigation through data collection and data curation. John Douglas Crawford contributed to the conceptualization of the study, funding acquisition, project administration, supervision, and manuscript review and editing.

9.2 Chapter 3

This chapter is based on collaborative work by Lina Musa, Gaelle Nsamba Luabeya, Brando Sheldrick, Ali Rezaei, Saihong Sun, Xiaogang Yan, Michael Vesia, and John Douglas Crawford. Lina Musa led the conceptualization of the study, data curation, formal analysis, investigation, visualization, and preparation of the original manuscript draft. Gaelle Nsamba Luabeya contributed to investigation through data collection and

manuscript review and editing. Brando Sheldrick and Ali Rezaei contributed to investigation through data collection. Saihong Sun contributed software development and methodological expertise. Xiaogang Yan contributed resources and methodological expertise. Michael Vesia contributed to methodology through TMS training and manuscript review and editing. John Douglas Crawford contributed to the conceptualization of the study, funding acquisition, project administration, supervision, and manuscript review and editing.